TRANSIENT RADIATION FROM RESISTIVELY LOADED TRANSMISSION LINES AND THIN BICONICAL ANTENNAS

by
Harold Edwin Foster

A dissertation submitted in partial fulfillment
of the requirements for the degree of
Doctor of Philosophy
(Electrical Engineering)
in The University of Michigan
1973

Doctoral Committee:

Professor Chen-To Tai, Co-Chairman
Professor Ralph E. Hiatt, Co-Chairman
Associate Professor Roger D. Low
Professor John A. M. Lyon
Professor Lawrence L. Rauch

ABSTRACT

TRANSIENT RADIATION FROM RESISTIVELY LOADED TRANSMISSION LINES AND THIN BICONICAL ANTENNAS

by
Harold Edwin Foster

Co-Chairmen: Chen-To Tai, Ralph E. Hiatt

This dissertation presents a theoretical analysis of the radiation and reception of transient electromagnetic signals by resistively loaded transmission lines and thin biconical antennas. The resistively loaded transmission line analysis, in addition to providing an advance in its own right, supplies a basis for the study of transients in antennas. Transmission line theory and mechanisms apply to the modeling of a variety of antennas and to the detailed understanding of their performance.

The transient analysis is attacked by the Fourier transform approach to make use of established concepts such as that of impedance. Investigations are performed first in the frequency domain and then transformed into the time domain for inspection of transient results. The Fast Fourier Transform technique of truncating series of sinusoids provides some economy where numerical computations are needed for the transformations.

General transmission line equations are developed to account for time-dependent and position-dependent transmission line parameters. These equations are then specialized to accommodate the case under investigation which is that of an open-circuited transmission line loaded with series resistance. Several functional distributions of resistance along the transmission line are considered. For a resistive loading that varies linearly with position along the line, a closed form expression for the resulting current on the line is found in terms of Airy functions with complex arguments. For resistance distributions other than linear, the transmission line equation does

not in general possess a closed form functional solution. These problems are solved by a numerical analysis which is implemented digitally on a computer.

An examination is made of the control which the different resistance distributions exert over the transmission line's input impedance, current distribution, radiated transient waveform and received transient waveform. It is shown that an inverse functional form of resistance loading is optimum, based on criteria of maximizing current on the transmission line while minimizing reflections.

Discretely lumped resistance loadings as well as continuous resistance distributions are analyzed. Results of the discrete and continuous analyses are in excellent agreement when the discrete resistances are sufficiently close together.

The concept of a position-dependent characteristic impedance is developed for the resistively loaded transmission line. In addition to varying with position along the line, this quantity also differs in the forward and backward directions. Such characteristic impedances are formulated in general and for the several resistance loading functions that are treated in this dissertation.

An approximate step function voltage source is considered to energize the loaded transmission lines. The resulting current waveforms at positions along the line and the resulting transient radiated fields are computed. The different shapes of the transient waveforms that are radiated in different directions from the loaded transmission line are shown. The radiation patterns which change shape with time are also computed and shown. The maximum amplitude of radiation, over all time, is shown to be in an off-broadside direction that is consistent with a predominantly traveling wave. This occurs for the optimally loaded transmission line in which reflected waves are minimized.

Reception of transient signals by a resistively loaded transmission line is formulated in terms of the vector effective height function. Transient radiation coupling between different loaded transmission lines is also formulated

in this way.

The conical transmission line fields associated with a thin biconical antenna are used in an analysis of the transient behavior of this antenna. Determination of transient currents on the antenna takes account of internal complementary fields. Radiation of transient waveforms is analyzed. Transient reception is analyzed via the vector effective height function of the antenna.

ACKNOWLEDGEMENTS

Professor Chen-To Tai and Professor Ralph E. Hiatt have the eternal gratitude of the author for their guidance in this work. The National Science Foundation supported a portion of this research.

TABLE OF CONTENTS

	ACKNOWLEDGEMENTS	ii
	LIST OF TABLES	iv
	LIST OF ILLUSTRATIONS	v
	LIST OF APPENDICES	x
I	INTRODUCTION	1
II	RESISTIVELY LOADED TRANSMISSION LINES	4
	2.1 Transmission Line Equations	4
	2.2 Uniform Resistance Distribution	7
	2.3 Linear Resistance Distribution	8
	2.4 Nonlinear Resistance Distributions	11
	2.5 Transmission Line Currents	15
	2.6 Transmission Line Impedances	32
	2.7 Position-Dependent Characteristic Impedance	33
	2.8 Discrete Resistance Loading	45
	2.9 Excitation Voltage Source	72
	2.10 Transmission Line Waveforms	80
	2.11 Radiation from Transmission Lines	81
	2.12 Reception by Transmission Lines	90
	2.13 Transient Coupling of Transmission Lines	94
III	BICONICAL ANTENNA	95
	3.1 Antenna Considerations	95
	3.2 Antenna Fields	96
	3.3 Antenna Impedances	98
	3.4 Transient Currents and Voltages	99
	3.5 Radiation from Biconical Antenna	102
	3.6 Reception by Biconical Antenna	112
	3.7 Transient Coupling of Biconical Antennas	114
IV	CONCLUSIONS	116
V	RECOMMENDATIONS	118
	REFERENCES	119
	APPENDIX A	124
	APPENDIX B	137

LIST OF TABLES

Table		Page
2-1	Optimum Magnitude Coefficients For Various Continuous Resistance Distributions.	30
2-2	Preferential Order of Various Continuous Resistance Distributions.	31
2-3	Optimum Magnitude Coefficients for Various Discrete Resistance Distributions.	51
2-4	Preferential Order of Various Discrete Resistance Distributions.	64

LIST OF ILLUSTRATIONS

Figure		
2-1	Parameters of Balanced Two-Wire Transmission Line	6
2-2	Complex Propagation Factor γ For Uniform Resistance-Loaded Transmission Line	9
2-3	Normalized Resistance Distributions	16
2-4	Amplitude of Current Along Transmission Line Produced by Continuous Uniform Resistance Loading	17
2-5	Phase of Current Along Transmission Line Produced by Continuous Uniform Resistance Loading	18
2-6	Amplitude of Current Along Transmission Line Produced by Continuous Logarithmic Resistance Loading	19
2-7	Phase of Current Along Transmission Line Produced by Continuous Logarithmic Resistance Loading	20
2-8	Amplitude of Current Along Transmission Line Produced by Continuous Linear Resistance Loading	21
2-9	Phase of Current Along Transmission Line Produced by Continuous Linear Resistance Loading	22
2-10	Amplitude of Current Along Transmission Line Produced by Continuous Inverse Resistance Loading	23
2-11	Phase of Current Along Transmission Line Produced by Continuous Inverse Resistance Loading	24
2-12	Amplitude of Current Along Transmission Line Produced by Continuous Exponential Resistance Loading	25
2-13	Phase of Current Along Transmission Line Produced by Continuous Exponential Resistance Loading	26
2-14	Amplitude of Current Along Transmission Line Produced by Continuous Impulse Resistance Loading	27
2-15	Phase of Current Along Transmission Line Produced by Continuous Impulse Resistance Loading	28

2-16	Impedances Along Transmission Line With Uniform Continuous Resistance Loading $\frac{R(z)}{Z_0} = 3.6$.	34
2-17	Impedances Along Transmission Line With Logarithmic Continuous Resistance Loading $\frac{R(z)}{Z_0} = 8.3 \frac{\log(z+1)}{\log 1\frac{8}{9}}$.	35
2-18	Impedances Along Transmission Line With Linear Continuous Resistance Loading $\frac{R(z)}{Z_0} = 7.2 \frac{9z}{8}$.	36
2-19	Impedances Along Transmission Line With Inverse Continuous Resistance Loading $\frac{R(z)}{Z_0} = \frac{18}{8}(\frac{1}{1-z} - 1)$.	37
2-20	Impedances Along Transmission Line With Exponential Continuous Resistance Loading $\frac{R(z)}{Z_0} = 18\frac{38.4^z - 1}{38.4^{8/9} - 1}$.	38
2-22	Impedances Along Transmission Line With Impulse Continuous Resistance Loading $\frac{R(z)}{Z_0} = 1.4\delta(z-\frac{8}{9})$.	39
2-22	Input Reflection Coefficients Produced by Various Continuous Resistance Distributions.	40
2-23	Discrete Resistance Loaded Transmission Line Configuration.	46
2-24	Amplitude of Current Along Transmission Line Produced by Discrete Uniform Resistance Loading.	52
2-25	Phase of Current Along Transmission Line Produced by Discrete Uniform Resistance Loading.	53
2-26	Amplitude of Current Along Transmission Line Produced by Discrete Logarithmic Resistance Loading.	54
2-27	Phase of Current Along Transmission Line Produced by Discrete Logarithmic Resistance Loading.	55
2-28	Amplitude of Current Along Transmission Line Produced by Discrete Linear Resistance Loading.	56

2-29	Phase of Current Along Transmission Line Produced by Discrete Linear Resistance Loading.	57
2-30	Amplitude of Current Along Transmission Line Produced by Discrete Inverse Resistance Loading.	58
2-31	Phase of Current Along Transmission Line Produced by Discrete Inverse Resistance Loading.	59
2-32	Amplitude of Current Along Transmission Line Produced by Discrete Exponential Resistance Loading.	60
2-33	Phase of Current Along Transmission Line Produced by Discrete Exponential Resistance Loading.	61
2-34	Amplitude of Current Along Transmission Line Produced by Discrete Impulse Resistance Loading.	62
2-35	Phase of Current Along Transmission Line Produced by Discrete Impulse Resistance Loading.	63
2-36	Impedances Along Transmission Line With Uniform Discrete Resistance Loading $\frac{R_n}{Z_0} = 0.4$.	65
2-37	Impedances Along Transmission Line With Logarithmic Discrete Resistance Loading $\frac{R_n}{Z_0} = 8.3\frac{\log n}{9 \log 9}$.	66
2-38	Impedances Along Transmission Line With Linear Discrete Resistance Loading $\frac{R_n}{Z_0} = 7.2\frac{n-1}{72}$.	67
2-39	Impedances Along Transmission Line With Inverse Discrete Resistance Loading $\frac{R_n}{Z_0} = 18(\frac{1}{72})(\frac{9}{10-n}-1)$.	68
2-40	Impedances Along Transmission Line With Exponential Discrete Resistance Loading $\frac{R_n}{Z_0} = 18(\frac{1}{9})(\frac{1.5^{n-1}-1}{1.5^{8}-1})$.	69

2-41	Impedances Along Transmission Line With Impulse Discrete Resistance Loading $\frac{R_n}{Z_0} = 1.4\,\delta_n^9$.	70
2-42	Input Reflection Coefficients Produced by Various Discrete Resistance Distributions.	71
2-43	Square Wave Voltage Source Waveform.	74
2-44	Transmission Line With Source of Excitation in the Frequency Domain.	76
2-45	Input Impedance Versus Frequency for Optimum Resistance-Loaded Transmission Line.	77
2-46	Frequency Domain Amplitude and Phase of Source Voltage $V_s(\omega)$ and Input Current $I(0,\omega)$. $K = 50$.	78
2-47	Time Waveforms of Source Voltage $v_s(t)$ and Input Current $i(0,t)$. $K = 50$.	79
2-48	Time Waveform of Current $i(\frac{h}{2},t)$ at Center of Transmission Line.	81
2-49	Coordinates for Describing Radiation From Transmission Line.	82
2-50	Transient Time Waveforms Radiated in Various θ Directions From Step-Excited Transmission Line With Optimum Resistance Loading.	87
2-51	Maximum Amplitude of Radiated Transient Waveform as a Function of Radiation Direction.	89
2-52	Time Sequence of Radiation Patterns for Optimally Loaded Transmission Line Excited by Approximate Step Voltage.	91
2-53	Transient Time Waveforms Radiated in Various Broadside Directions From Step-Excited Transmission Line With Optimum Resistance Loading.	92
3-1	Biconical Antenna	95
3-2	Frequency Domain Input Current of Biconical Antenna. $K = 50$.	100

3-3	Time Waveforms of Source Voltage $v_s(t)$ and Input Current $i(0,t)$ of Biconical Antenna.	101
3-4	Transient Waveforms Radiated in Various θ Directions From Step-Excited Biconical Antenna.	106
3-5	Idealized Step Function Current Waves Traveling on Arms of Antenna.	107
3-6	Component Idealization of Transient Waveform Radiated in $\theta = \frac{\pi}{10}$ Direction.	109
3-7	Component Idealization of Transient Waveform Radiated in $\theta = \frac{\pi}{4}$ Direction.	110
3-8	Component Idealization of Transient Waveform Radiated in $\theta = \frac{\pi}{2}$ Direction.	111
3-9	Biconical Antenna in Reception.	113

LIST OF APPENDICES

APPENDIX A:	Computation of Current on Resistively Loaded Transmission Lines	124
APPENDIX B:	Computation of Transient Radiation Field of Resistively Loaded Transmission Line	137

Chapter I
INTRODUCTION

The research undertaken in this dissertation is intended to add to the knowledge about transmission, radiation and reception of transient electromagnetic signals by basic types of wave guiding and launching structures. Transmission lines are emphasized due to their direct applicability to the understanding and physical modeling of transient waves on basic types of antennas. Dipoles, loops, spirals, helices, surface wave antennas and various endfire antennas are included among the types that employ transmission line concepts in their transient analyses.

Prior work on the subject of transient phenomena associated with transmission lines has concentrated on lines which have a uniform resistance loading[1,2,3,....,18]. Even in the uniform resistance case, solutions have been primarily in the form of small loss approximations or for the distortionless constraint $\frac{R}{L} = \frac{G}{C}$ on the usual transmission line parameters. The present study gives exact closed form analytic solutions for uniform series resistance loading of any magnitude and for resistance loading which varies linearly with distance along the transmission line. For nonlinear distributions of resistance, numerical solution of the general transmission line equation is possible.

In the past several years, some attention has been given to the related problem of resistively loaded linear antennas[19, 20, 21,....,33]. To date, the number of different resistance distributions which has been reported is small. The present study, which includes several nonlinear functional distributions of resistance along transmission lines, may be useful in providing a model and representative data for the linear antenna problem. In particular, the results of the present transmission line investigation may be applicable to the optimization of resistance loading functions to produce a desired transient antenna current and thereby a desired radiated or received transient waveform. The adequacy of modeling a linear antenna by a transmission line should be

improved by the presence of resistive loading in both. This is due to the reduction in the influence of terminal end effects by the attenuation of waves on the structures.

A thin biconical antenna can be treated from a conical transmission line point of view and also can be considered as an approximation to a linear antenna. Prior work on the biconical antenna has been extensive[34,35,....,48] although concentrated in the frequency domain. A transient analysis of biconical antennas has been conducted[49] but only for wide angle antennas. A wide angle biconical antenna is not amenable to accurate field matching as is a thin biconical antenna. Published analyses have suffered from not including interior complementary modes in matching fields at the hypothetical spherical surface which bounds the antenna. This caused some uncertainties in the determination of an effective terminating admittance which in turn was responsible for uncertainties in the antenna current and thereby in the radiated field. This also led to limitations in the antenna effective height function which describes the antenna's receiving properties. By dealing with a biconical antenna of small cone angle, the present dissertation is able to use an exact closed expression for the terminating admittance and the quantities that it effects.

The present investigation has been stimulated by current interest in electromagnetic pulse problems. The electromagnetic pulse radiated from a thermonuclear explosion can produce harmful transient field intensities or undesirable transient signals in structures or equipment upon which the radiation is incident. Antennas which radiate transient signals of the same shape as this electromagnetic pulse are needed for performing tests on the vulnerability of equipment and the effectiveness of shields. Resistively loaded antennas, of basic types which may be modeled as resistively loaded transmission lines, are expected to be used for radiating simulated electromagnetic pulses. The pulse shape can be controlled by selection of appropriate resistance loading functions.

The formulation techniques employed in this dissertation include the dyadic Green's function formulation[50] of radiated field in terms of surface

current density. Another is the vector effective height function[59] which is used to express the receiving and radiation coupling properties of the transmission lines and biconical antennas. These techniques afford a measure of generality and conciseness to the treatment. Fast Fourier Transform techniques are used for economy in transforming quantities between the time and frequency domains.

Chapter II

RESISTIVELY LOADED TRANSMISSION LINES

2.1 Transmission Line Equations

The differential equations relating voltage v and current i on a transmission line whose parameters R, G, L, C are position-dependent and time-dependent are

$$\frac{\partial v(z,t)}{\partial z} = - R(z,t)\, i(z,t) - L(z,t) \frac{\partial i(z,t)}{\partial t} \quad , \tag{2.1}$$

$$\frac{\partial i(z,t)}{\partial z} = - G(z,t)\, v(z,t) - C(z,t) \frac{\partial v(z,t)}{\partial t} \quad , \tag{2.2}$$

where z = the linear dimension along the transmission line,

t = time,

$R(z,t)$ = series resistance per unit length,

$G(z,t)$ = shunt conductance per unit length,

$L(z,t)$ = series inductance per unit length,

$C(z,t)$ = shunt capacitance per unit length.

Performing the operations

$$\frac{\partial (2.1)}{\partial z} \bigcap (2.2) \bigcap \frac{\partial (2.2)}{\partial t} \, ,$$

$$\frac{\partial (2.2)}{\partial z} \bigcap (2.1) \bigcap \frac{\partial (2.1)}{\partial t} \, ,$$

yields the transmission line equations

$$\frac{\partial^2 v(z,t)}{\partial z^2} = L(z,t)\, C(z,t) \frac{\partial^2 v(z,t)}{\partial t^2}$$

$$+ \left[R(z,t)\, C(z,t) + G(z,t)\, L(z,t) + L(z,t) \frac{\partial C(z,t)}{\partial t} \right] \frac{\partial v(z,t)}{\partial t}$$

$$+ \left[R(z,t)\, G(z,t) + L(z,t) \frac{\partial G(z,t)}{\partial t} \right] v(z,t)$$

$$- \frac{\partial R(z,t)}{\partial z} i(z,t) - \frac{\partial L(z,t)}{\partial z} \frac{\partial i(z,t)}{\partial t} , \qquad (2.3)$$

$$\frac{\partial^2 i(z,t)}{\partial z^2} = L(z,t)\, C(z,t) \frac{\partial^2 i(z,t)}{\partial t^2}$$

$$+ \left[R(z,t)\, C(z,t) + G(z,t)\, L(z,t) + C(z,t) \frac{\partial L(z,t)}{\partial t} \right] \frac{\partial i(z,t)}{\partial t}$$

$$+ \left[R(z,t)\, G(z,t) + C(z,t) \frac{\partial R(z,t)}{\partial t} \right] i(z,t)$$

$$- \frac{\partial G(z,t)}{\partial z} v(z,t) - \frac{\partial C(z,t)}{\partial z} \frac{\partial v(z,t)}{\partial t} . \qquad (2.4)$$

A special case of these general transmission line equations which is used in the present research embodies only constant inductance per unit length L and capacitance per unit length C as well as a resistance per unit length R (z) which varies with position along the line but is time-invariant. The arrangement of a balanced two-wire transmission line is sketched in Fig. 2-1. Under these special conditions, the transmission line equations reduce to

$$\frac{\partial^2 v(z,t)}{\partial z^2} = LC \frac{\partial^2 v(z,t)}{\partial t^2} + R(z)\, C \frac{\partial v(z,t)}{\partial t} - \frac{dR(z)}{dz} i(z,t) , \qquad (2.5)$$

$$\frac{\partial^2 i(z,t)}{\partial z^2} = LC \frac{\partial^2 i(z,t)}{\partial t^2} + R(z)\, C \frac{\partial i(z,t)}{\partial t} . \qquad (2.6)$$

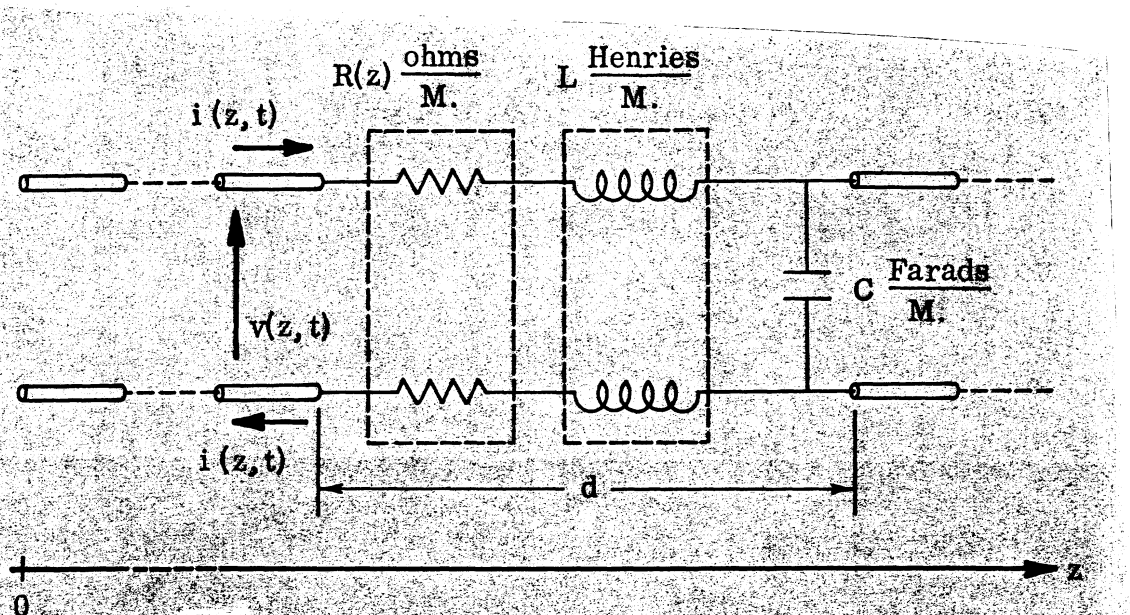

FIG. 2-1: PARAMETERS OF BALANCED TWO-WIRE TRANSMISSION LINE.

Both v and i appear in the first of these transmission line equations, making it less convenient to use than the second equation. Due to the absence of non-uniform shunt conductance or capacitance in the transmission line considered here, the second transmission line equation contains only i. An additional advantage to the second equation is that its solution directly gives i which will be used in determining the radiation field of the transmission line by the dyadic Green's function formulation[50].

A boundary condition to be imposed on on (2.6) is

$$i(h, t) = 0, \tag{2.7}$$

where h is the length of the transmission line. This condition at the terminal end of the line z = h describes an open-circuited transmission line which is chosen for study because of its applicability to the modeling of a linear antenna.

The Fourier transform method is applied to the problem of solving (2.5) and (2.6) for the transient voltage and current. With an $e^{j\omega t}$ dependence (2.5) and (2.6) are transformed to

$$\frac{\partial^2 V(z,\omega)}{\partial z^2} = \left[k_0^2 - j\, R(z)\, C\right] V(z,\omega) - \frac{dR(z)}{dz} I(z,\omega), \tag{2.8}$$

$$\frac{\partial^2 I(z,\omega)}{\partial z^2} = \left[k_0^2 - j\, R(z)\, C\right] I(z,\omega)\ , \tag{2.9}$$

where ω = the Fourier transform radian frequency variable,

$k_0 = \omega\sqrt{L\,C}$,

V = voltage in the frequency domain,

I = current in the frequency domain.

The boundary condition is

$$I(h, \omega) = 0\ . \tag{2.10}$$

Solution of the differential equation (2.9) for the transmission line current $I(z,\omega)$ will be examined for various resistance distributions R (z).

2.2 Uniform Resistance Distribution

The transmission line equatinn (2.9) subject to (2.10) has a conventional exponential form of solution for the current $I(z,\omega)$ in the case where R is constant, that is, where the resistance loading is uniformly distributed along the line.

$$I(z,\omega) = \frac{I(0,\omega)}{1 - \Gamma(\omega)}\left[e^{-\gamma(\omega)z} - \Gamma(\omega)\, e^{\gamma(\omega)z}\right], \tag{2.11}$$

where $$\gamma(\omega) = \left[\sin\left(\frac{\arctan\frac{R}{\omega L}}{2}\right) + j\cos\left(\frac{\arctan\frac{R}{\omega L}}{2}\right)\right]\left[1+\left(\frac{R}{\omega L}\right)^2\right]^{1/4} k_0$$

is a complex propagation factor separated into real and imaginary parts for convenient reference,

$\Gamma(\omega) = e^{-j2\left(1-j\frac{R}{\omega L}\right)^{1/2} k_0 h}$ is a complex reflection coefficient.

For $R << \omega L$, $\gamma(\omega)$ is approximately $j k_0$ the propagation factor of a lossless transmission line, For $R >> \omega L$, $\gamma(\omega)$ is approximately $\left(\frac{\omega RC}{2}\right)^{1/2}(1+j)$ which is recognized as the propagation factor of a very lossy transmission line. Figure 2-2 shows the transition of $\gamma(\omega)$ between the low loss and high loss cases. More interesting results are obtained from non-uniform resistance loading distributions.

2.3 Linear Resistance Distribution

A type of resistance distribution $R(z)$ for which the transmission line equation (2.9) possesses a solution in closed functional form is a function which varies linearly along the line:

$$R(z) = R_0 + r_1 z, \tag{2.12}$$

where R_0 and r_1 are real coefficients whose units are, respectively, $\frac{\text{resistance}}{\text{length}}$ and $\frac{\text{resistance}}{(\text{length})^2}$.

The key step in solving (2.9) for $I(z,\omega)$ with this resistance distribution is the introduction of the variable

$$\zeta(z,\omega) = \left(\frac{j\omega C}{r_1}\right)^{1/3}(R_0 + r_1 z + j\omega L), \tag{2.13}$$

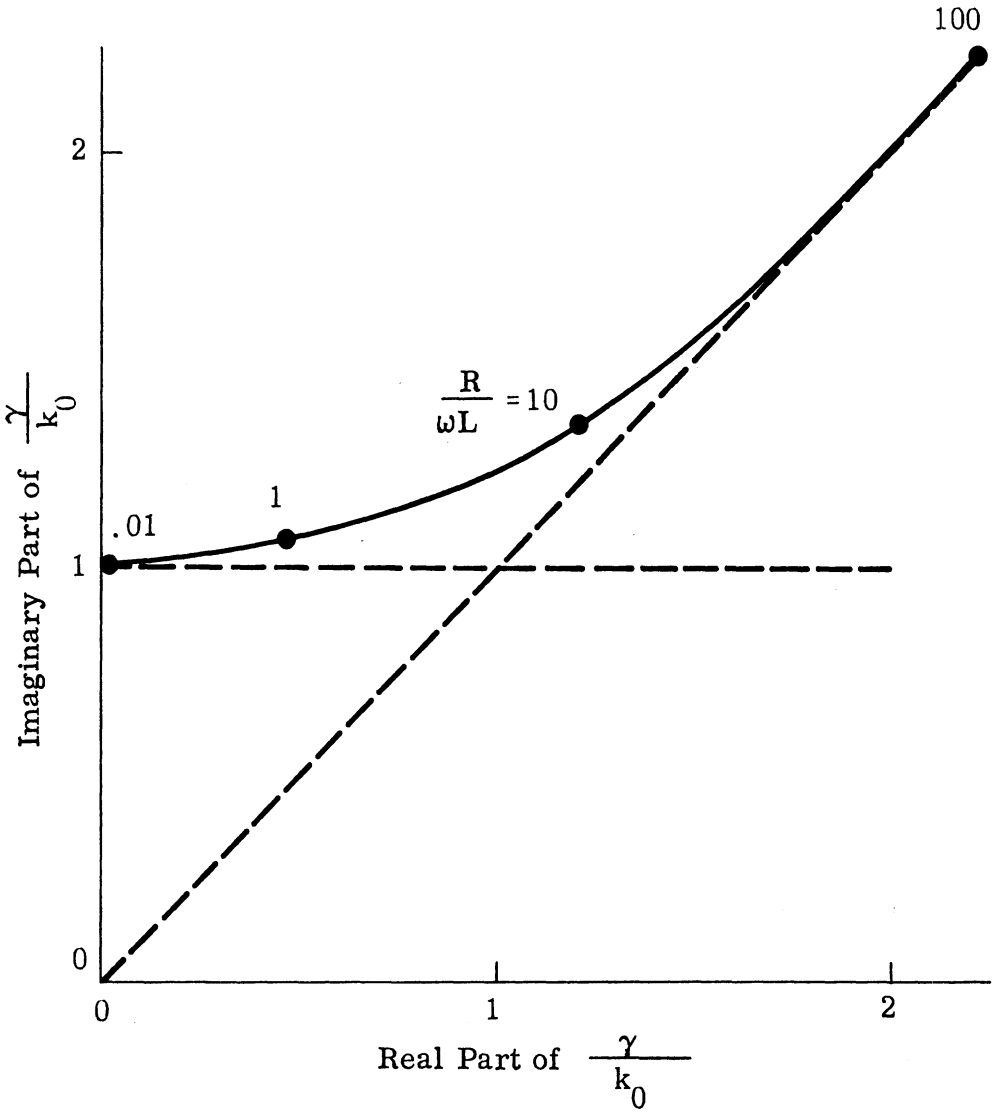

FIG. 2-2: COMPLEX PROPAGATION FACTOR γ FOR UNIFORM RESISTANCE-LOADED TRANSMISSION LINE.

which reduces (2.9) to the standard form of Stokes' differential equation, namely,

$$\frac{d^2 I(\zeta)}{d\zeta^2} = \zeta I(\zeta) \quad . \tag{2.14}$$

The solution of (2.14) may be expressed in terms of Airy functions with complex arguments[51] as

$$I(\zeta) = a\, A\, i(\zeta) + b\, B\, i(\zeta) \quad . \tag{2.15}$$

The coefficients a and b are determined by the boundary conditions imposed on the current at the terminals of the transmission line.

$$a = \frac{I\left[\zeta\ (0,\omega)\right]}{A\ i\ \left[\zeta\ (0,\omega)\right] - B\ i\ \left[\zeta\ (0,\omega)\right] \frac{A\ i\ \left[\zeta\ (h,\omega)\right]}{B\ i\ \left[\zeta\ (h,\omega)\right]}} \quad , \tag{2.16}$$

$$b = \frac{I\left[\zeta\ (0,\omega)\right]}{B\ i\ \left[\zeta\ (0,\omega)\right] - A\ i\ \left[\zeta\ (0,\omega)\right] \frac{B\ i\ \left[\zeta\ (h,\omega)\right]}{A\ i\left[\zeta\ (h,\omega)\right]}} \quad . \tag{2.17}$$

Calculation of the current $I(z,\omega)$ thus requires only stipulation of the transmission line parameters R_0, r_1, L, C and access to a table of Airy functions of complex argument[52]. Alternatives to the use of the tabulated functions are numerical computations of the Airy functions from their integral representations[53].

$$A\ i(\zeta) = \frac{(3c)^{1/3}}{\pi} \int_0^\infty \cos\left[c\,u^3 + (3c)^{1/3}\,\zeta\,u\right]\, du\,, \tag{2.18}$$

$$B\ i(\zeta) = \frac{(3c)^{1/3}}{\pi} \int_0^\infty \left\{ e^{-cu^3 + (3c)^{1/3}\zeta u} + \sin\left[cu^3 + (3c)^{1/3}\zeta u\right] \right\} du\,, \tag{2.19}$$

or from their relation to Bessel functions of fractional order [53]

$$A\,i(\zeta) = \frac{\zeta^{1/2}}{3}\left[I_{-1/3}\left(\frac{2}{3}\zeta^{3/2}\right) - I_{1/3}\left(\frac{2}{3}\zeta^{3/2}\right)\right], \tag{2.20}$$

$$B\,i(\zeta) = \left(\frac{\zeta}{3}\right)^{1/2}\left[I_{-1/3}\left(\frac{2}{3}\zeta^{3/2}\right) + I_{1/3}\left(\frac{2}{3}\zeta^{3/2}\right)\right], \tag{2.21}$$

or from an ascending series [53]

$$A\,i(\zeta) = \sum_{n=0}^{\infty} 3^n \frac{\zeta^{3n}}{(3n)!}\left[A\,i(0)\left(\frac{1}{3}\right)_n + A\,i'(0)\left(\frac{2}{3}\right)_n \frac{\zeta}{3n+1}\right], \tag{2.22}$$

$$B\,i(\zeta) = \sum_{n=0}^{\infty} 3^n \frac{\zeta^{3n}}{(3n)!}\left[B\,i(0)\left(\frac{1}{3}\right)_n - Bi'(0)\left(\frac{2}{3}\right)_n \frac{\zeta}{3n+1}\right], \tag{2.23}$$

where c is an arbitrary constant,

$$\left(c+\frac{1}{3}\right)_0 = 1,$$

$$\left(c+\frac{1}{3}\right)_n = \frac{1}{3^n}(3c+1)(3c+4)\text{-----}(3c+3n-2),$$

and the primes denote differentiation.

2.4 Nonlinear Resistance Distributions

Except for the uniform and linear resistance distributions, the transmission line equation (2.9) does not in general possess a closed form functional solution for the current $I(z,\omega)$. A numerical solution is required when the resistance distribution function $R(z)$ is a nonlinear form. To make the problem amenable to numerical solution, the second order differential equation with a variable complex coefficient (2.9) is reduced to a set of four

simultaneous first order equations with real coefficients by the substitutions

$$I(z,\omega) = I_1(z,\omega) + j\, I_2(z,\omega),$$

$$I_3(z,\omega) = \frac{\partial I_1(z,\omega)}{\partial z},$$

$$I_4(z,\omega) = \frac{\partial I_2(z,\omega)}{\partial z} \quad .$$

The resulting set of equations in matrix notation is

$$\bar{I}'(z,\omega) = \bar{\bar{A}}(z,\omega)\, \bar{I}(z,\omega) \tag{2.24}$$

where $\bar{I}'(z,\omega) = \begin{bmatrix} \frac{\partial I_1(z,\omega)}{\partial z} \\ \frac{\partial I_2(z,\omega)}{\partial z} \\ \frac{\partial I_3(z,\omega)}{\partial z} \\ \frac{\partial I_4(z,\omega)}{\partial z} \end{bmatrix}$, $\bar{I}(z,\omega) = \begin{bmatrix} I_1(z,\omega) \\ I_2(z,\omega) \\ I_3(z,\omega) \\ I_4(z,\omega) \end{bmatrix}$,

$$\bar{\bar{A}}(z,\omega) = \begin{bmatrix} 0 & 0 & 1 & 0 \\ 0 & 0 & 0 & 1 \\ -k_0^2 & -\omega CR(z) & 0 & 0 \\ \omega CR(z) & -k_0^2 & 0 & 0 \end{bmatrix} .$$

The boundary conditions become

$$\bar{\bar{B}}\, \bar{I}(0,\omega) + \bar{\bar{C}}\, \bar{I}(h,\omega) = \bar{R} \tag{2.25}$$

where $\overline{\overline{B}} = \begin{bmatrix} 1 & 0 & 0 & 0 \\ 0 & 1 & 0 & 0 \\ 0 & 0 & 0 & 0 \\ 0 & 0 & 0 & 0 \end{bmatrix}$,

$\overline{\overline{C}} = \begin{bmatrix} 0 & 0 & 0 & 0 \\ 0 & 0 & 0 & 0 \\ 1 & 0 & 0 & 0 \\ 0 & 1 & 0 & 0 \end{bmatrix}$,

$\overline{R} = \begin{bmatrix} I(0,\omega) \\ 0 \\ 0 \\ 0 \end{bmatrix}$.

This reduced problem can be solved numerically even when the resistance distribution R (z) has a general functional form or is specified by quantized data.

In the numerical solution, the current amplitude $|I(z)|$ and phase $\psi(z)$ are sampled at discrete values of z. Values of z which are separated by increments d that are no larger than $\frac{1}{32}$ of a free space wavelength λ_0 are used to produce accurate solutions with reasonable computational economy. For computational economy, the current is sampled at equidistant intervals at each frequency. For each frequency in the input waveform spectrum, the computer program provides a different increment

$$d = \frac{h}{N-1} , \tag{2.26}$$

such that

$$N - 1 = \ell.\ i.\ g.\ t.\left(\frac{32\,h}{\lambda_0}\right) , \tag{2.27}$$

where h = the transmission line length,

N = the number of sampling positions.

The integer index n in the range $1 \leq n \leq N$ identifies the location along the transmission line's linear dimension where $0 \leq z \leq h$. Thus,

$$I(nd-d,\omega) = \left|I_n(\omega)\right| e^{j\psi_n(\omega)} . \tag{2.28}$$

A subroutine of the computer program makes an additional provision of multiply subdividing d in regions where the current varies rapidly so that the accuracy to which the current is computed is everywhere better than a selectable parameter which is set at 1 percent for computations that are performed here. Other parameters that are readily variable in the computer program are : a description of the Fourier frequency spectrum of the source waveform, h, $R(z)$ and the characteristic impedance Z_0 of the associated unloaded transmission line.

Without loss of generality, the input boundary condition is normalized to

$$I(0,\omega) = 1 + j\,0 \tag{2.29}$$

in the program. This is done for convenience to allow the computed and stored complex $I(z,\omega)$ to be weighted subsequently by the complex Fourier coefficients of various input current waveforms.

The computer program employs the numerical method of adjoint equations which generates, successively, adjoint initial value problems from the given set of boundary value problems. Solutions to the resulting simultaneous initial value problems are then obtained by Gauss elimination and Hamming's predictor-corrector method. The program provides for the computation and storage in a file of $I(z,\omega)$ and $\frac{\partial I(z,\omega)}{\partial z}$. In addition, these data are provided on computer printed output in tabular and graphical forms. A detailed listing of the program appears in Appendix A.

2.5 Transmission Line Currents

Markedly different current distributions $I(z,\omega)$ are produced by the uniform, linear and nonlinear resistance loading functions $R(z)$. To illustrate, the program of Appendix A has computed the monochromatic complex current distributions along transmission lines which are loaded by the following resistance distributions:

UNIFORM $$\frac{R(z)}{Z_0} = C_0 \ , \tag{2.30a}$$

LOGARITHMIC $$\frac{R(z)}{Z_0} = C_0 \frac{\log (z+1)}{\log 1\frac{8}{9}} \ , \tag{2.30b}$$

LINEAR $$\frac{R(z)}{Z_0} = C_0 \frac{9\,z}{8} \ , \tag{2.30c}$$

INVERSE $$\frac{R(z)}{Z_0} = C_0 \frac{1}{8} \left(\frac{1}{1-z} - 1\right) \ , \tag{2.30d}$$

EXPONENTIAL $$\frac{R(z)}{Z_0} = C_0 \frac{b^z - 1}{b^{8/9} - 1} \ , \tag{2.30e}$$

IMPULSE $$\frac{R(z)}{Z_0} = C_0 \, \delta\left(z - \frac{8}{9}\right) \ , \tag{2.30f}$$

where $\delta\left(z - \frac{8}{9}\right)$ is the Dirac delta function and b is an exponential base which may be varied as a parameter. C_0 is a parameter which establishes the magnitude of the resistance distribution. The resistance distributions are normalized to $Z_0 = \sqrt{\frac{L}{C}}$, the characteristic impedance of a transmission line without loading. The above resistance loading functions are adjusted such that they all equal zero at $Z = 0$ and rise monotonically to the value C_0, at a distance of 1 free-space wavelength from the source end of the line. In these examples, the free-space wavelength is $\frac{8}{9}$ meter and the transmission line length is 1 meter. These resistance distributions are graphed in Fig. 2-3.

Figures 2-4 through 2-15 are plots of the amplitudes $|I|$ and phases ψ of the currents as functions of position along transmission lines which are loaded

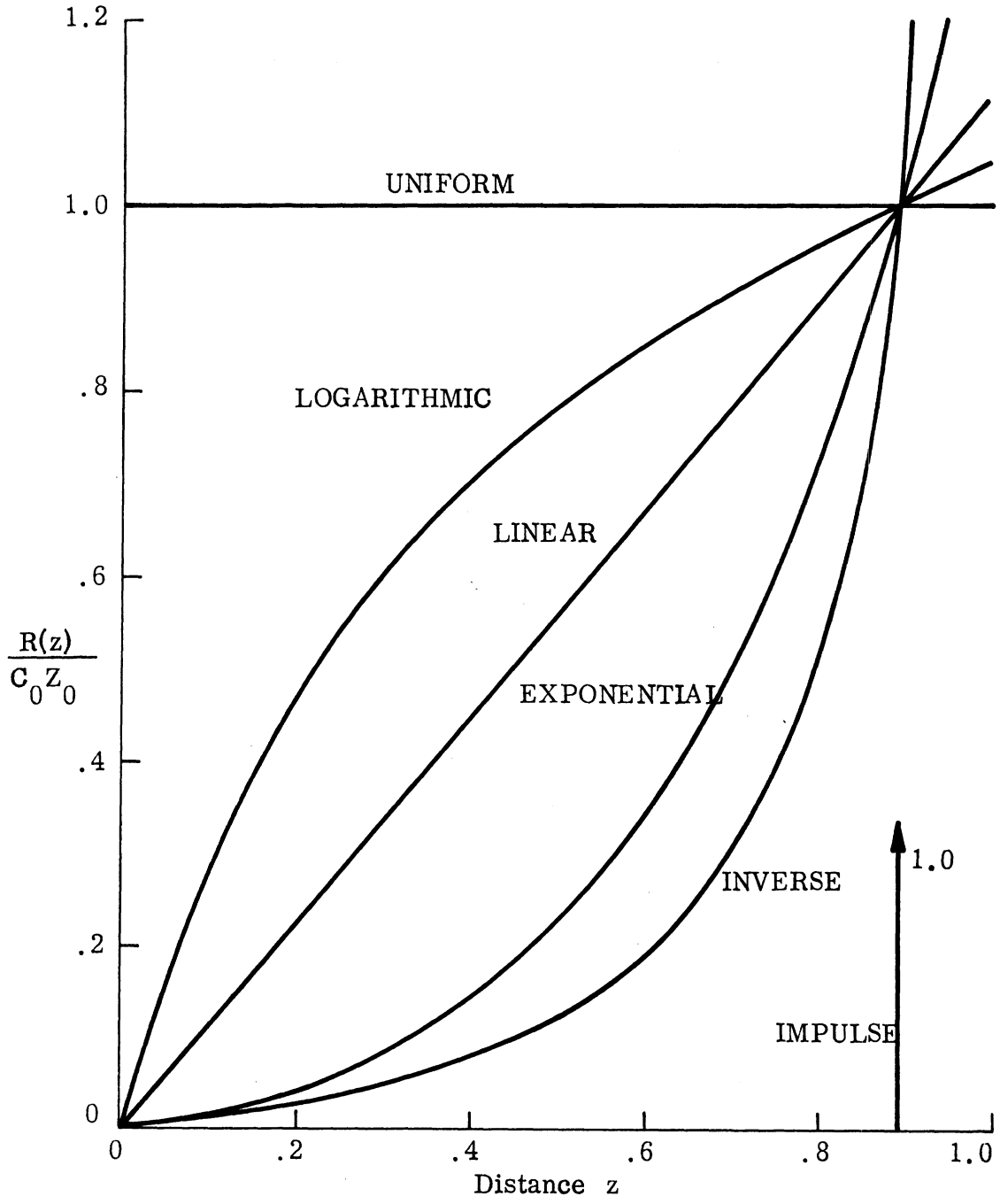

FIG. 2-3: NORMALIZED RESISTANCE DISTRIBUTIONS.

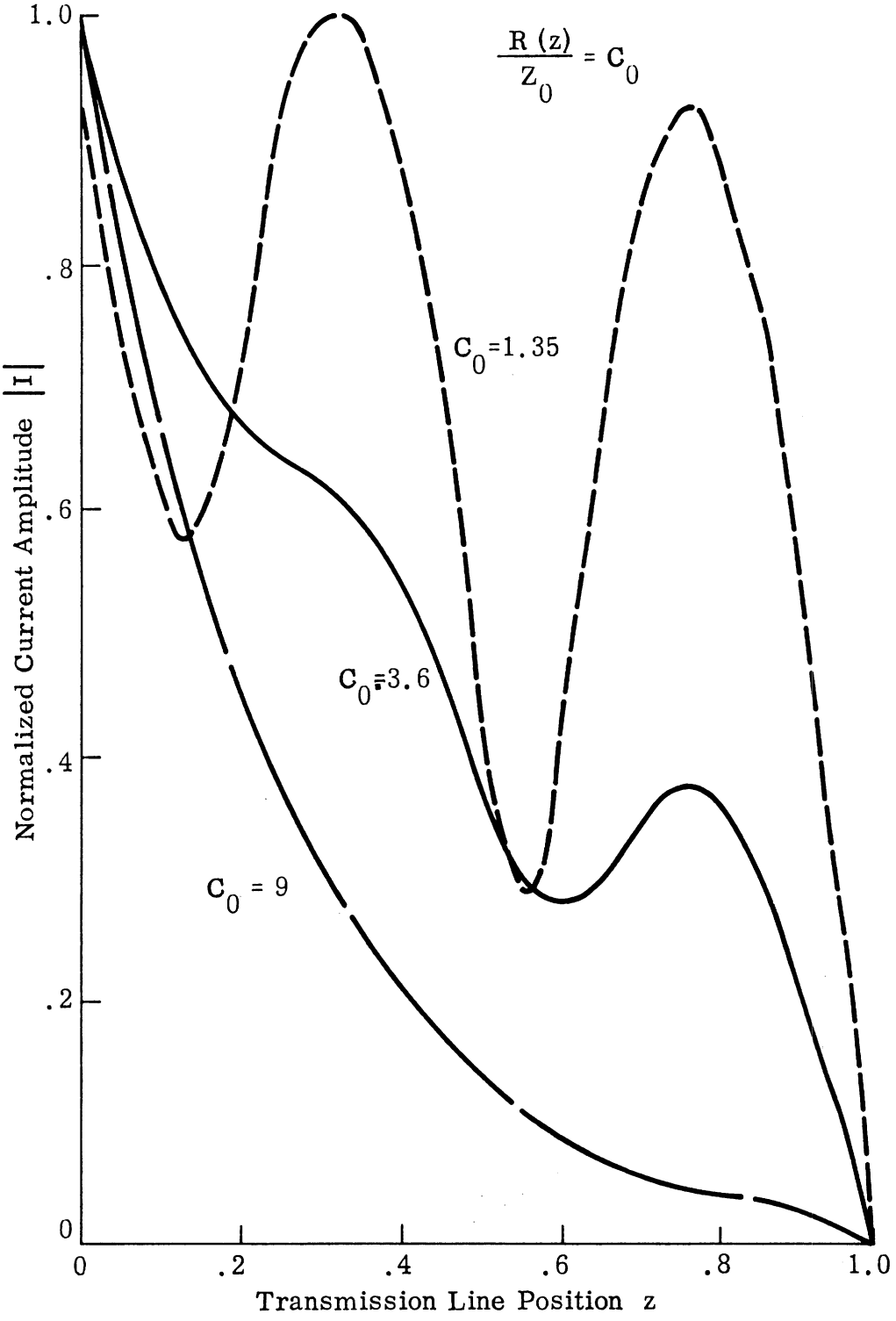

FIG. 2-4: AMPLITUDE OF CURRENT ALONG TRANSMISSION LINE PRODUCED BY CONTINUOUS UNIFORM RESISTANCE LOADING.

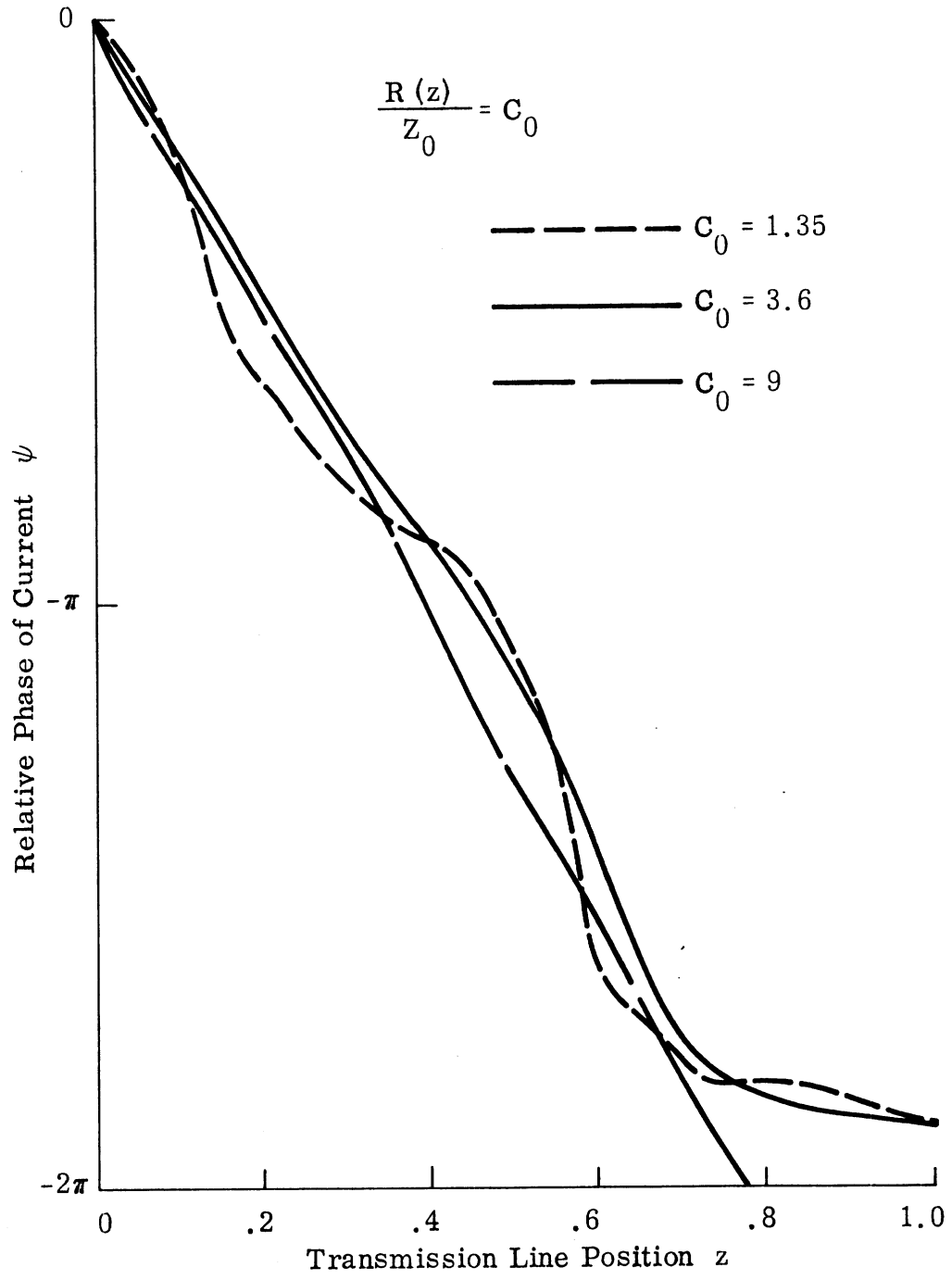

FIG. 2-5: PHASE OF CURRENT ALONG TRANSMISSION LINE PRODUCED BY CONTINUOUS UNIFORM RESISTANCE LOADING.

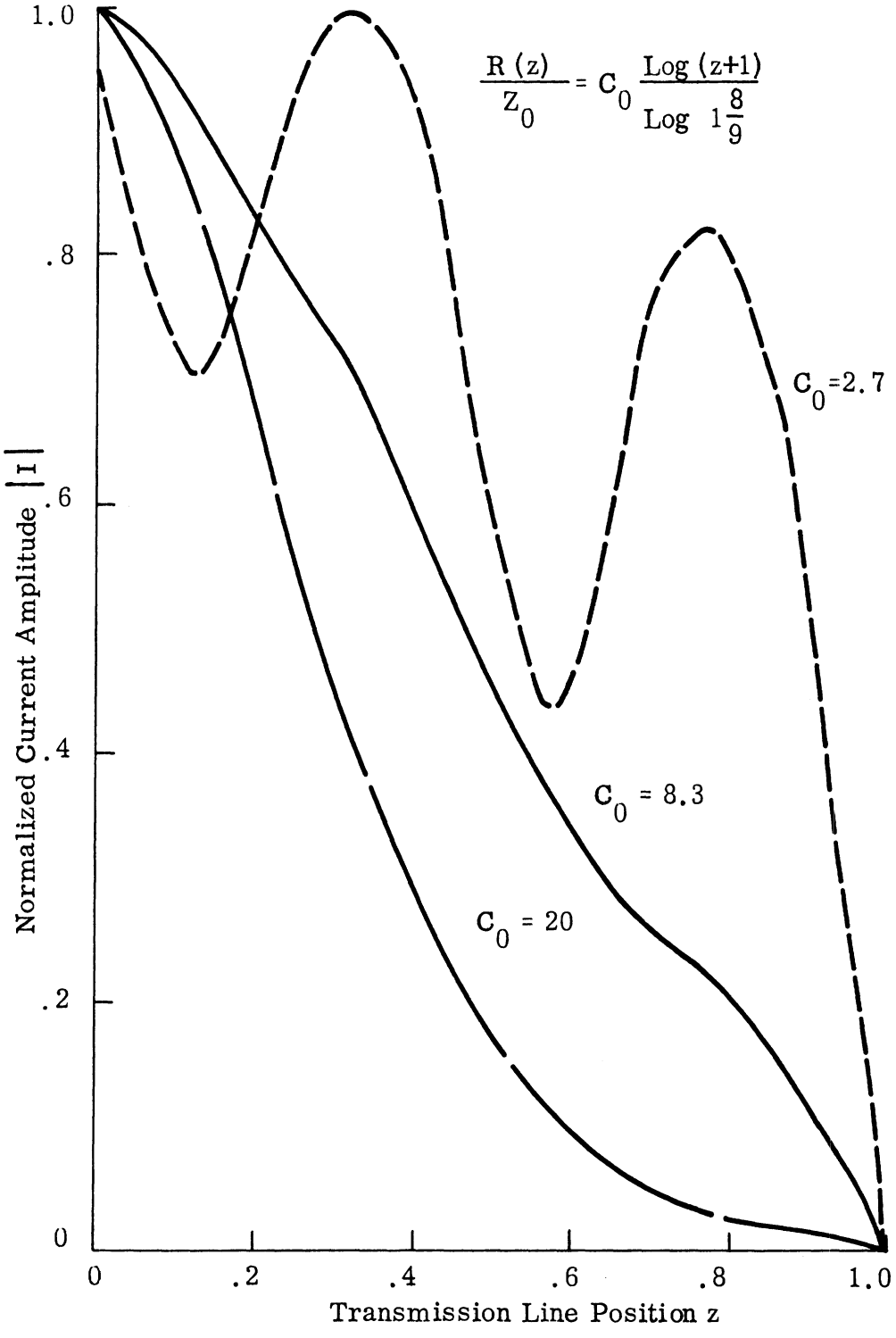

FIG. 2-6: AMPLITUDE OF CURRENT ALONG TRANSMISSION LINE PRODUCED BY CONTINUOUS LOGARITHMIC RESISTANCE LOADING.

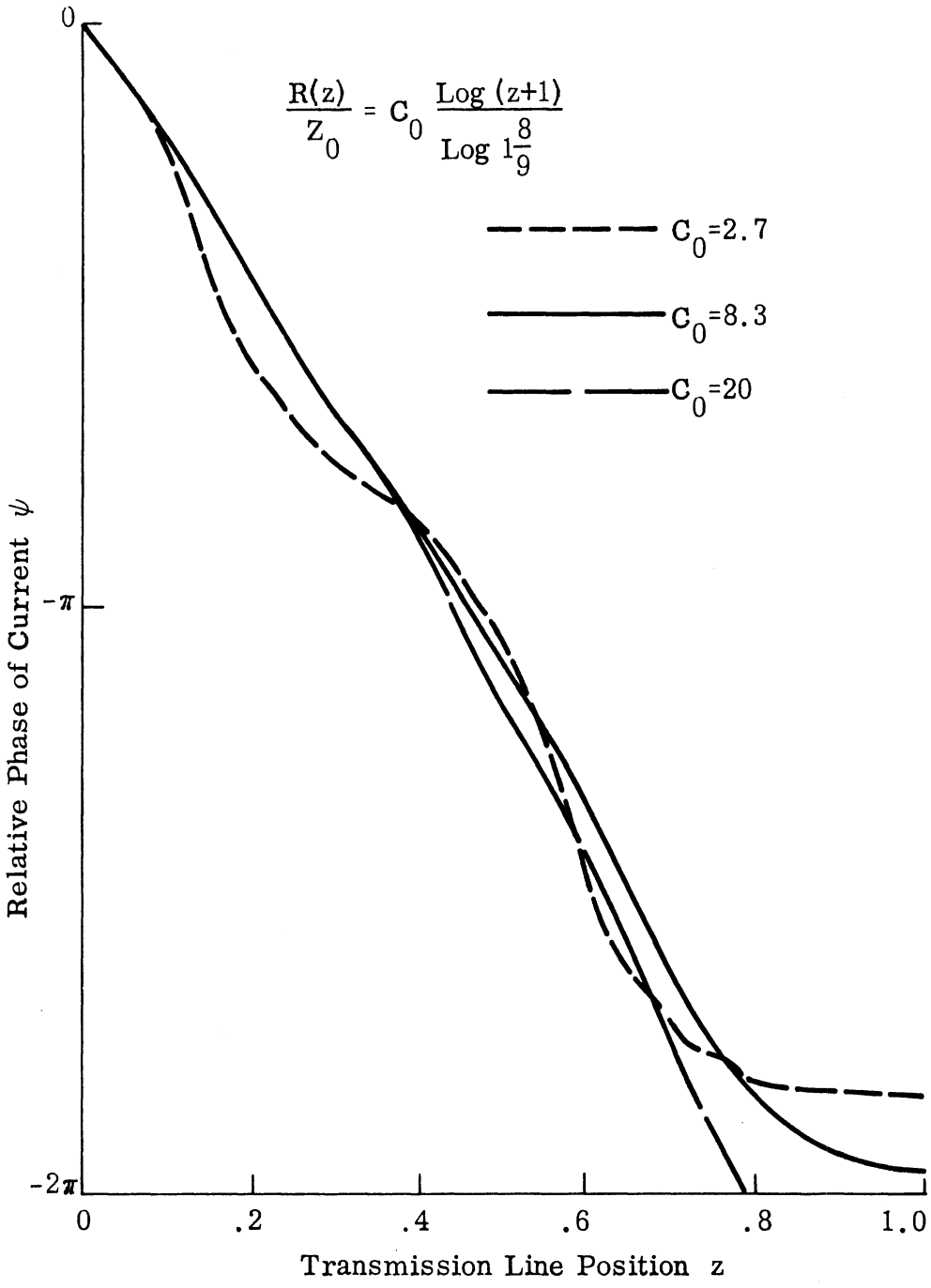

FIG. 2-7: PHASE OF CURRENT ALONG TRANSMISSION LINE PRODUCED BY CONTINUOUS LOGARITHMIC RESISTANCE LOADING.

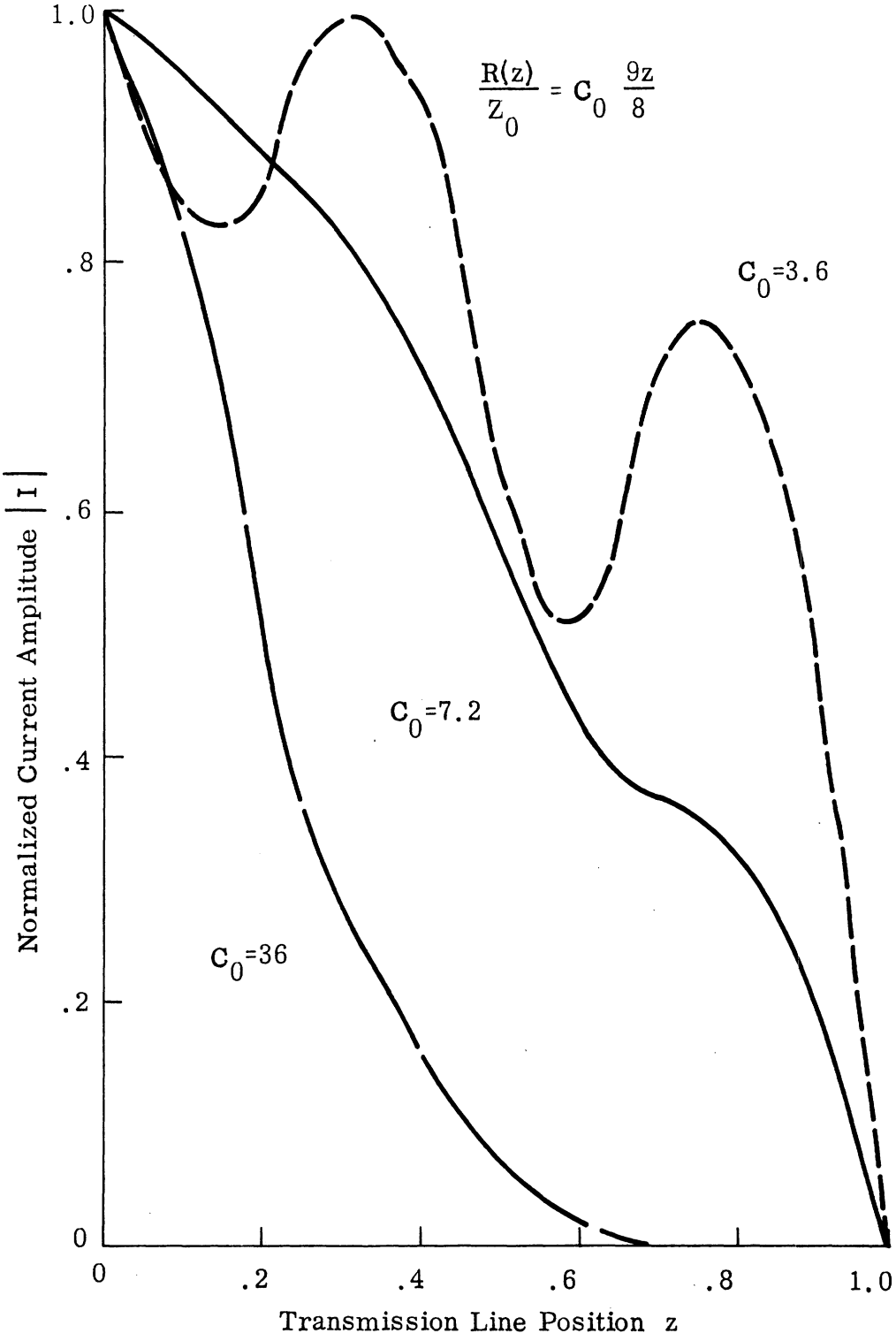

FIG. 2-8: AMPLITUDE OF CURRENT ALONG TRANSMISSION LINE PRODUCED BY CONTINUOUS LINEAR RESISTANCE LOADING.

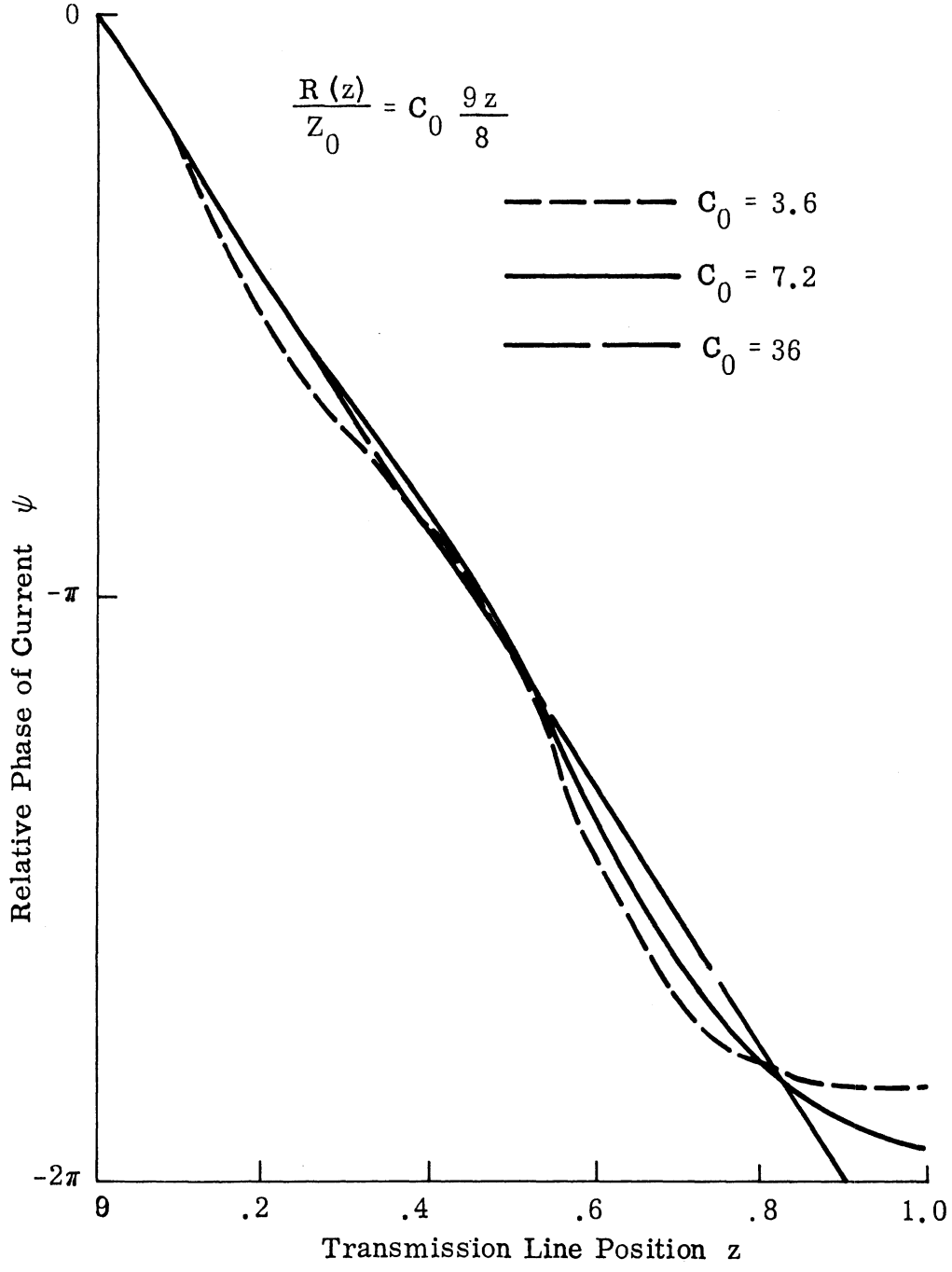

FIG. 2-9: PHASE OF CURRENT ALONG TRANSMISSION LINE PRODUCED BY CONTINUOUS LINEAR RESISTANCE LOADING.

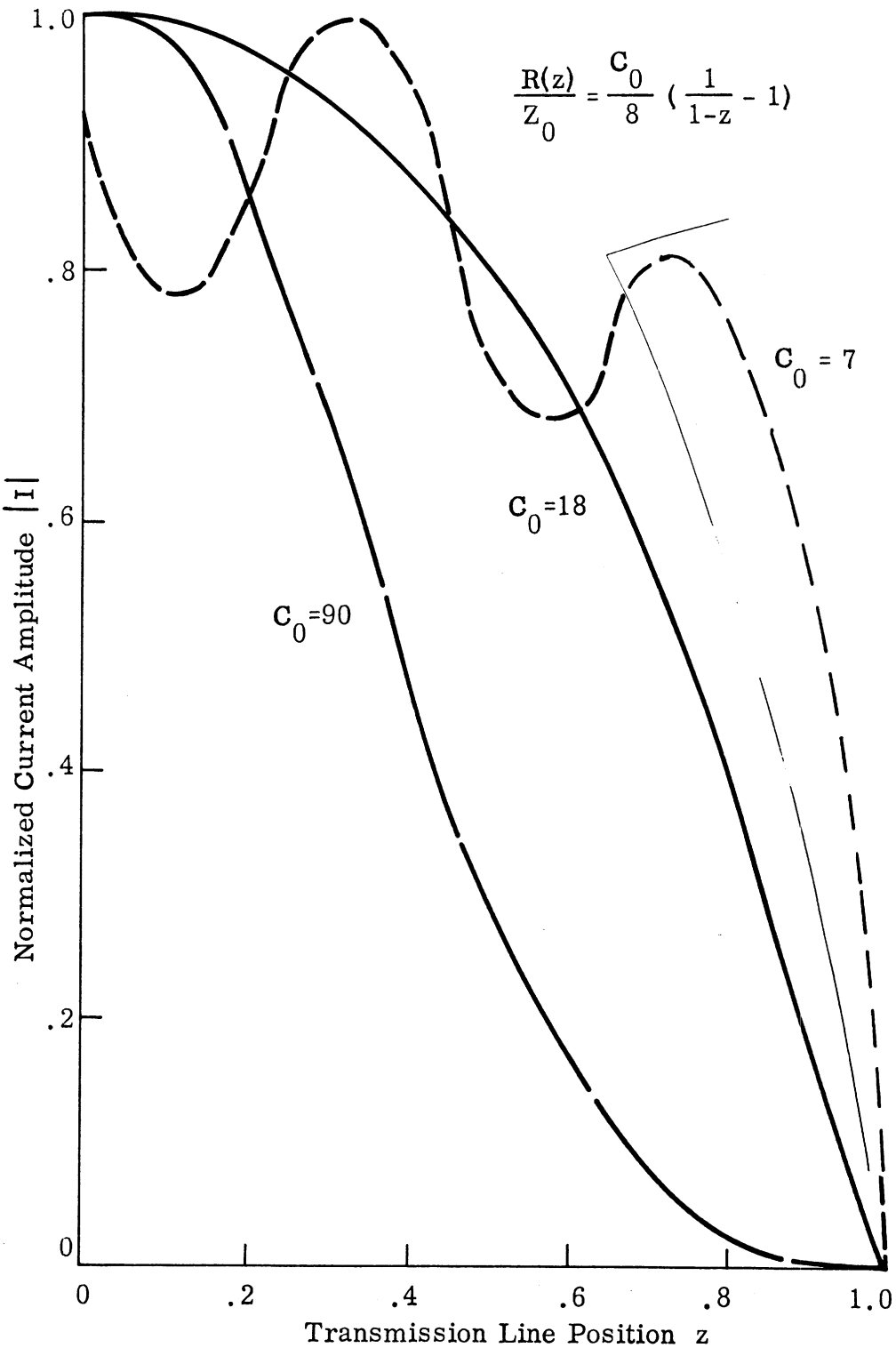

FIG. 2-10: AMPLITUDE OF CURRENT ALONG TRANSMISSION LINE PRODUCED BY CONTINUOUS INVERSE RESISTANCE LOADING.

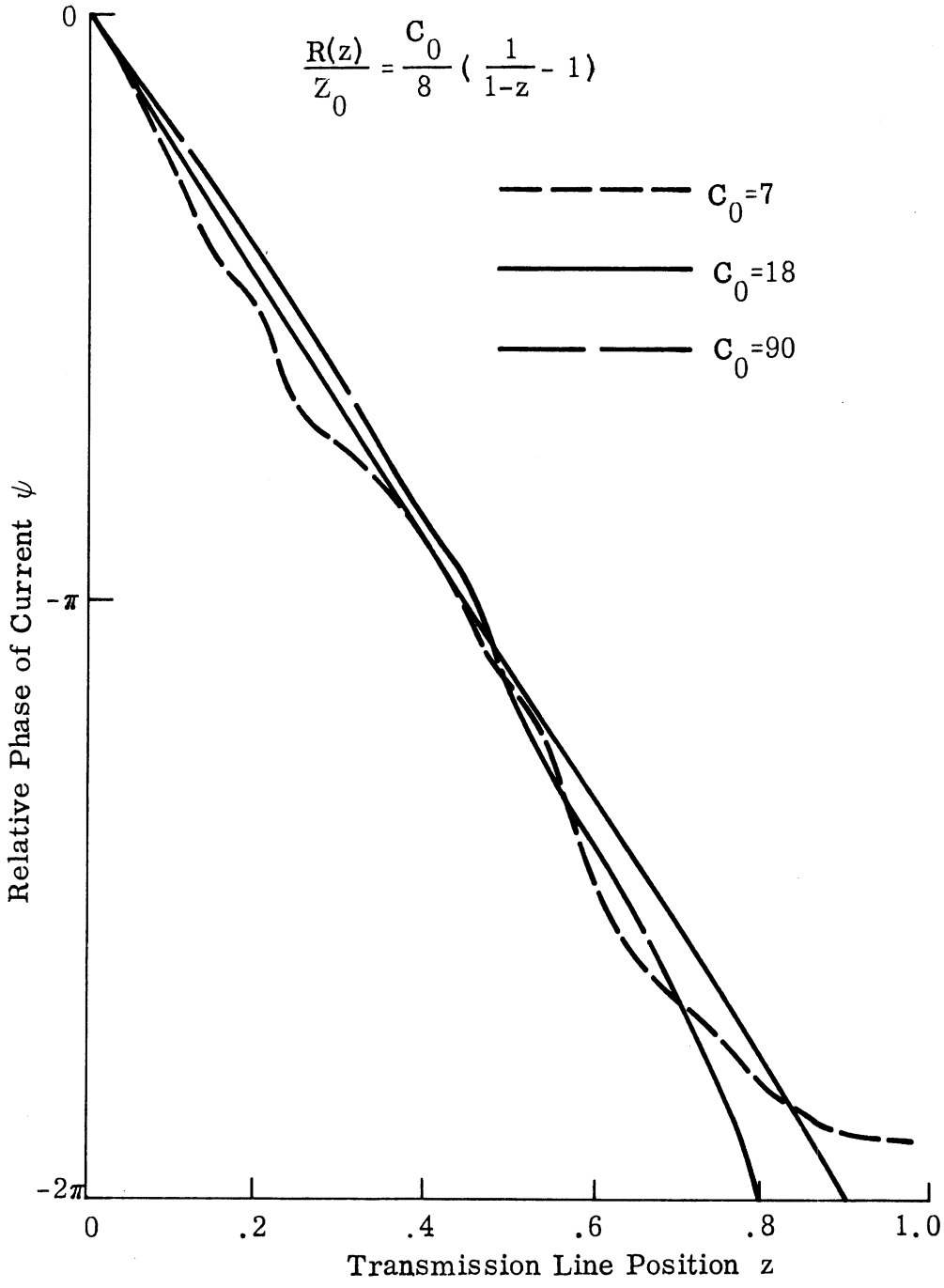

FIG. 2-11: PHASE OF CURRENT ALONG TRANSMISSION LINE PRODUCED BY CONTINUOUS INVERSE RESISTANCE LOADING.

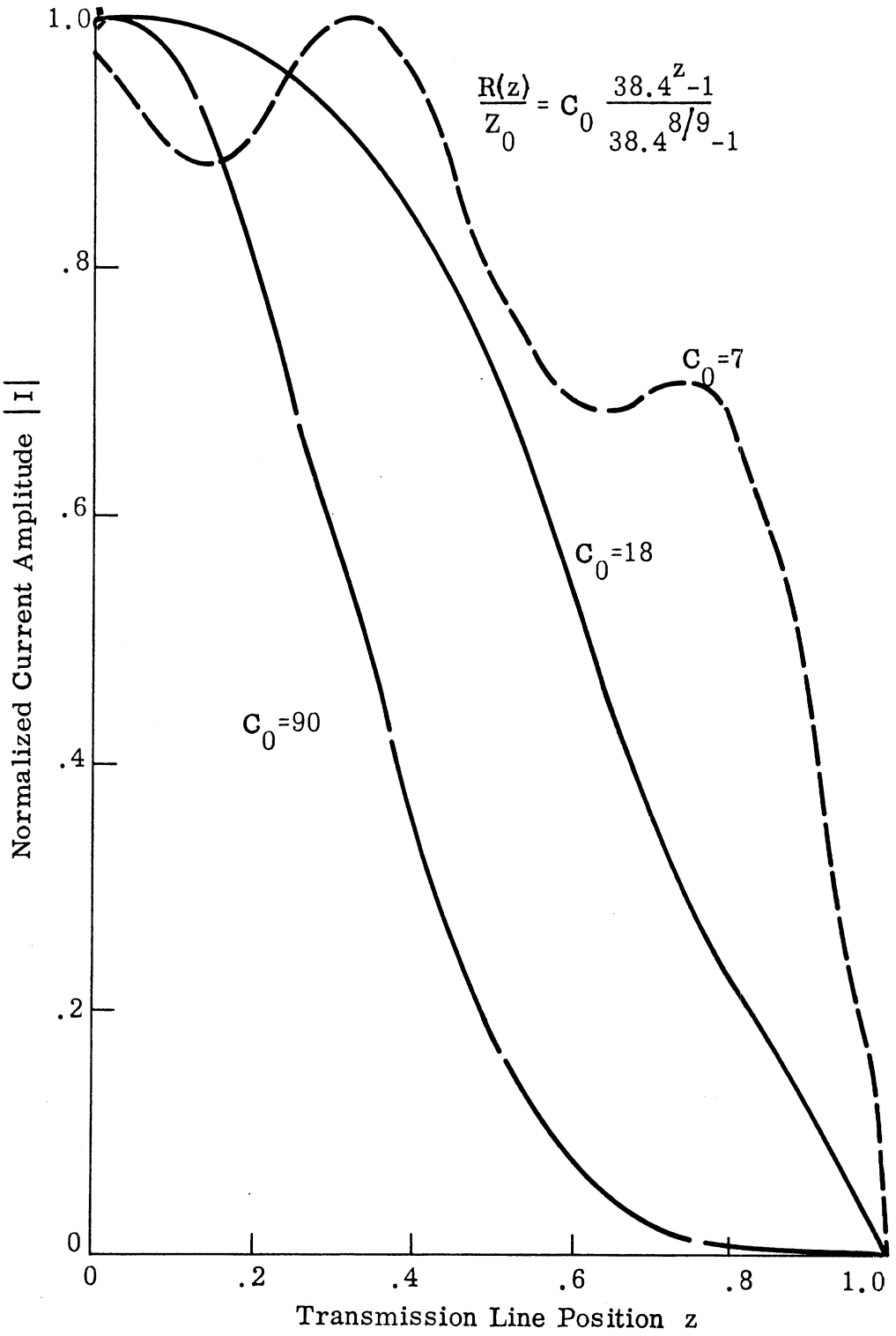

FIG. 2-12: AMPLITUDE OF CURRENT ALONG TRANSMISSION LINE PRODUCED BY CONTINUOUS EXPONENTIAL RESISTANCE LOADING.

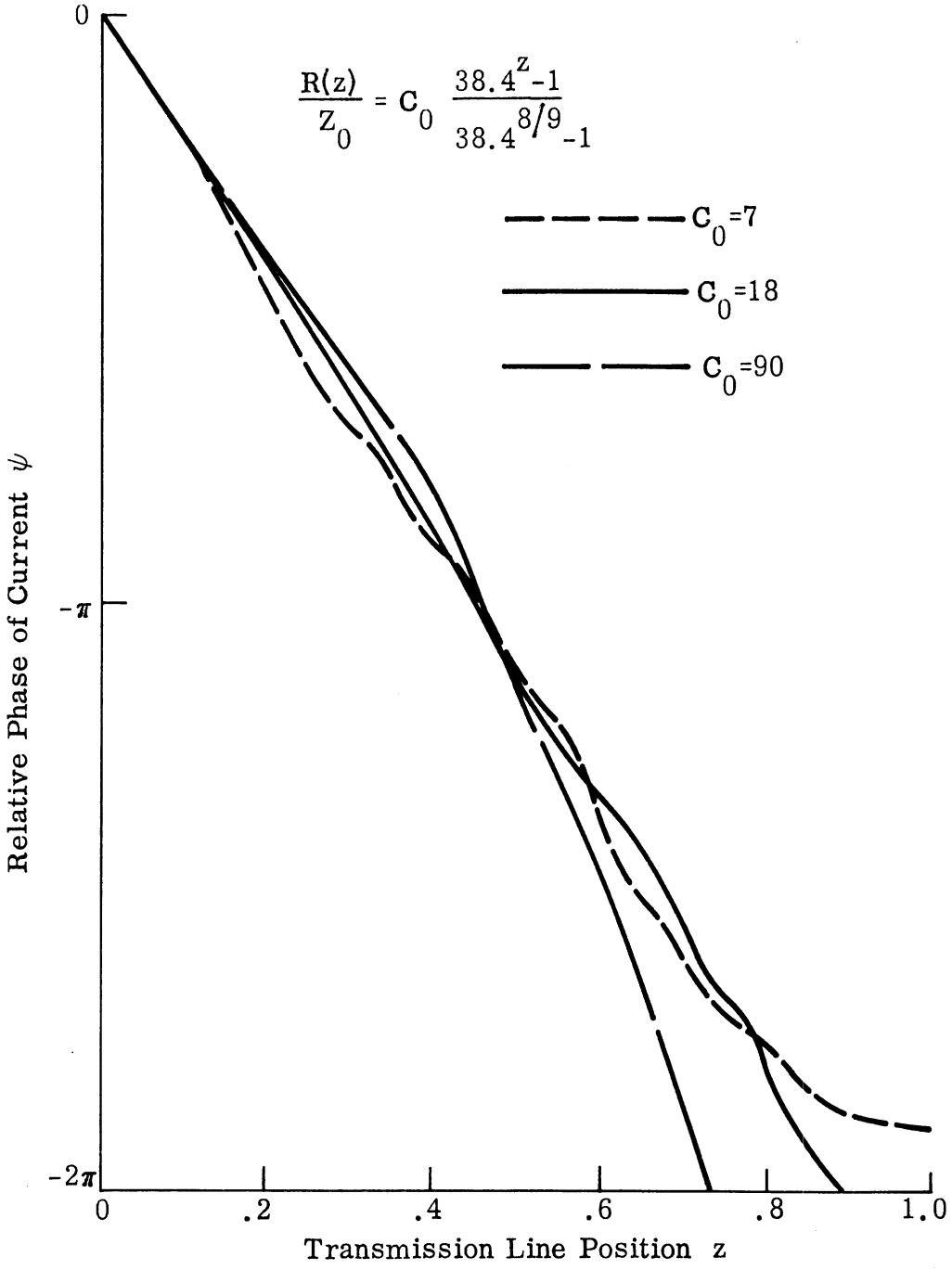

FIG. 2-13: PHASE OF CURRENT ALONG TRANSMISSION LINE PRODUCED BY CONTINUOUS EXPONENTIAL RESISTANCE LOADING.

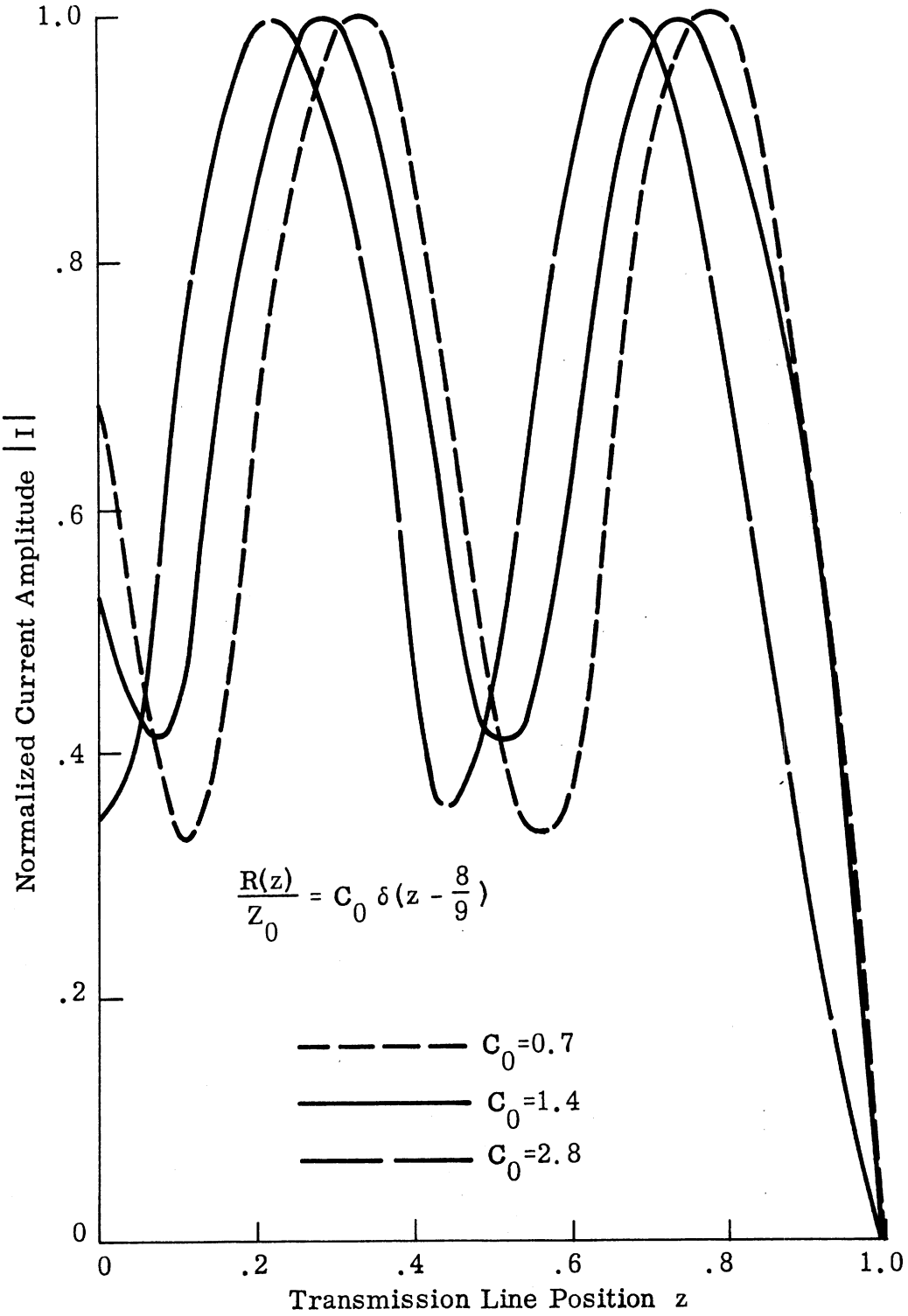

FIG. 2-14: AMPLITUDE OF CURRENT ALONG TRANSMISSION LINE PRODUCED BY CONTINUOUS IMPULSE RESISTANCE LOADING.

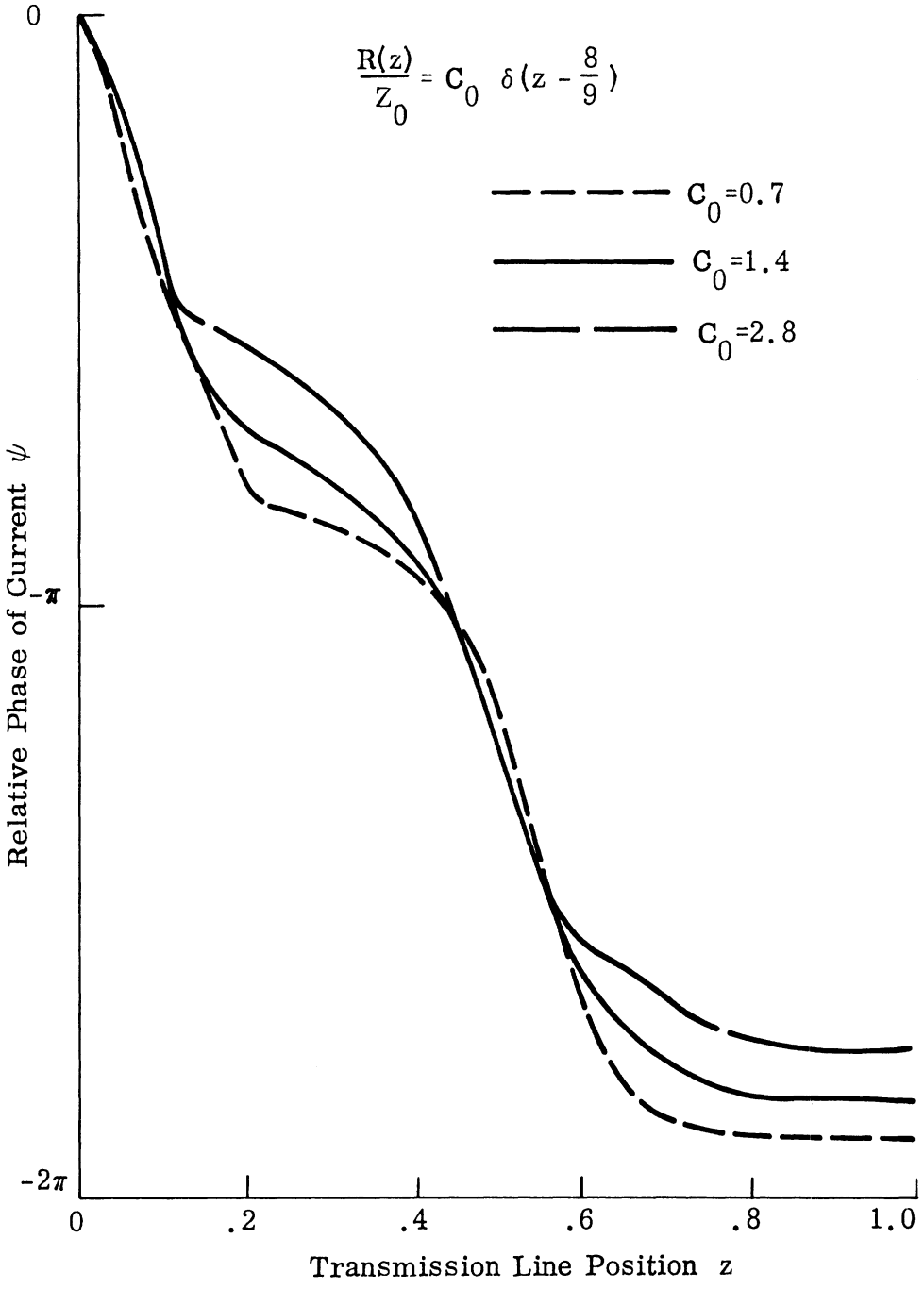

FIG. 2-15: PHASE OF CURRENT ALONG TRANSMISSION LINE PRODUCED BY CONTINUOUS IMPULSE RESISTANCE LOADING.

by the resistance distributions (2.30). For the sake of visibility in these plots, the maximum values of $|I|$ have been normalized to unity and the range of ψ has been translated to $0 \geq \psi \geq -2\pi$.

Each figure shows the effects of varying the magnitudes of the resistive loadings by the parameter C_0. The small resistive loadings attenuate traveling current waves only small amounts so that the transmission line terminations reflect appreciable current waves. The resulting current distributions are observed to contain appreciable standing wave components. In an extreme case of $C_0 = 0$, a pure standing wave would result. The current amplitude would be a sinusoidal function of z and the phase would be constant. In the cases of large C_0, the large resistive loadings attenuate traveling current waves to the extent that no appreciable current waves reach the ends of the transmission lines to be reflected. In these cases, the current distributions are seen to be essentially damped traveling waves. With extremely large C_0, $|I|$ would be an exponentially decreasing curve and ψ would be a linear curve. The values of C_0 for which curves are presented here are intermediate values which reveal the details of the transition between the extreme small and large magnitudes of each functional form of resistance distribution.

An optimum magnitude coefficient C_0 may be found for each form of resistance distribution, based on criteria which can be postulated for the resulting complex current distribution. Where it is desired to maximize radiation from the transmission line, optimization criteria would be to maximize $\int_0^h |I|\, dz$ and simultaneously to require a predominently traveling wave. The latter requirement may be interpreted as requiring that the ψ versus z variation be linear to within some established tolerance, for example $\pm \frac{\pi}{16}$. These criteria can be applied to the transmission line which is used as an illustration here. Examination of the curves in Figs. 2-4 through 2-15 and

intermediate curves which have been omitted for clarity shows the following optimum values of the magnitude coefficient C_0:

Functional Form of Continuous Resistance Distribution	Optimum Magnitude Coefficient C_0
UNIFORM	3.6
LOGARITHMIC	8.3
LINEAR	7.2
INVERSE	18.0
EXPONENTIAL	18.0
IMPULSE	1.4

TABLE 2-1: OPTIMUM MAGNITUDE COEFFICIENTS FOR VARIOUS CONTINUOUS RESISTANCE DISTRIBUTIONS.

The $|I|$ and ψ plots resulting from the optimum C_0 in each of the Figs. 2-4 through 2-15 have been drawn as solid curves.

The best of the individually optimized resistance distribution functions can now be selected. Applying the same optimization criteria to the sequence of Figs. 2-4 through 2-15 leads to the Table 2-2 list of resistance loading functions in order of decreasing effectiveness.

Thus the best of all the resistance loading functions which have been examined here is the inverse function

$$R(z) = \frac{9}{4} Z_0 \left(\frac{1}{1 - z} - 1 \right) \text{ ohms/meter} \qquad (2.31)$$

and the resulting optimum complex current distribution is that which appears as the solid curves in Figs. 2-10 and 2-11.

INVERSE	$\frac{R(z)}{Z_0} = 18\left(\frac{1}{8}\right)\left(\frac{1}{1-z} - 1\right)$
EXPONENTIAL	$\frac{R(z)}{Z_0} = 18\,\frac{38.4^{z}-1}{38.4^{8/9}-1}$
LINEAR	$\frac{R(z)}{Z_0} = 7.2\,\frac{9z}{8}$
LOGARITHMIC	$\frac{R(z)}{Z_0} = 8.3\,\frac{\log(z+1)}{\log 1\frac{8}{9}}$
UNIFORM	$\frac{R(z)}{Z_0} = 3.6$
IMPULSE	$\frac{R(z)}{Z_0} = 1.4\,\delta\left(z - \frac{8}{9}\right)$

TABLE 2-2: PREFERENTIAL ORDER OF VARIOUS CONTINUOUS RESISTANCE DISTRIBUTIONS.

The exponential form of resistance distribution,

$$\frac{R(z)}{Z_0} = C_0\,\frac{b^{z}-1}{b^{8/9}-1},$$

is nearly as effective as the inverse form. Figure 2-3 shows graphically how little quantitative difference exists between the two resistance distributions. The two resulting current distributions are similar as has been observed in Figs. 2-10 through 2-13. Two parameters, the magnitude coefficient C_0 and the exponential base b, have been optimized for the exponential distribution. Optimization of C_0 to the value $C_0 = 18.0$ resulted from data which includes that in Figs. 2-12 and 2-13. The optimum value of $b = 38.4$ was determined similarly by computing sets of $|I|$ and ψ curves with $C_0 = 18$ and b variable.

Uniform resistance loading, which is most commonly encountered due to its analytic tractability, is seen to be relatively poor in its ability to produce a current distribution that will enhance radiation.

The impulse resistance loading is perhaps the simplest to fabricate as it consists of a single lumped resistor in an otherwise lossless transmission line. Its performance is the worst of all the loading functions that have been considered here.

Properties of resistance distributions which are responsible for producing the desirable features in a current distribution are evident. High resistance near the end of the transmission line is needed to reduce the reflected current wave. Low resistance loading over the rest of the line is necessary to retain a large amplitude of the outward traveling current wave. The proper smooth transition between low and high resistance regions is needed to reduce reflections from the transition.

2.6 Transmission Line Impedances

The impedance $Z(z)$ at any position z along a loaded transmission line can be computed readily in terms of the current and the spatial derivative of current at that position. The transmission line relation

$$\frac{\partial I(z)}{\partial z} = - j \omega C V(z)$$

is employed in the expression for this impedance

$$Z(z) = \frac{j \frac{\partial I(z)}{\partial z}}{\omega C I(z)} \quad . \tag{2.32}$$

The computer program of Appendix A solves (2.9) for both $I(z)$ and $\frac{\partial I(z)}{\partial z}$.

The various resistance distribution functions produce quite different transmission line impedances $Z(z)$. Smith chart plots of $\frac{Z(z)}{Z_0}$ produced by each of the optimized resistance loadings of Table 2-2 appear in Figs. 2-16

through 2-21. These plots verify the expectation that the best input impedance match and the most direct transition from an open circuit termination to a well-matched impedance is produced by the inverse resistance loading (2.31). The good impedance match along the transmission line that has the inverse loading allows the maximum value of $\int_0^h |I|\, dz$ and essentially an outward traveling current wave with minimum net reflections. This is the same conclusion that had been reached from another point of view: that of current distributed along the transmission line. In fact, the impedance plots show that the relative effectiveness of the various resistance loading functions in producing matched impedances along the transmission line is the same as was indicated in Table 2-2.

At the input terminals of the transmission line, the reflection coefficient related to Z_0 is

$$\Gamma_{in} = \frac{\omega C Z_0 I(0) - j \frac{\partial I(0)}{\partial z}}{\omega C Z_0 I(0) + j \frac{\partial I(0)}{\partial z}} \quad . \tag{2.33}$$

Minimization of input reflection coefficient can be used as a criterion for selecting a value of C_0 for each resistance loading function and for selecting the best function. Figure 2-22 is a display of data computed for these purposes. The same set of optimum values of C_0 (Table 2-1) and the same relative ranking of the loading functions (Table 2-2) are found as in the case of optimization based on current distribution considerations. The most effective resistance distribution function is the inverse form (2.31)

2.7 Position-Dependent Characteristic Impedance

In the frequency domain, a transmission line loaded with position-dependent resistance may be considered to possess a characteristic impedance which is also position dependent. The characteristic impedance $Z_c^{(+)}(z)$ encountered by waves traveling away from the source differs from the

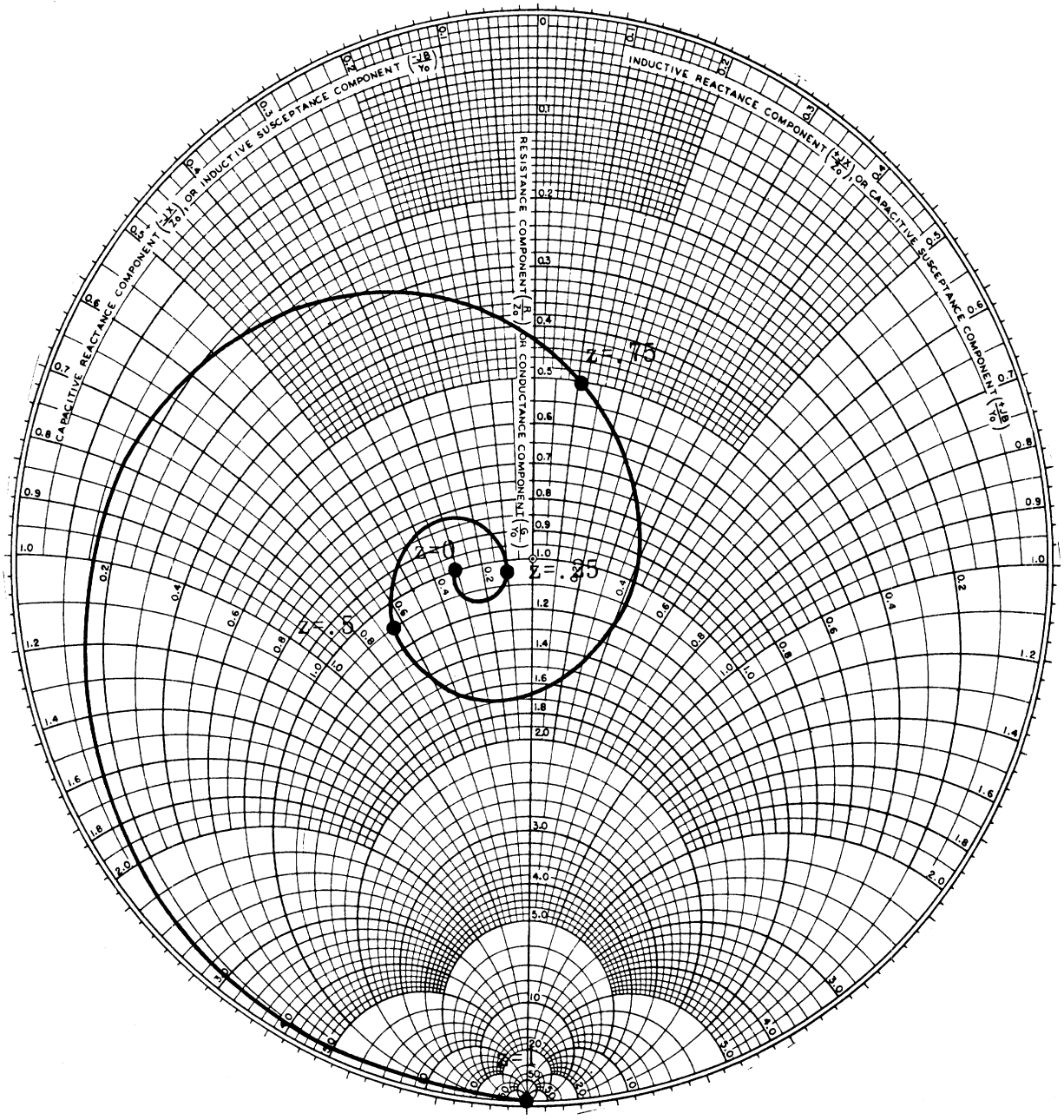

Normalized Impedance $\frac{Z(z)}{Z_0}$

FIG. 2-16: IMPEDANCES ALONG TRANSMISSION LINE WITH UNIFORM CONTINUOUS RESISTANCE LOADING $\frac{R(z)}{Z_0} = 3.6$.

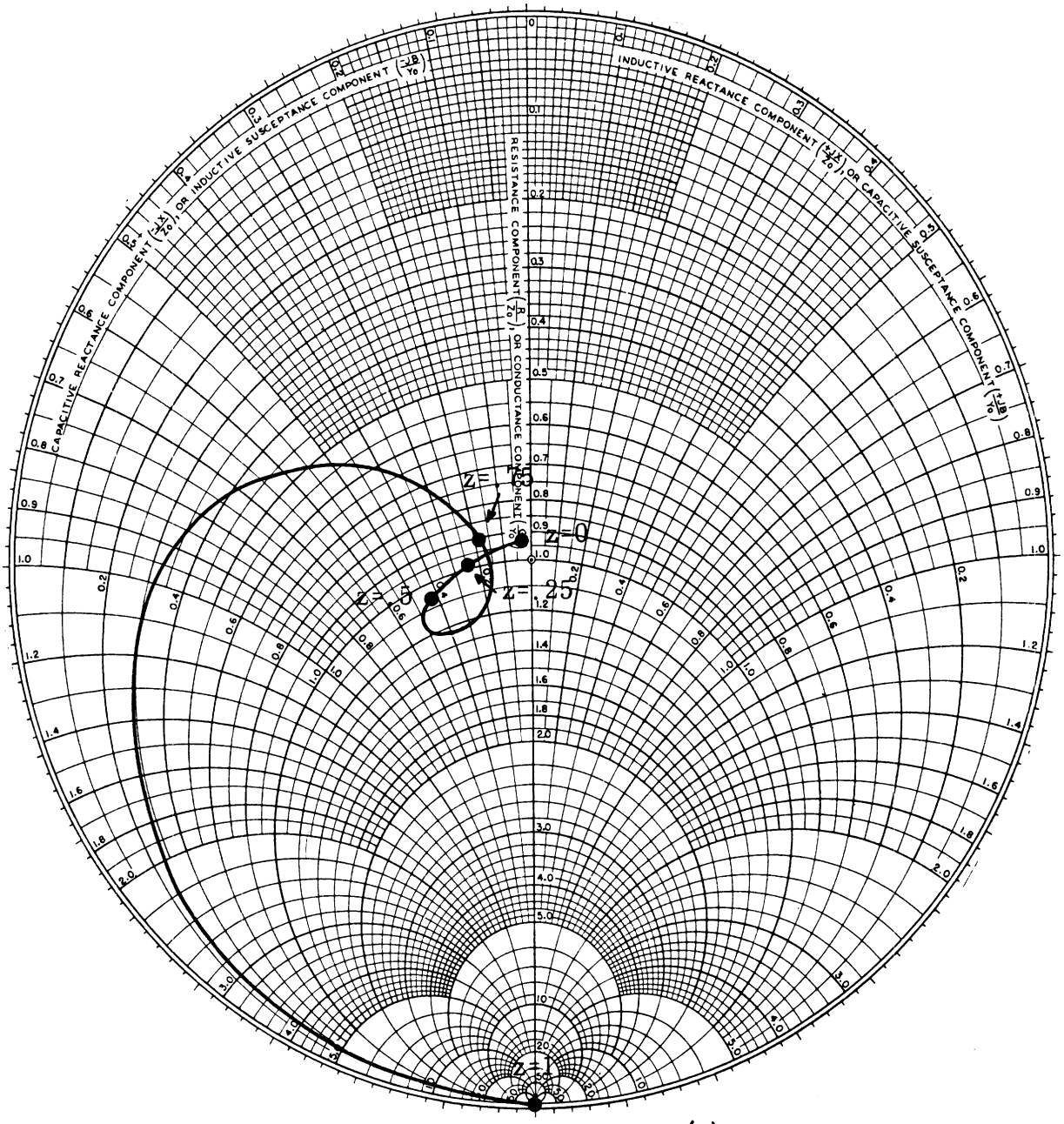

FIG. 2-17: IMPEDANCES ALONG TRANSMISSION LINE WITH LOGARITHMIC CONTINUOUS RESISTANCE LOADING $\frac{R(z)}{Z_0} = 8.3 \frac{\log (z+1)}{\log 1\frac{8}{9}}$.

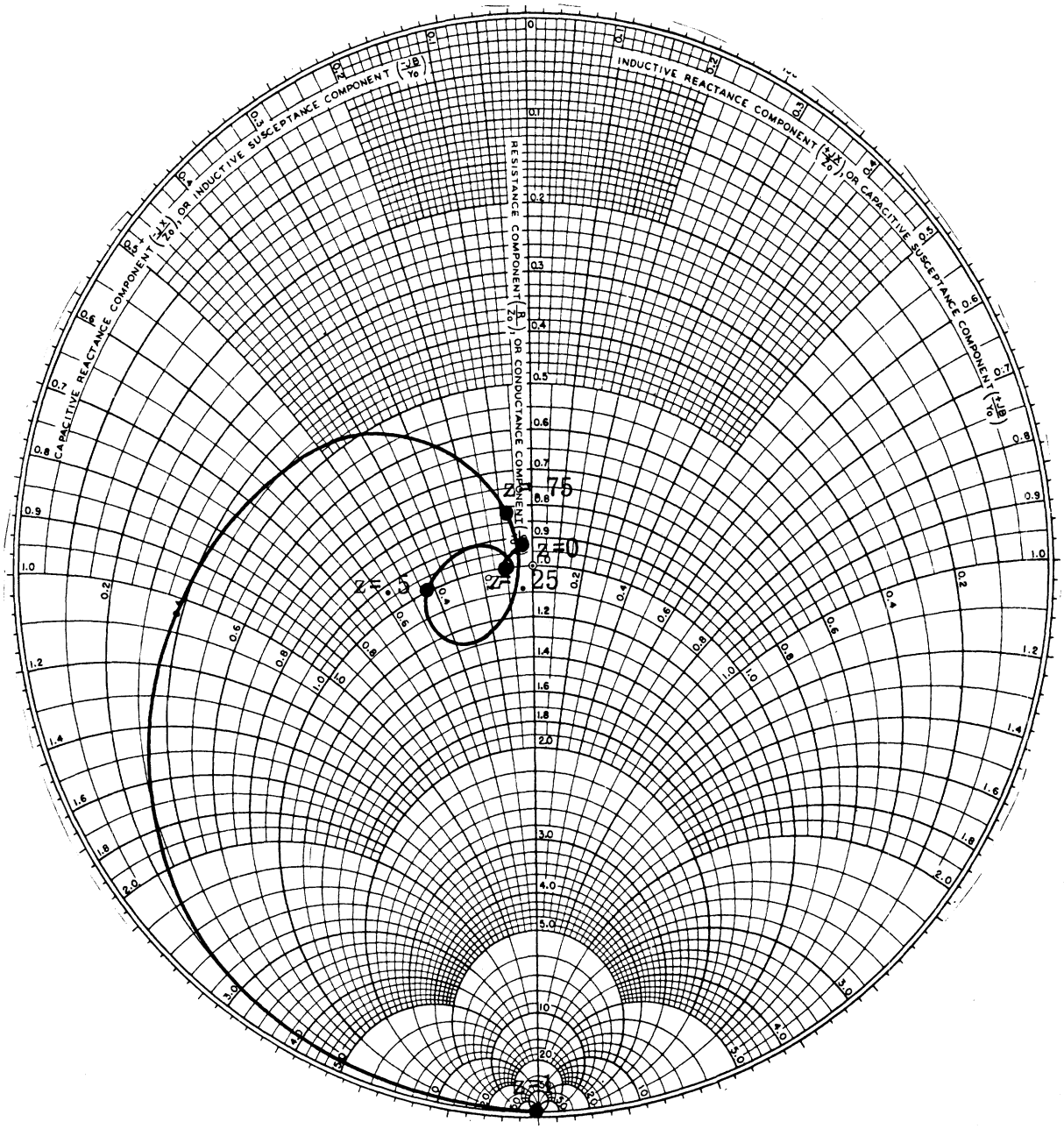

Normalized Impedance $\frac{Z(z)}{Z_0}$

FIG. 2-18: IMPEDANCES ALONG TRANSMISSION LINE WITH LINEAR CONTINUOUS RESISTANCE LOADING

$$\frac{R(z)}{Z_0} = 7.2\,\frac{9\,z}{8}\,.$$

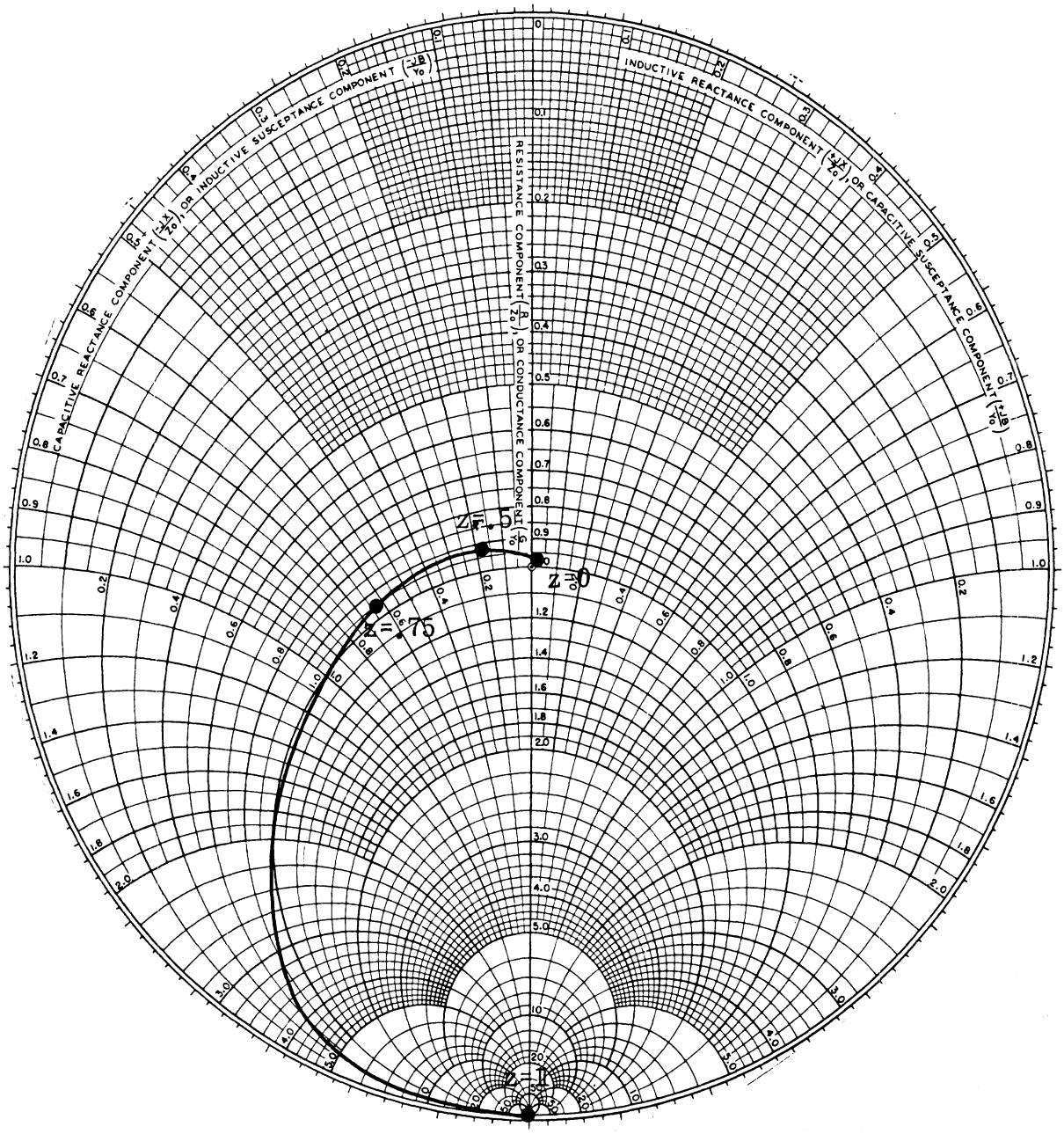

Normalized Impedance $\frac{Z(z)}{Z_0}$

FIG. 2-19: IMPEDANCES ALONG TRANSMISSION LINE WITH INVERSE CONTINUOUS RESISTANCE LOADING $\frac{R(z)}{Z_0} = \frac{18}{8}\left(\frac{1}{1-z} - 1\right)$.

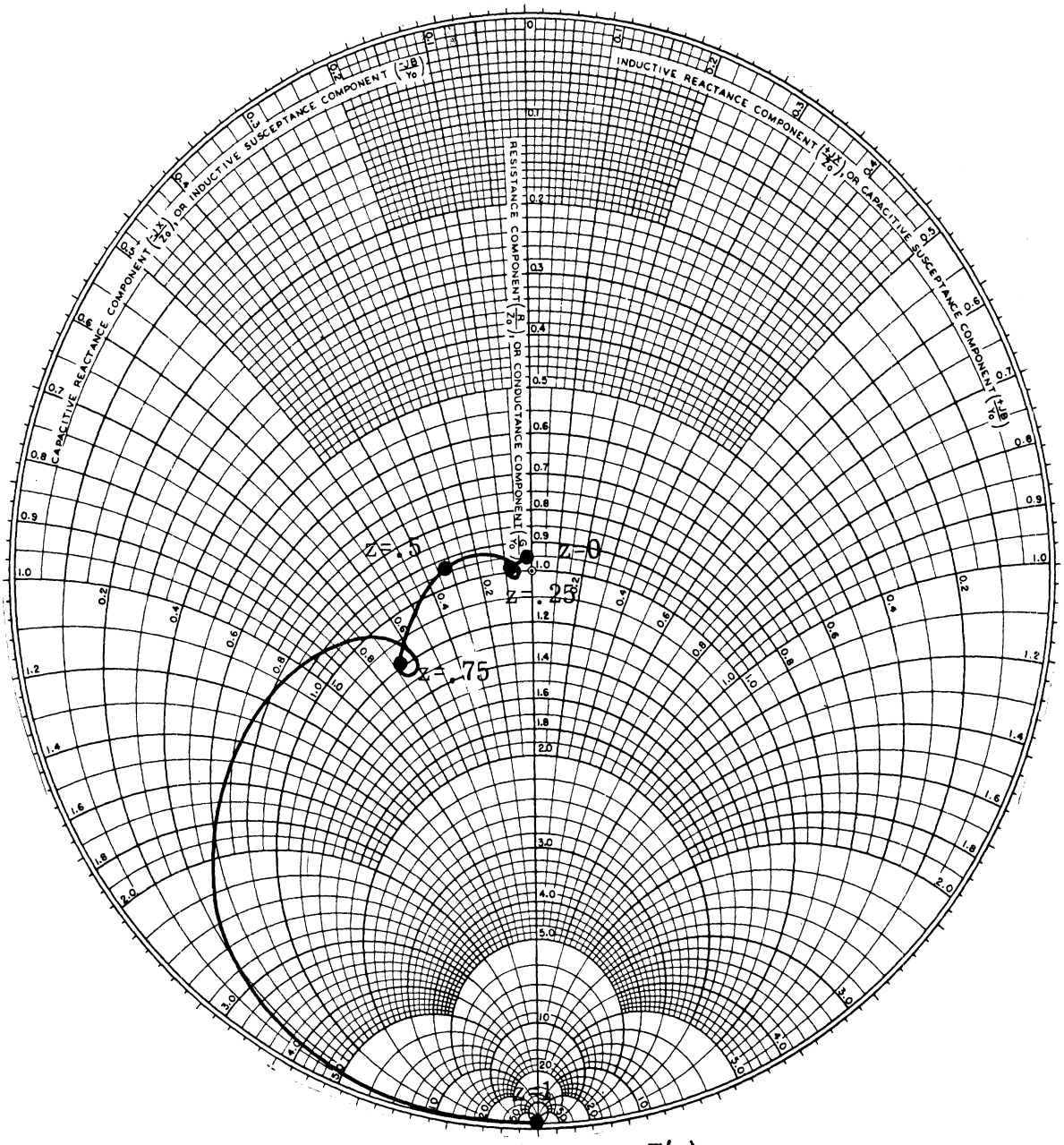

FIG. 2-20: IMPEDANCES ALONG TRANSMISSION LINE WITH EXPONENTIAL CONTINUOUS RESISTANCE LOADING

$$\frac{R(z)}{Z_0} = 18\,\frac{38.4^{z}-1}{38.4^{8/9}-1}\,.$$

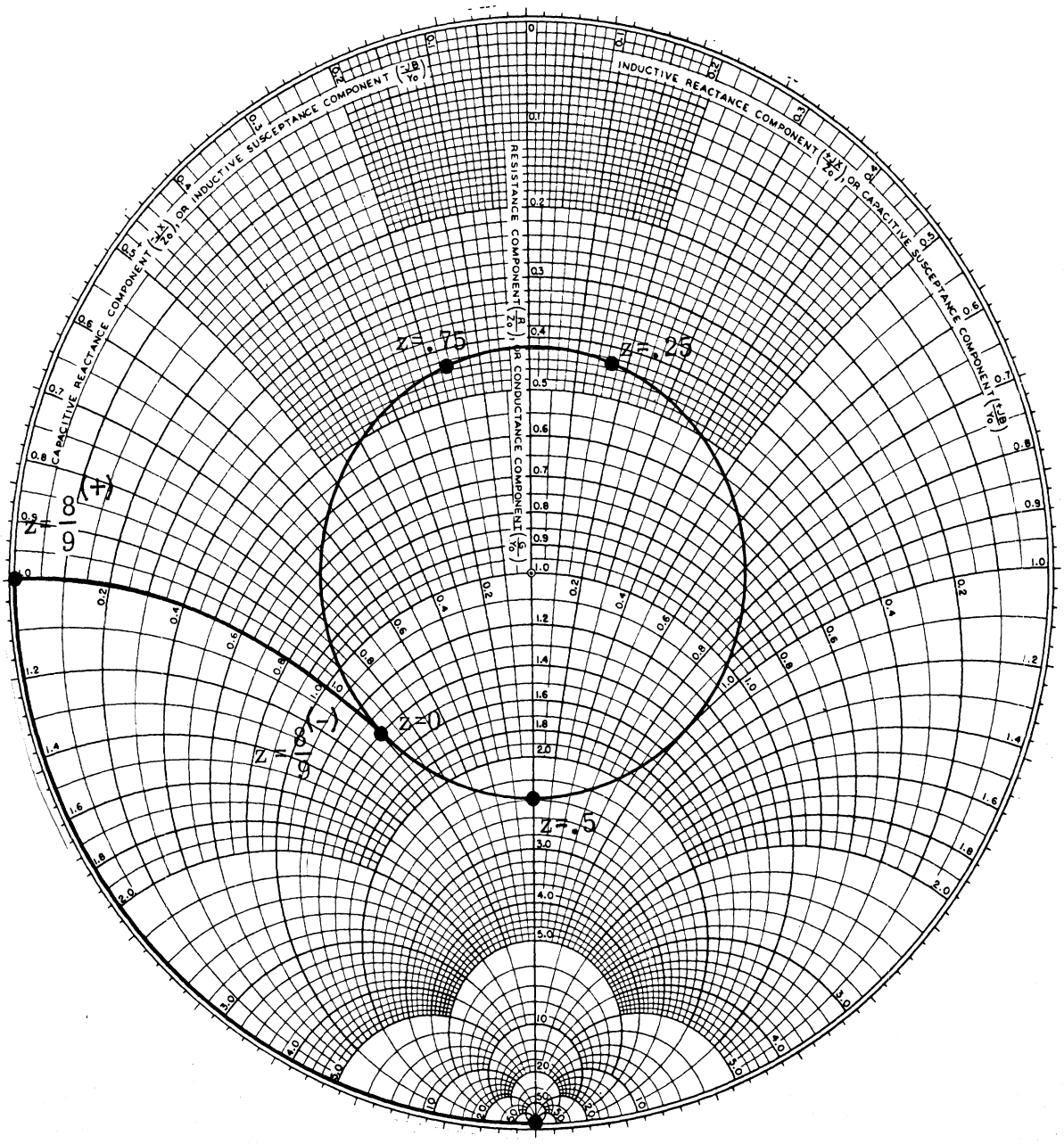

Normalized Impedance $\frac{Z(z)}{Z_0}$

FIG. 2-21: IMPEDANCES ALONG TRANSMISSION LINE WITH IMPULSE CONTINUOUS RESISTANCE LOADING $\frac{R(z)}{Z_0} = 1.4\,\delta\left(z - \frac{8}{9}\right)$.

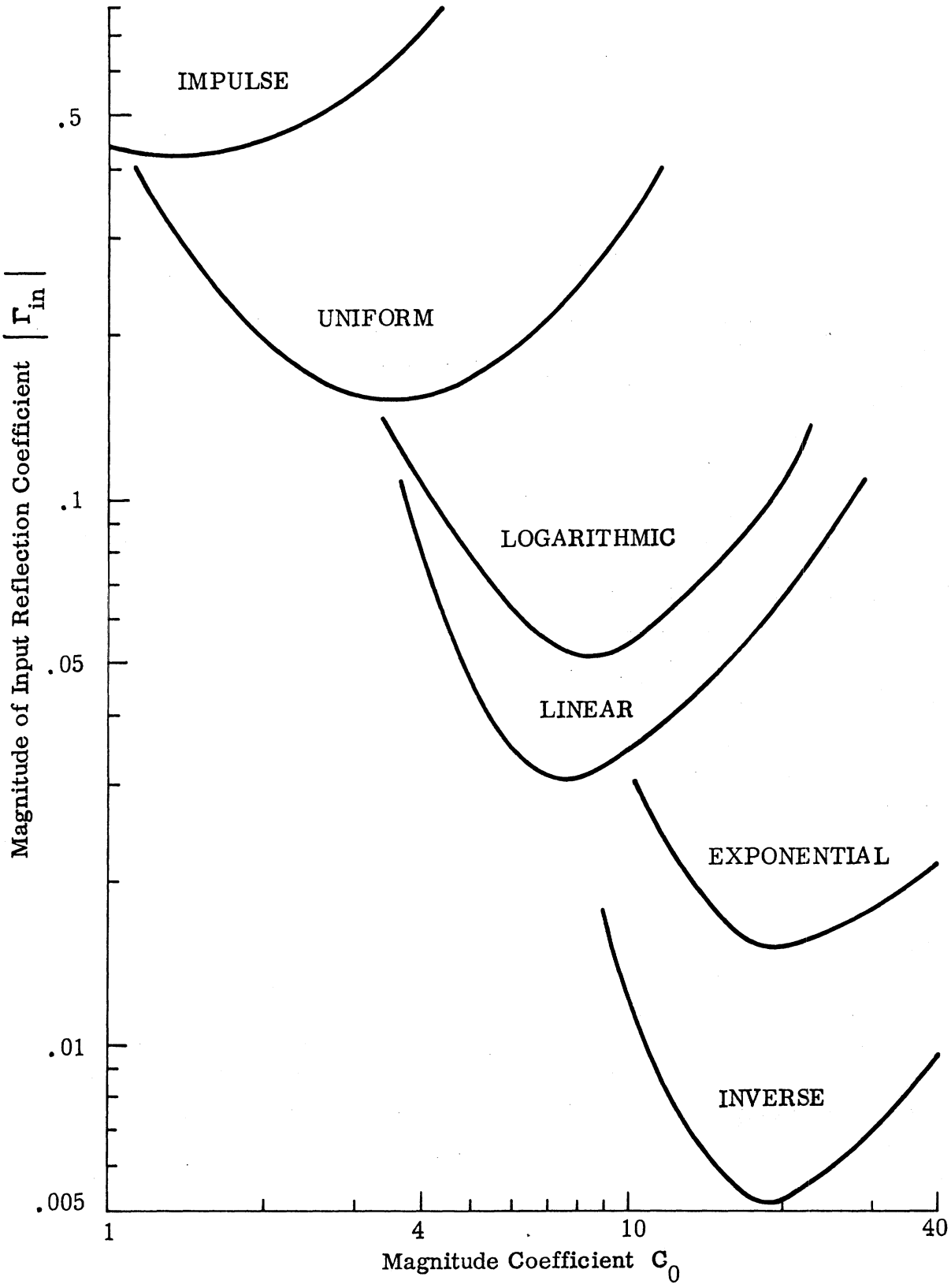

FIG. 2-22: INPUT REFLECTION COEFFICIENTS PRODUCED BY VARIOUS CONTINUOUS RESISTANCE DISTRIBUTIONS.

characteristic impedance $Z_c^{(-)}(z)$ seen by waves traveling toward the source. To obtain expressions for these quantities, an invariant imbedding approach is applied. The analysis avoids reflections from the ends of the transmission line by considering a line that is infinitely long or terminated in reflection-less impedances. The transmission line is characterized by the parameters $R(z)$, L, C as was shown in Fig. 2-1.

The impedances, looking away from the source end of the line, at two positions separated by the infinitesimal distance d are

$$Z^{(+)}(z) = Z_c^{(+)}(z) \ , \tag{2.34}$$

$$Z^{(+)}(z-d) = Z_c^{(+)}(z) - Z_c^{(+)'}(z)\, d, \tag{2.35}$$

where the prime indicates differentiation of a function with respect to its argument. Relating (2.34) and (2.35) through the parameters of the transmission line cell yields

$$Z_c^{(+)}(z) - Z_c^{(+)'}(z)d = R(z)d + j\omega Ld + \frac{1}{j\omega Cd + \dfrac{1}{Z_c^{(+)}(z)}} \ . \tag{2.36}$$

Equation (2.36) can be rearranged algebraically, including division by d, to the form

$$j\omega C \left[Z_c^{(+)}(z)\right]^2 \left[1 - \frac{Z_c^{(+)'}(z)}{Z_c^{(+)}(z)}\, d\right] - Z_c^{(+)'}(z) = j\omega CR(z)\, Z_c^{(+)}(z)d - \omega^2 LC\, Z_c^{(+)}(z)\, d$$

$$+ R(z) + j\omega L \ . \tag{2.37}$$

Letting $d \longrightarrow 0$ in (2.37) leads to an expression for the position-dependent characteristic impedance

$$Z_c^{(+)}(z) = \sqrt{\frac{L}{C}\left[1 - j\frac{R(z) + Z_c^{(+)'}(z)}{\omega L}\right]} \quad . \tag{2.38}$$

If $Z_c^{(+)'}(z) \approx -R(z)$, then $\left|R(z) + Z_c^{(+)'}(z)\right| << \omega L$ and

$$Z_c^{(+)}(z) \approx \sqrt{\frac{L}{C}\left[1 - j\frac{R(z) + Z_c^{(+)'}(z)}{2\omega L}\right]} \quad . \tag{2.39}$$

Treated as a linear first order differential equation in the standard form

$$Z_c^{(+)'}(z) - j2k_0 Z_c^{(+)}(z) + R(z) + j2\omega L = 0 \ ,$$

(2.39) is seen to possess the integrating factor $e^{-j2k_0 z}$ and the solution

$$Z_c^{(+)}(z) = \sqrt{\frac{L}{C}} - e^{j2k_0 z}\int R(z)\, e^{-j2k_0 z}\, dz \ , \tag{2.40}$$

where $k_0 = \omega\sqrt{LC}$.

The impedances, looking toward the source, at two positions separated by the infinitesimal distance d are:

$$Z^{(-)}(z) = Z_c^{(-)}(z) \ , \tag{2.41}$$

$$Z^{(-)}(z+d) = Z_c^{(-)}(z) + Z_c^{(-)'}(z)\, d. \quad . \tag{2.42}$$

Again using the parameters of the infinitesimal section of transmission line to relate (2.41) and (2.42) yields

$$Z_c^{(-)}(z) + Z_c^{(-)'} d = R(z)d + j\omega L d + \frac{1}{j\omega C d + \dfrac{1}{Z_c^{(-)}(z)}} \quad . \tag{2.43}$$

Algebraic rearrangement of (2.43), including division by d, produces the form

$$j\omega C\left[Z_c^{(-)}(z)\right]^2\left[1+\frac{Z_c^{(-)'}(z)}{Z_c^{(-)}(z)}\,d\right]+Z_c^{(-)'}(z)$$

$$=j\omega CR(z)\,Z_c^{(-)}(z)\,d-k_0^2\,Z_c^{(-)}(z)\,d+R(z)+j\omega L \qquad (2.44)$$

which becomes

$$Z_c^{(-)}(z)=\sqrt{\frac{L}{C}\left[1-j\frac{R(z)-Z_c^{(-)'}(z)}{\omega L}\right]} \qquad (2.45)$$

as $d\to 0$. If $Z_c^{(-)'}(z)\approx R(z)$, then $\left|R(z)-Z_c^{(-)'}(z)\right| << \omega L$ and

$$Z_c^{(-)}(z)\approx\sqrt{\frac{L}{C}}\left[1-j\frac{R(z)-Z_c^{(-)'}(z)}{2\omega L}\right]. \qquad (2.46)$$

In the standard form

$$Z_c^{(-)'}(z)+j\,2\,k_0\,Z_c^{(-)}(z)-R(z)-j\,2\omega L=0,$$

the differential equation has the solution

$$Z_c^{(-)}(z)=\sqrt{\frac{L}{C}}+e^{-j2k_0z}\int R(z)\,e^{j2k_0z}\,dz \qquad (2.47)$$

Equations (2.40) and (2.47) are the expressions for the position-dependent characteristic impedances looking in the two directions on a transmission line which is loaded with a non-uniform resistance R (z). In the special case of uniform resistance loading R (z) = R = constant, the

characteristic impedance is the same in both directions and equations (2.40) and (2.47) reduce to the known result

$$Z_c = \sqrt{\frac{L}{C}} - j\frac{R}{2k_0} \quad . \tag{2.48}$$

The various resistance distribution functions (2.30) which have been studied can be substituted into (2.40) and (2.47) to give

UNIFORM
$$\frac{Z_c^{(\pm)}(z)}{Z_0} = 1 - \frac{j\,C_0}{2k_0} \quad , \tag{2.49a}$$

LOGARITHMIC
$$\frac{Z_c^{(\pm)}(z)}{Z_0} \approx 1 - j\,\frac{C_0 \log e}{k_0 \log 1\frac{8}{9}} + \frac{4C_0 \log e}{\log 1\frac{8}{9}}\, e^{\pm j2k_0(z+2)} \cdot \left\{ \pm \ell n(z+2) - j2k_0(z+2) \pm \frac{\left[j2k_0(z+2)\right]^2}{2 \cdot 2!} - \frac{\left[j2k_0(z+2)\right]^3}{3 \cdot 3!} \pm \text{-------} \right\} \quad , \tag{2.49b}$$

LINEAR
$$\frac{Z_c^{(\pm)}(z)}{Z_0} = 1 - \frac{9\,C_0}{16\,k_0}\left(\pm\frac{1}{2k_0} + j\,z\right) \quad , \tag{2.49c}$$

INVERSE
$$\frac{Z_c^{(\pm)}(z)}{Z_0} = 1 + j\,\frac{C_0}{16\,k_0} + \frac{C_0}{8}\, e^{\pm j2k_0(z-1)} \cdot \left\{ \pm \ell n\,(1-z) - j2k_0(z-1) \pm \frac{\left[j2k_0(z-1)\right]^2}{2 \cdot 2!} - \frac{\left[j2k_0(z-1)\right]^3}{3 \cdot 3!} \pm \text{-----} \right\} , \tag{2.49d}$$

$$\text{EXPONENTIAL}\quad \frac{Z_c^{(\pm)}(z)}{Z_0} = 1 + j\,\frac{C_0}{2k_0\,(b^{8/9}-1)} + \frac{C_0 b^z}{(b^{8/9}-1)(j2k_0 \mp \ell nb)} \tag{2.49e}$$

$$\text{IMPULSE}\quad \frac{Z_c^{(\pm)}(z)}{Z_0} = 1 \mp C_0\, e^{\pm j2k_0(z-\frac{8}{9})} \quad . \tag{2.49f}$$

2.8 Discrete Resistance Loading

Continuous distributions of resistance along transmission lines have been analyzed in the preceding sections of this chapter. In the present section, a comparable development will be presented for transmission lines which are loaded by lumped resistances inserted at a finite number of discrete positions along the line. Physically constructing a discretely loaded transmission line would be somewhat simpler than constructing a continuously loaded line. The two forms of loading may be expected to produce similar results if the separation of the discrete resistances is sufficiently small in terms of wavelengths.

By employing generalized functions or numerical tabular functions to describe the discrete resistance distributions, the previous formulation of the continuous case can be applied also to the discrete case. However, it is more economical computationally to reformulate the problem to take advantage of the standard analysis of lossless transmission lines with lumped discontinuities.

Figure 2-23 shows the configuration of the discretely loaded transmission line. A lossless transmission line of length h is loaded by the insertion in series of N equispaced lumped resistances. The integer n which has the range $1 \leq n \leq N$ is used to index the consecutive resistances and associated quantities. The indexing notation employed here should not be

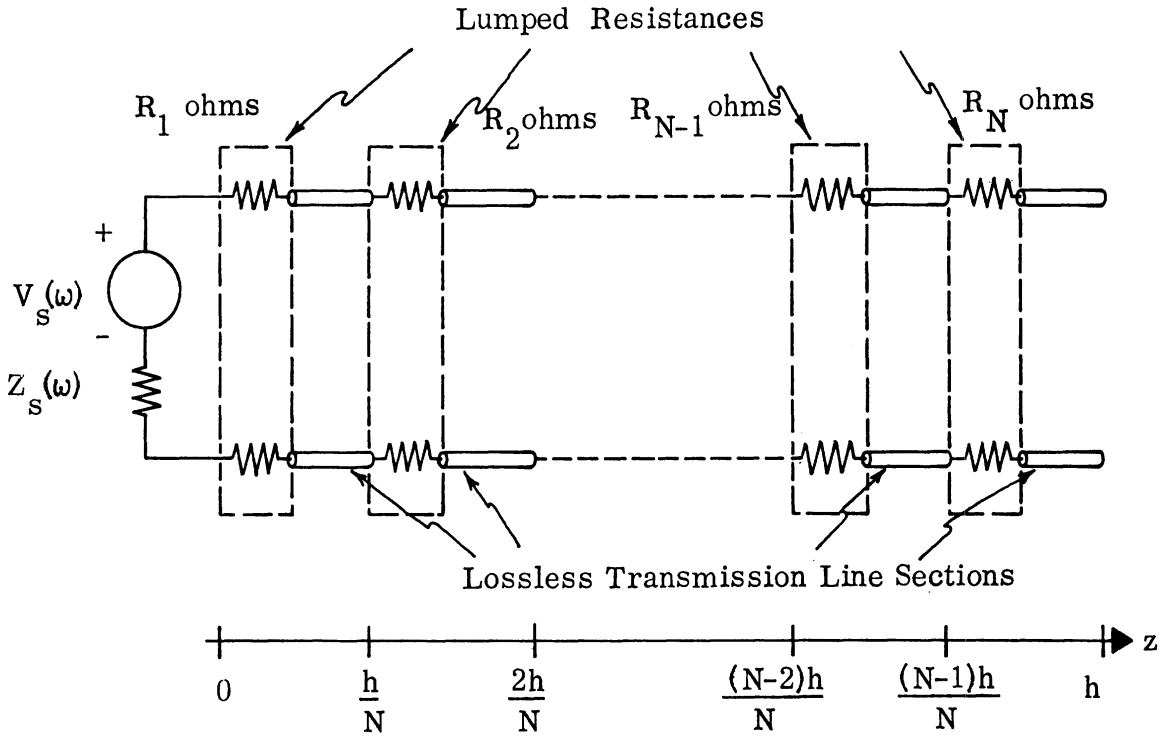

(A) Transmission Line Layout

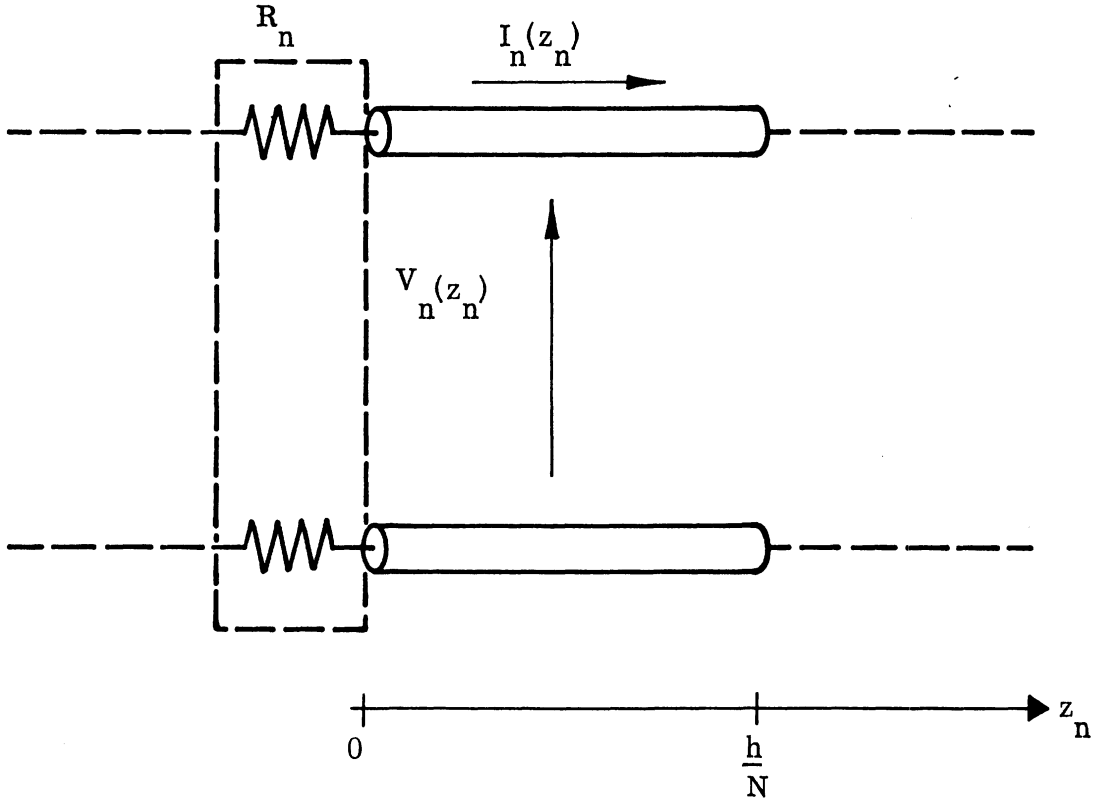

(B) Typical Section

FIG. 2-23: DISCRETE RESISTANCE LOADED TRANSMISSION LINE CONFIGURATION.

confused with similar notation which is elsewhere applied to the formulation of numerical solutions.

For a typical section of the transmission line as in Fig. 2-23b, the frequency domain voltage and current can be written in the forms

$$V_n(z_n) = A_n \left(e^{-jk_0 z_n} - \Gamma_n e^{jk_0 z_n}\right) , \tag{2.50}$$

$$I_n(z_n) = \frac{A_n}{Z_0} \left(e^{-jk_0 z_n} + \Gamma_n e^{jk_0 z_n}\right) , \tag{2.51}$$

where z_n = linear dimension along the nth section of transmission line,

k_0 = the propagation constant of the unloaded line,

Z_0 = the characteristic impedance of the unloaded line,

Γ_n = the current reflection coefficient at $z_n = 0$.

The complex amplitude coefficient A_n, which is determined from boundary conditions, can be expressed as

$$A_n = \frac{Z_0 I_n \left(\frac{h}{N}\right) e^{jk_0 \frac{h}{N}}}{1 + \Gamma_n e^{j2k_0 \frac{h}{N}}} . \tag{2.52}$$

The transmission line impedance looking toward the termination is

$$Z_n(z_n) = \frac{V_n(z_n)}{I_n(z_n)} .$$

Since R_n is a series resistance,

$$Z_{n-1}\left(\frac{h}{N}\right) = R_n + Z_n(0) . \tag{2.53}$$

$$Z_N(0) = -j Z_0 \cot \frac{k_0 h}{N} \quad , \tag{2.56h}$$

$$Z_N\left(\frac{h}{N}\right) = -j\infty \quad , \tag{2.56i}$$

$$\Gamma_N = -e^{-j2k_0 \frac{h}{N}} \quad , \tag{2.56j}$$

where B_N is merely a normalizing coefficient which is set by the amplitude of the source.

Due to cascade connection of the transmission line sections and loading resistances, the current distribution, impedances and current reflection coefficients along the entire line can be obtained by the usual procedure of starting with the stipulated terminal conditions (2.56) and proceeding toward the source. Thus repeated application of equations (2.51) through (2.55) provides the complete solution.

A discretely loaded transmission line analogous to the continuously loaded example that has been analyzed previously is formed by setting h = 1, N = 9, $k_o = \frac{9\pi}{4}$. In this case, the resistive loading consists of 9 lumped resistances spaced $\frac{1}{8}$ wavelength apart on an otherwise lossless uniform transmission line.

The discrete resistance loading functions to be considered here are the quantized analogs of the continuous resistance functions of equation (2.30). Each discrete resistance function has the properties $R_1 = 0$, $R_9 = \frac{C_0}{9}$ ohms to correspond with the continuous loading properties R(0)=0, $R\left(\frac{8}{9}\right) = C_0$ ohms/meter. The general relationship between the discrete and continuous resistance functions is

Thus

$$\Gamma_{n-1} = \frac{Z_0 - R_n - Z_n(0)}{Z_0 + R_n + Z_n(0)} \quad . \tag{2.54}$$

Continuity of current provides the relation

$$I_{n-1}\left(\frac{h}{N}\right) = I_n(0) \quad . \tag{2.55}$$

On the N^{th} or final section of transmission line adjacent to the open circuit termination, the voltage, current, impedance and current reflection coefficient can be stipulated as follows:

$$V_N(z_N) = -j B_N \frac{\cos k_0\left(\frac{h}{N} - z_N\right)}{\sin \frac{k_0 h}{N}} \quad , \tag{2.56a}$$

$$V_N(0) = -j B_N \cot \frac{k_0 h}{N} \quad , \tag{2.56b}$$

$$V_N\left(\frac{h}{N}\right) = -j B_N \csc \frac{k_0 h}{N} \quad , \tag{2.56c}$$

$$I_N(z_N) = \frac{B_N \sin k_0\left(\frac{h}{N} - z_N\right)}{Z_0 \sin \frac{k_0 h}{N}} \quad , \tag{2.56d}$$

$$I_N(0) = \frac{B_N}{Z_0} \quad , \tag{2.56e}$$

$$I_N\left(\frac{h}{N}\right) = 0, \tag{2.56f}$$

$$Z_N(z_n) = -j Z_0 \cot k_0\left(\frac{h}{N} - Z_N\right), \tag{2.56g}$$

$$R_n = \frac{h}{N} R\left(\frac{(n-1)\,h}{N}\right) . \tag{2.57}$$

Thus the discrete resistance distributions are

UNIFORM $$\frac{R_n}{Z_0} = \frac{C_0}{9} , \tag{2.58a}$$

LOGARITHMIC $$\frac{R_n}{Z_0} = \frac{C_0}{9} \frac{\log n}{\log 9} , \tag{2.58b}$$

LINEAR $$\frac{R_n}{Z_0} = \frac{C_0}{9} \frac{n-1}{8} , \tag{2.58c}$$

INVERSE $$\frac{R_n}{Z_0} = \frac{C_0}{9} \left(\frac{1}{8}\right)\left(\frac{9}{10-n} - 1\right), \tag{2.58d}$$

EXPONENTIAL $$\frac{R_n}{Z_0} = \frac{C_0}{9} \frac{a^{n-1} - 1}{a^8 - 1} , \tag{2.58e}$$

IMPULSE $$\frac{R_n}{Z_0} = C_0 \delta_n^9 , \tag{2.58f}$$

where δ_n^9 = the Kronecker delta function. The exponential base a can be expressed in terms of the exponential base b that was employed in the continuous resistance distribution (2.30e)

$$a = b^{1/9} . \tag{2.59}$$

Using the procedure developed above, the complex current distributions produced by each form of resistance function (2.58) have been determined for a range of the magntiude coefficient C_0. Plots of these current distributions, which were calculated at 1/8 wavelength increments along the

transmission lines, are presented in Figs. 2-24 through 2-35. By examining data of the sort included in these figures, an optimum value of C_0 can be determined for each of the forms of resistance loading functions. As was done with the continuous resistance loading, the optimization criterion is maximum radiation from the transmission line. To maximize radiation, $\int_0^h |I|\,dz$ is maximized within the constraint of requiring a nearly linear phase variation $\psi(z)$ for the current. The optimum values of C_0 that are determined in this way are listed in the following table.

Functional Form of Discrete Resistance Distribution	Optimum Magnitude Coefficient C_0
UNIFORM	3.6
LOGARITHMIC	8.3
LINEAR	7.2
INVERSE	18.0
EXPONENTIAL	18.0
IMPULSE	1.4

TABLE 2-3: OPTIMUM MAGNITUDE COEFFICIENTS FOR VARIOUS DISCRETE RESISTANCE DISTRIBUTIONS.

It is also seen from Figs. 2-24 through 2-35 that the inverse form of resistance distribution is more effective than the other functional forms in maximizing radiation. From this data, the set of individually optimized resistance loading functions can be ranked in order of decreasing effectiveness. Table 2-4 gives the ranking.

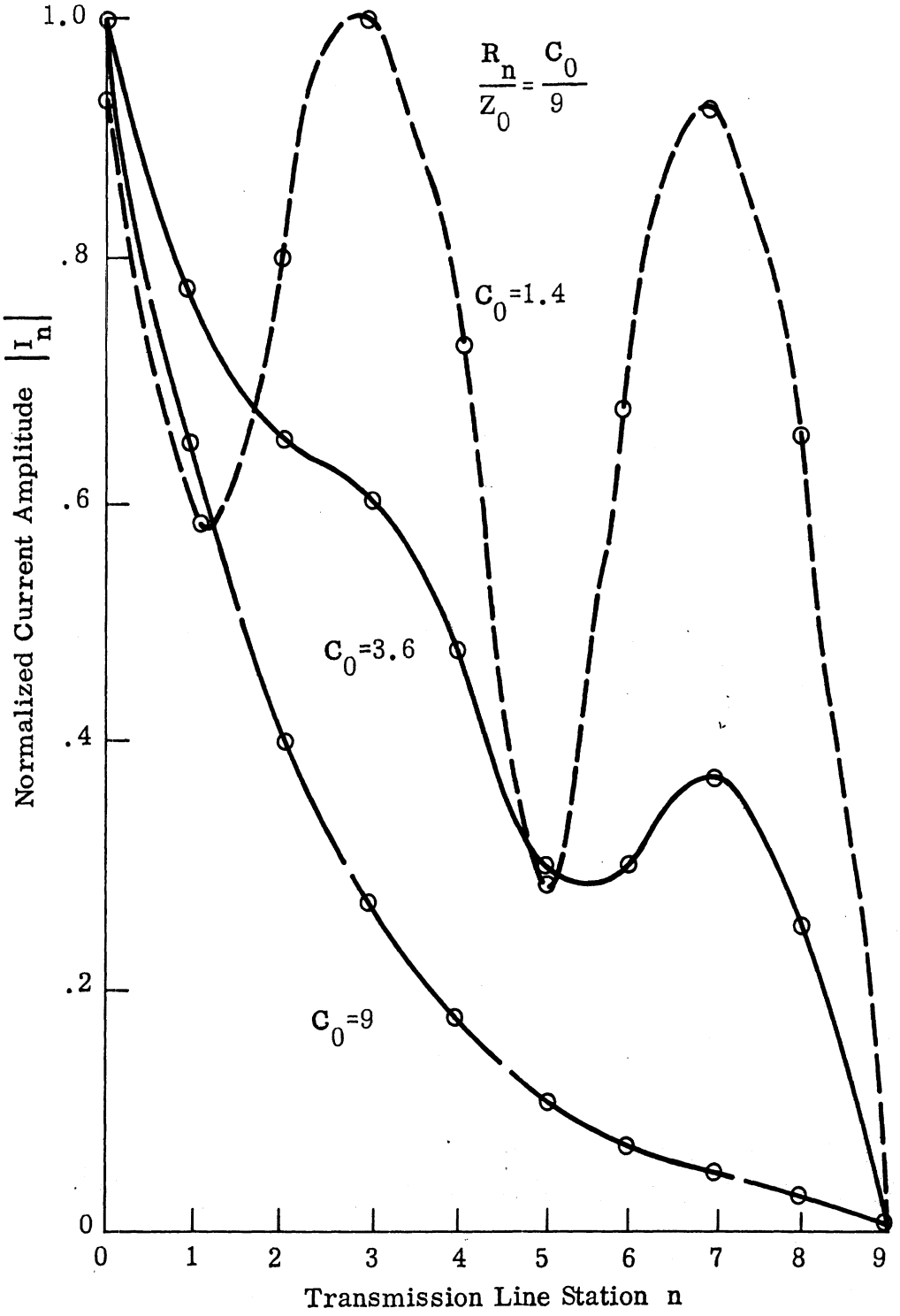

FIG. 2-24: AMPLITUDE OF CURRENT ALONG TRANSMISSION LINE PRODUCED BY DISCRETE UNIFORM RESISTANCE LOADING.

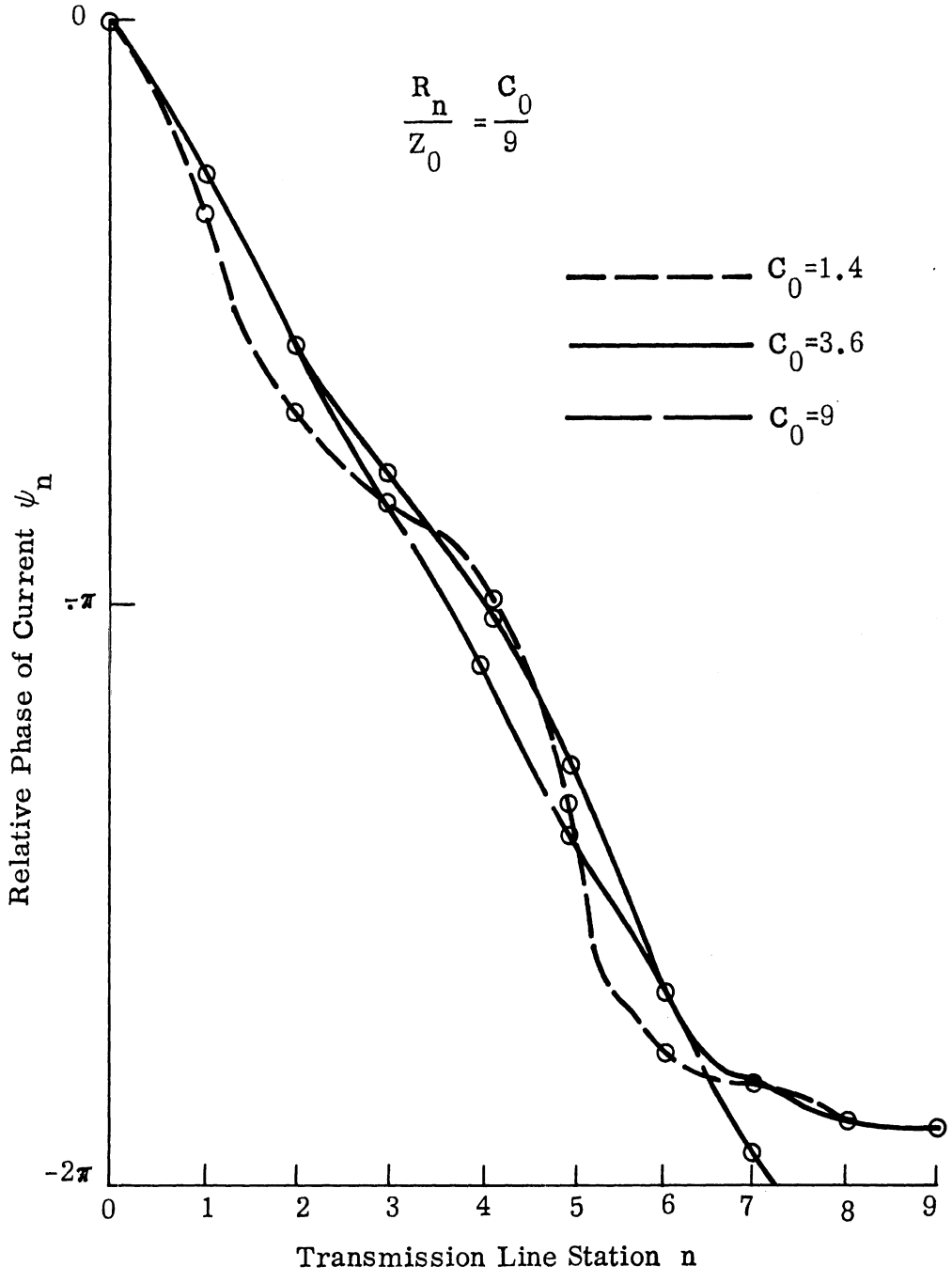

FIG. 2-25: PHASE OF CURRENT ALONG TRANSMISSION LINE PRODUCED BY DISCRETE UNIFORM RESISTANCE LOADING.

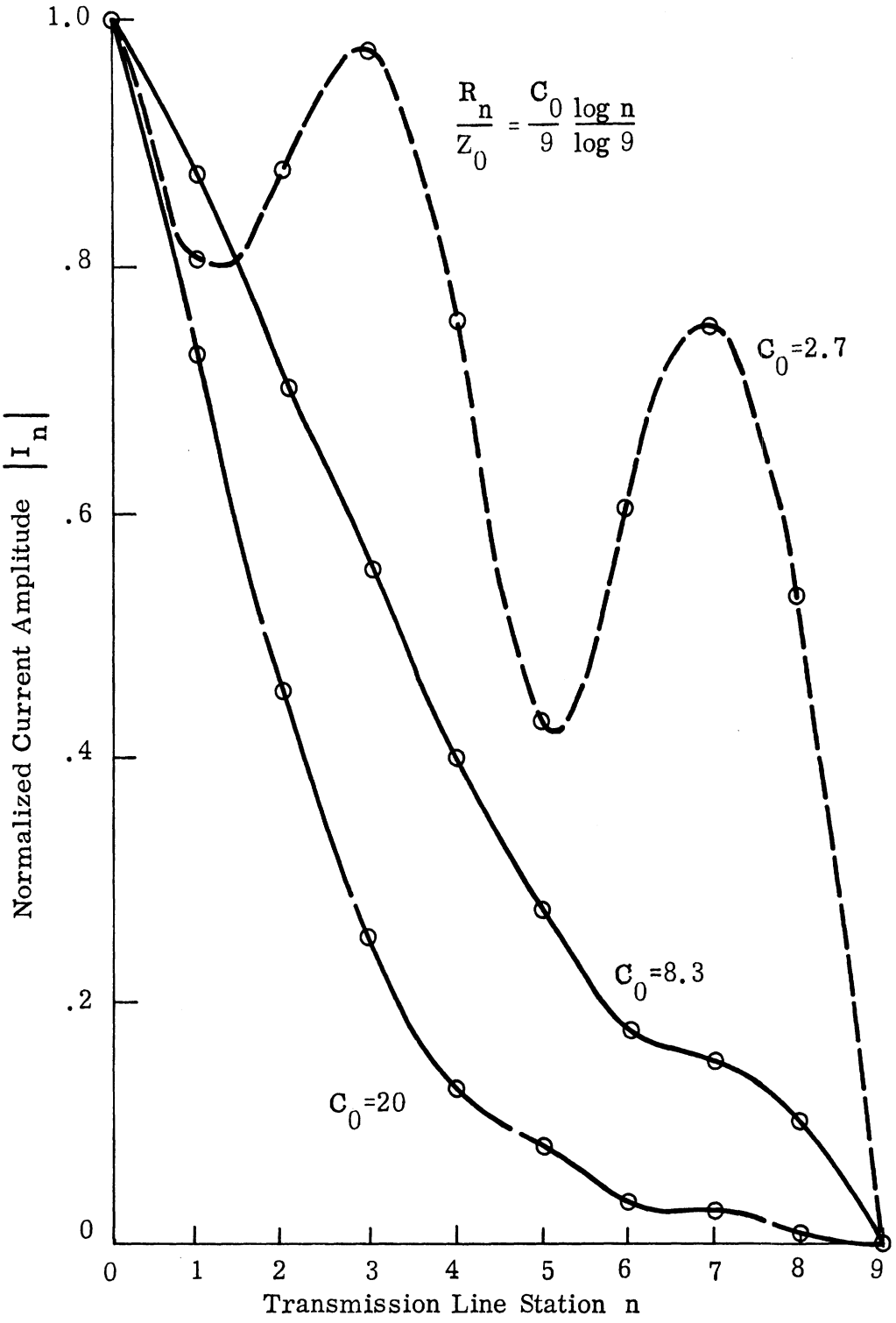

FIG. 2-26: AMPLITUDE OF CURRENT ALONG TRANSMISSION LINE PRODUCED BY DISCRETE LOGARITHMIC RESISTANCE LOADING.

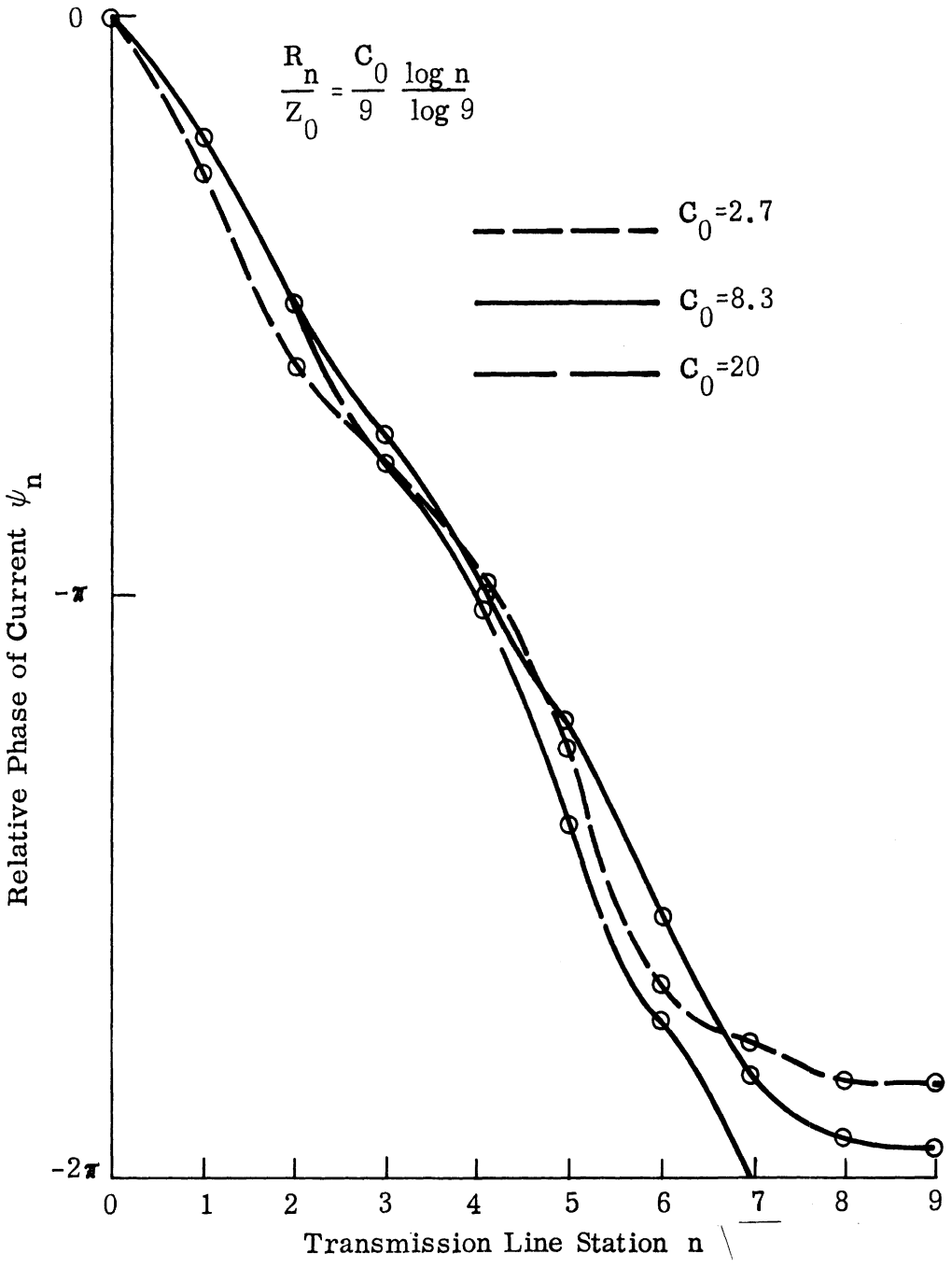

FIG. 2-27: PHASE OF CURRENT ALONG TRANSMISSION LINE PRODUCED BY DISCRETE LOGARITHMIC RESISTANCE LOADING.

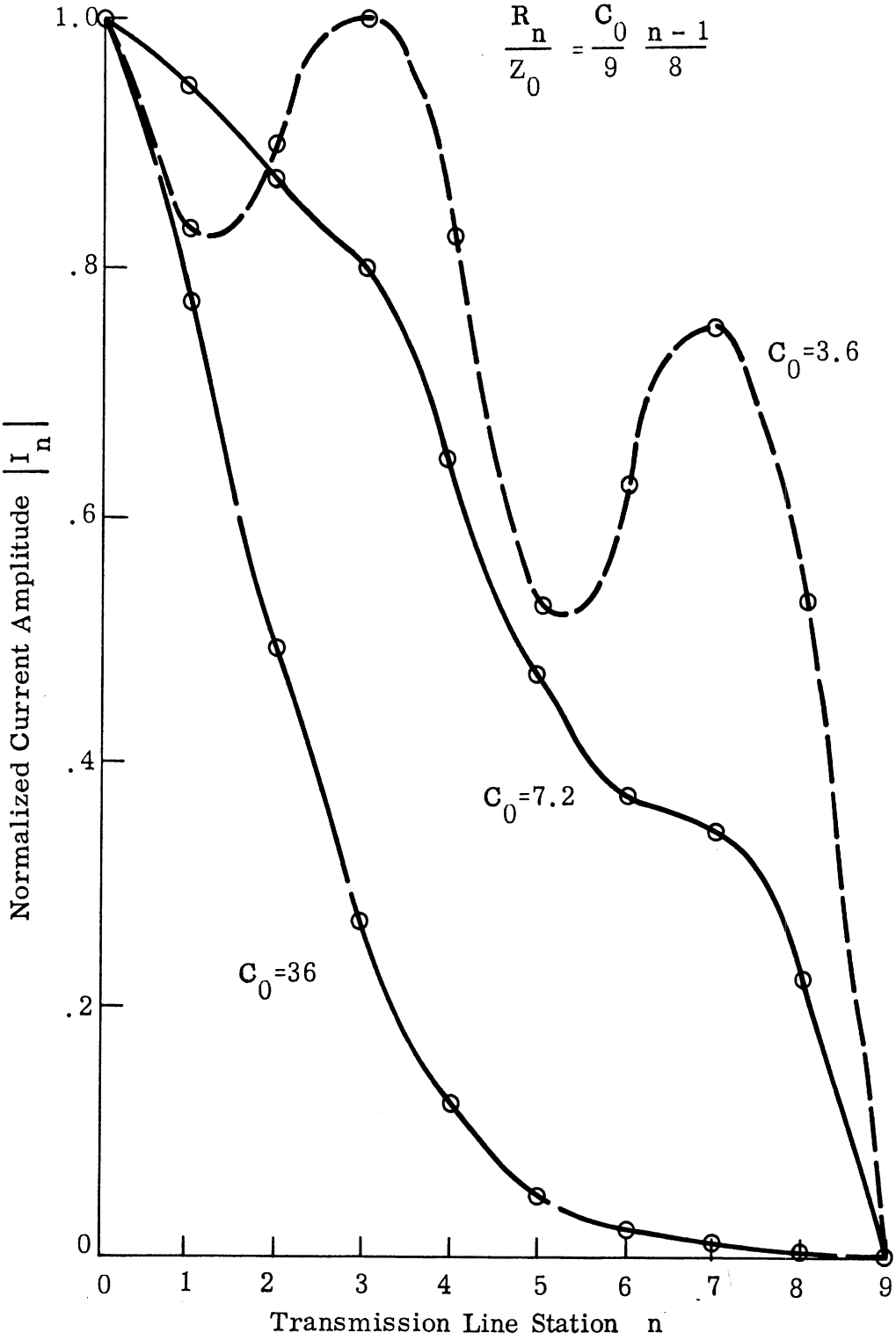

FIG. 2-28: AMPLITUDE OF CURRENT ALONG TRANSMISSION LINE PRODUCED BY DISCRETE LINEAR RESISTANCE LOADING.

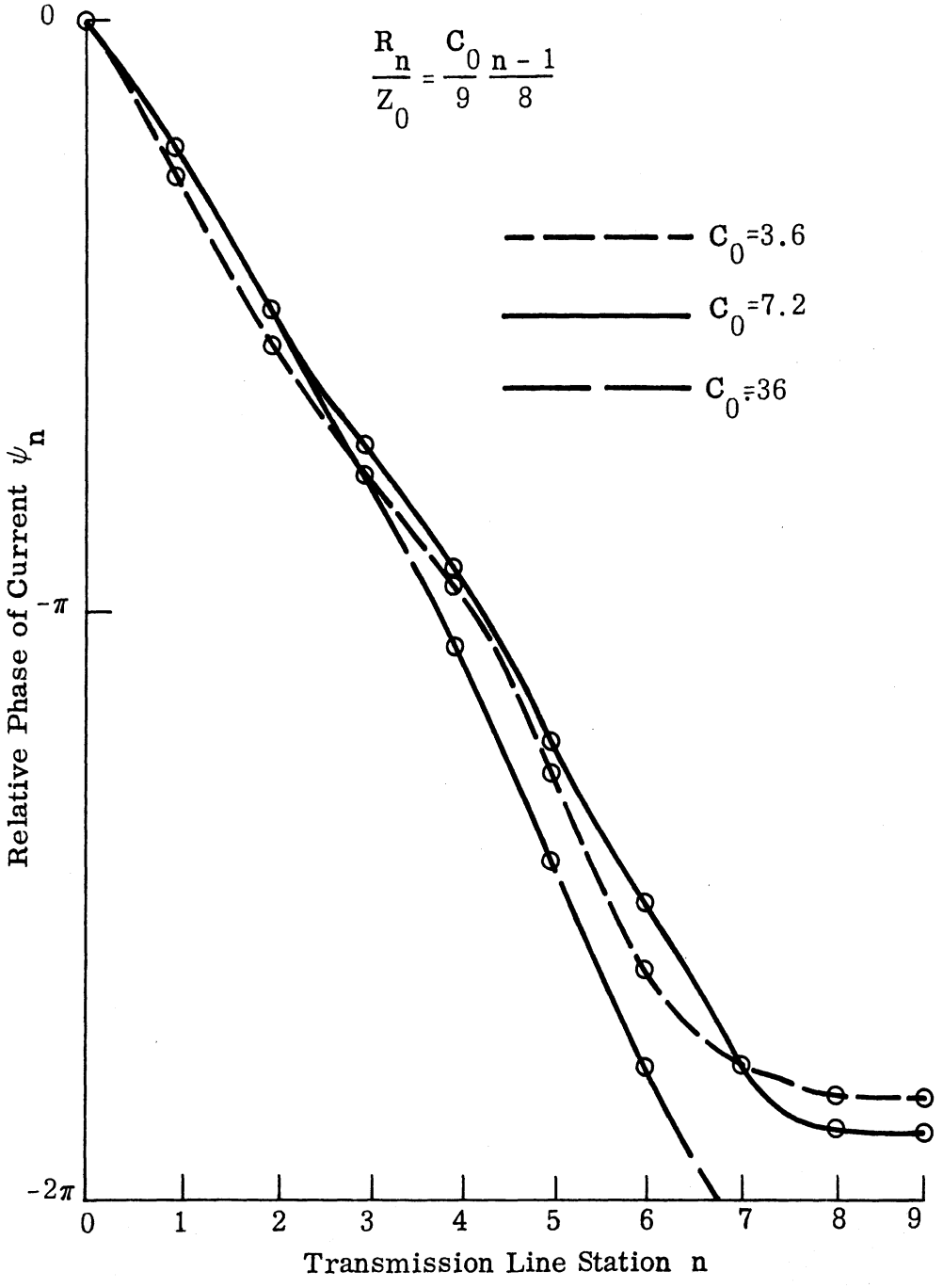

FIG. 2-29: PHASE OF CURRENT ALONG TRANSMISSION LINE PRODUCED BY DISCRETE LINEAR RESISTANCE LOADING.

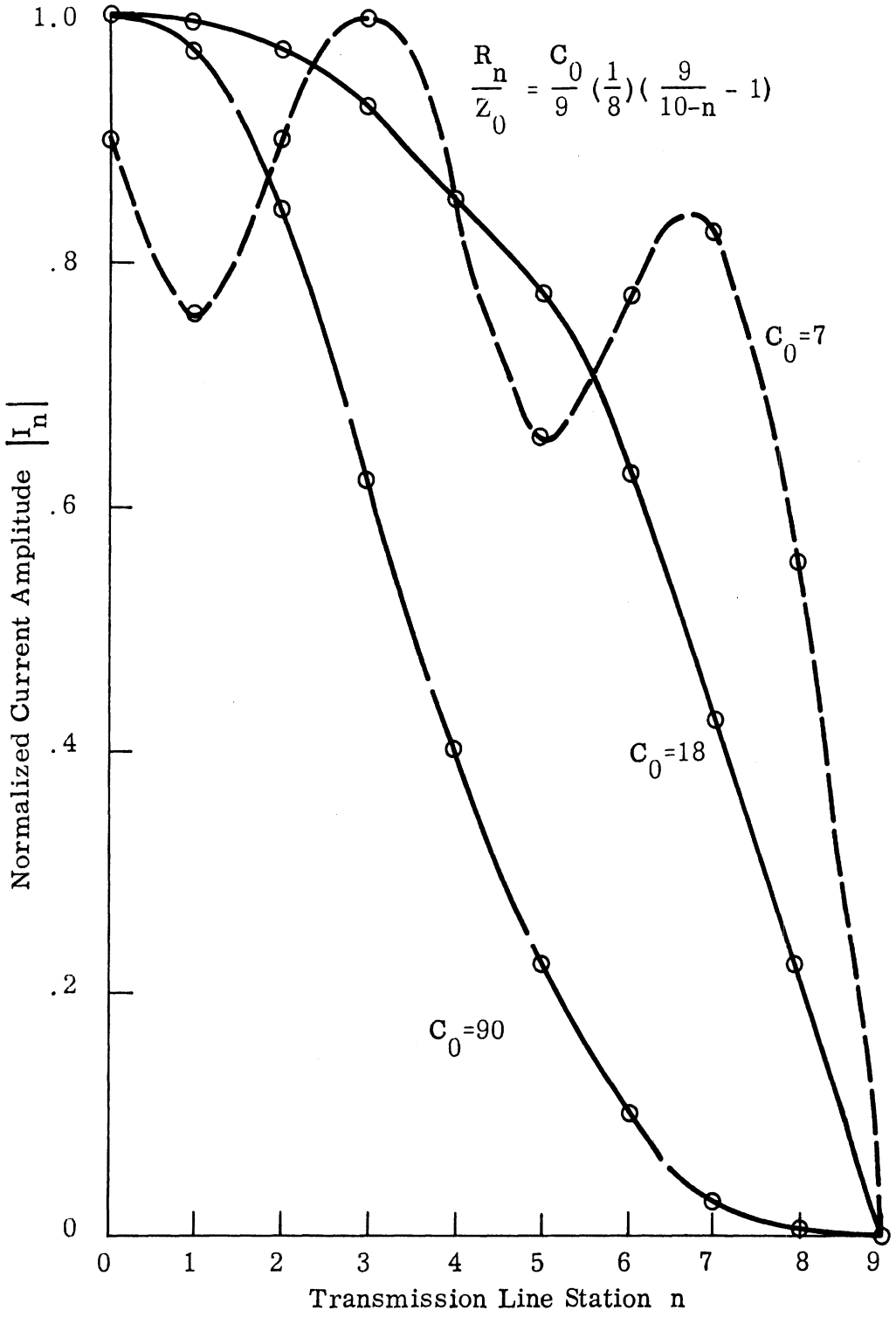

FIG. 2-30: AMPLITUDE OF CURRENT ALONG TRANSMISSION LINE PRODUCED BY DISCRETE INVERSE RESISTANCE LOADING.

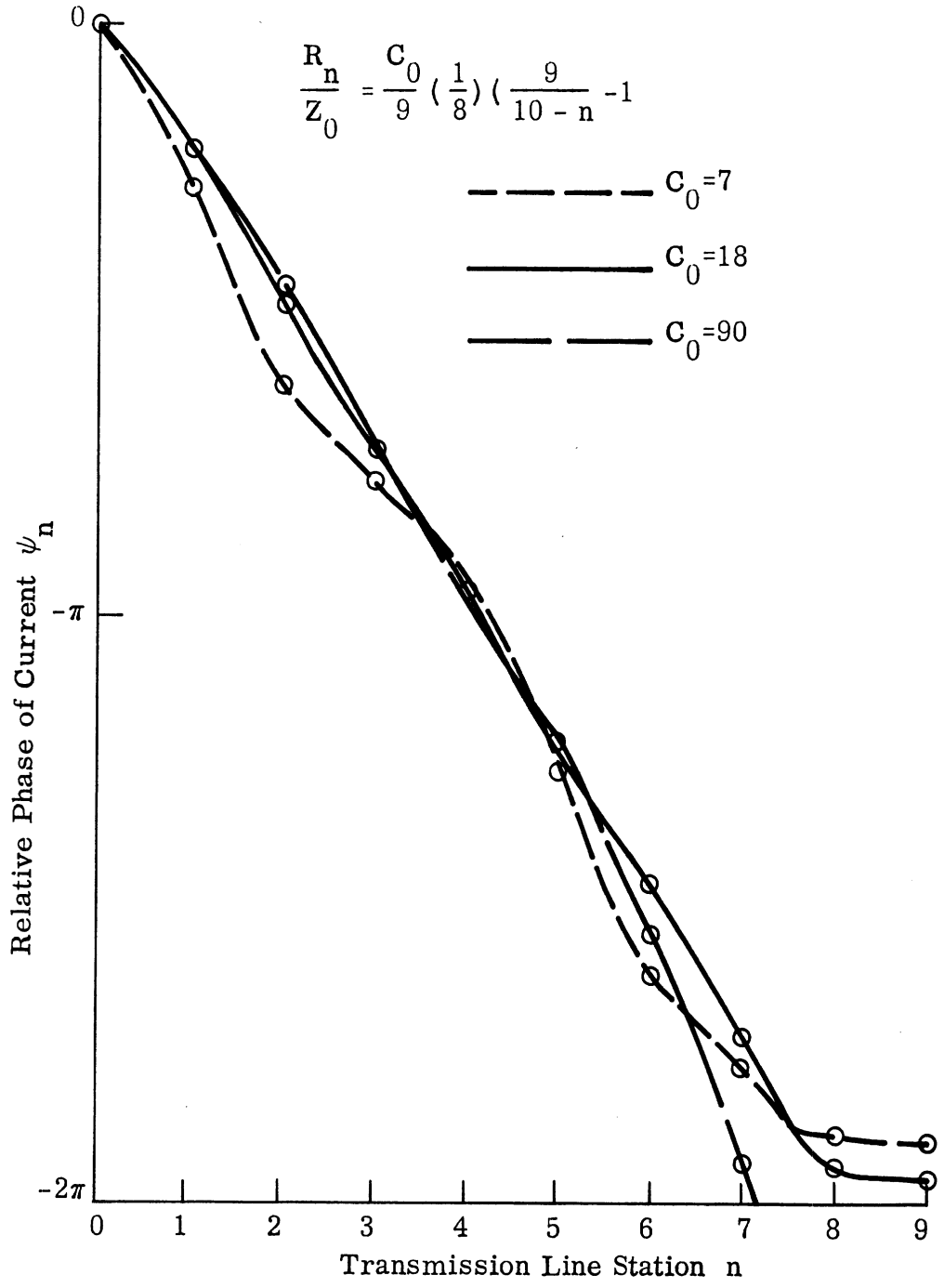

FIG. 2-31: PHASE OF CURRENT ALONG TRANSMISSION LINE PRODUCED BY DISCRETE INVERSE RESISTANCE LOADING.

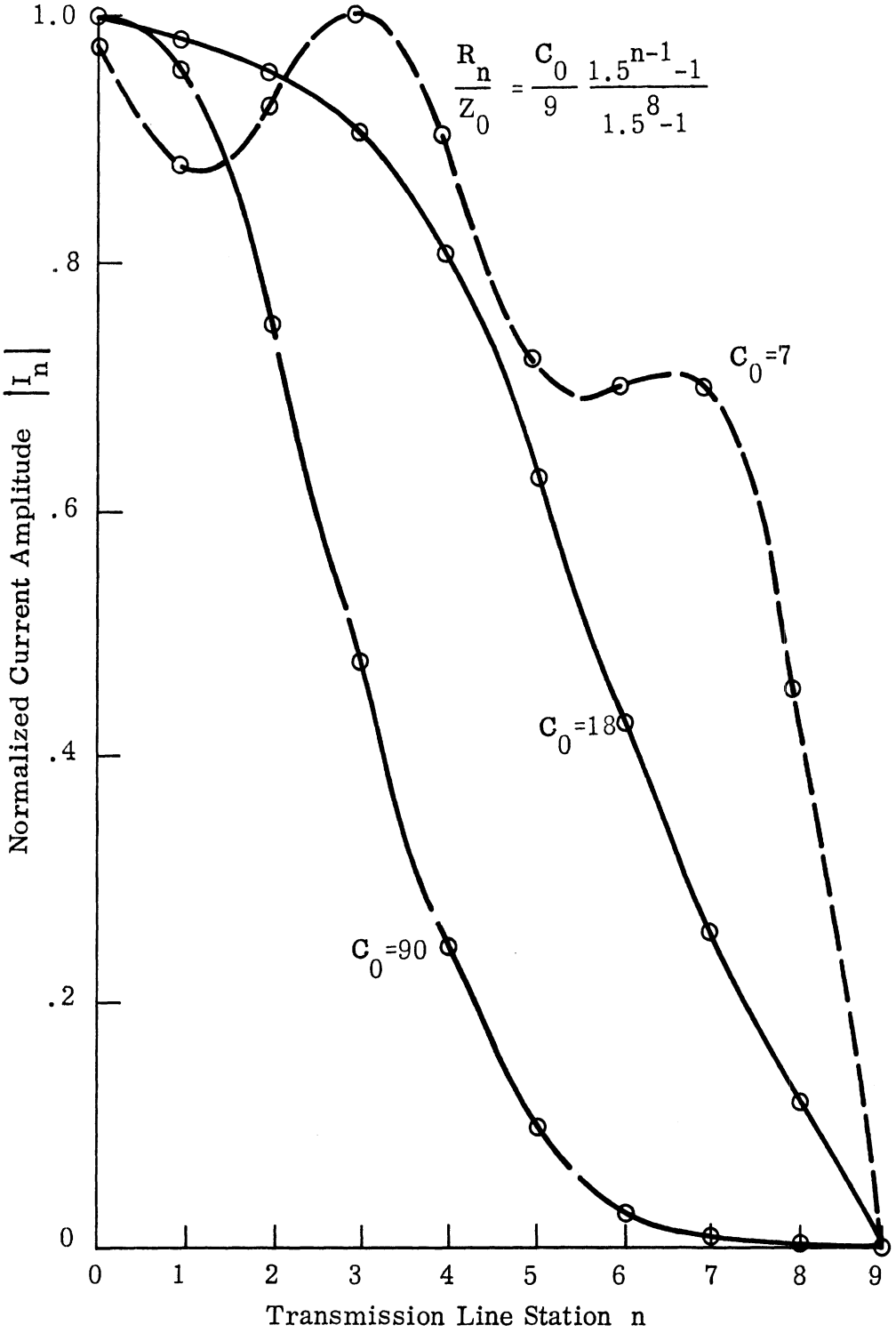

FIG. 2-32: AMPLITUDE OF CURRENT ALONG TRANSMISSION LINE PRODUCED BY DISCRETE EXPONENTIAL RESISTANCE LOADING.

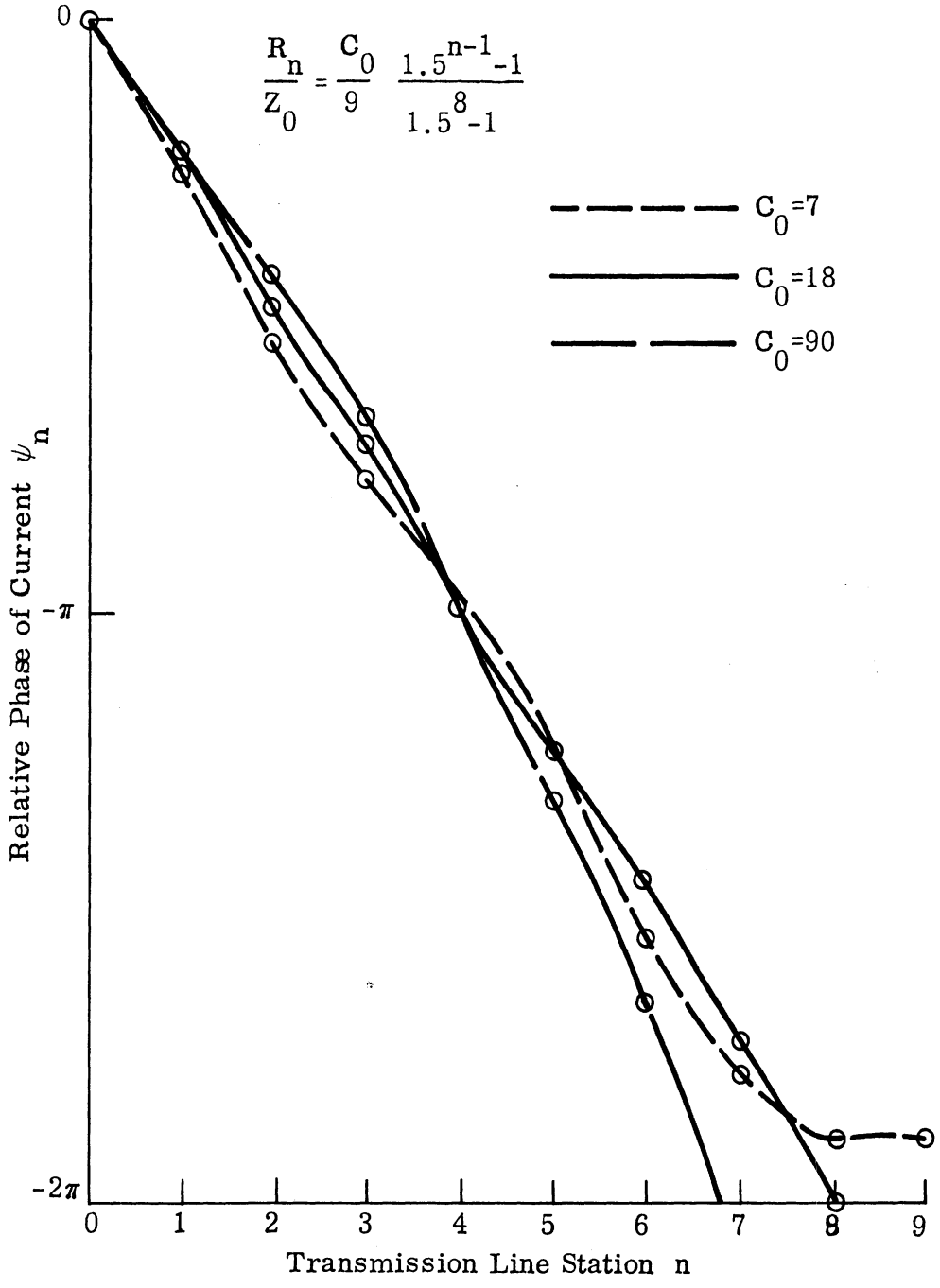

FIG. 2-33: PHASE OF CURRENT ALONG TRANSMISSION LINE PRODUCED BY DISCRETE EXPONENTIAL RESISTANCE LOADING.

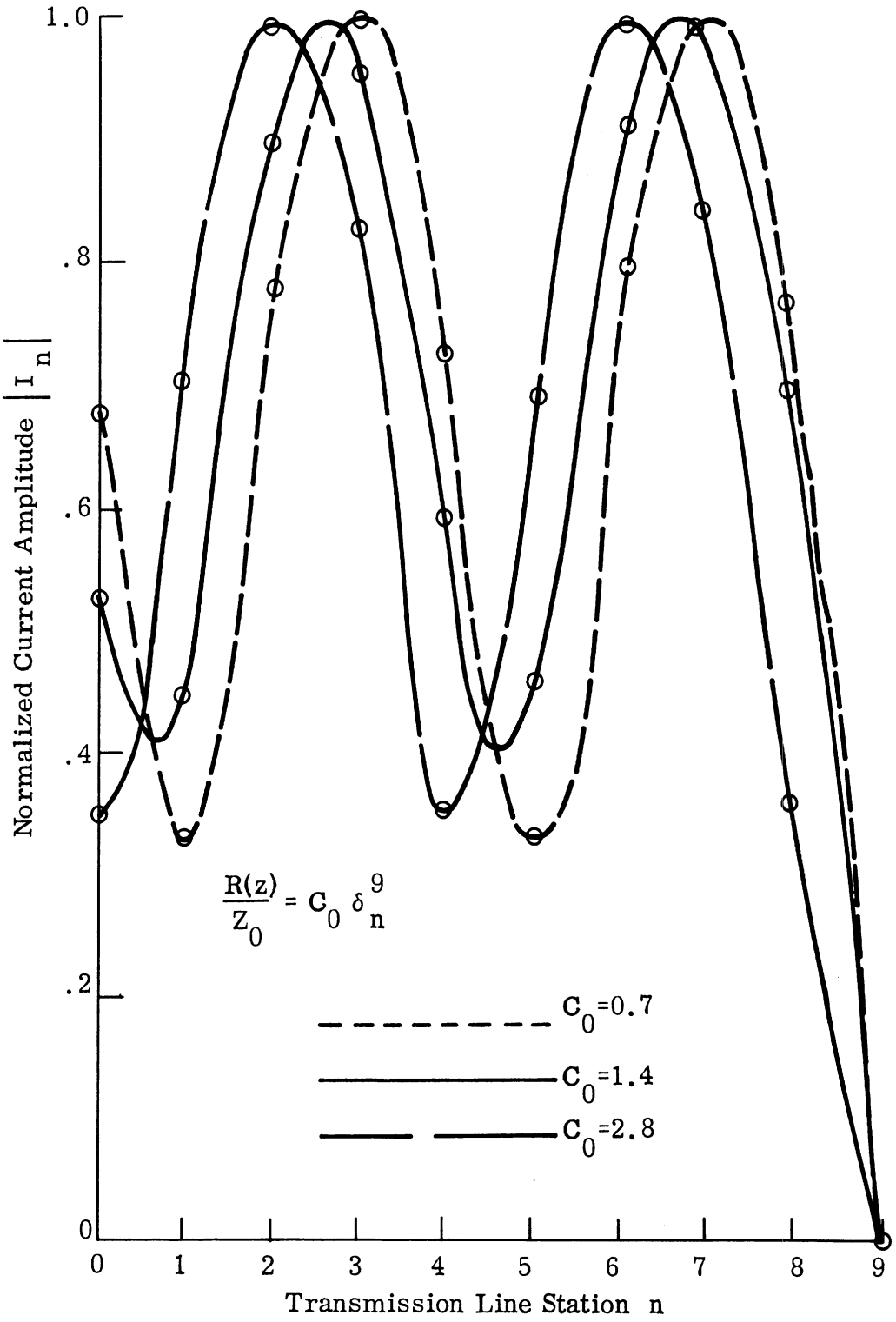

FIG. 2-34: AMPLITUDE OF CURRENT ALONG TRANSMISSION LINE PRODUCED BY DISCRETE IMPULSE RESISTANCE LOADING.

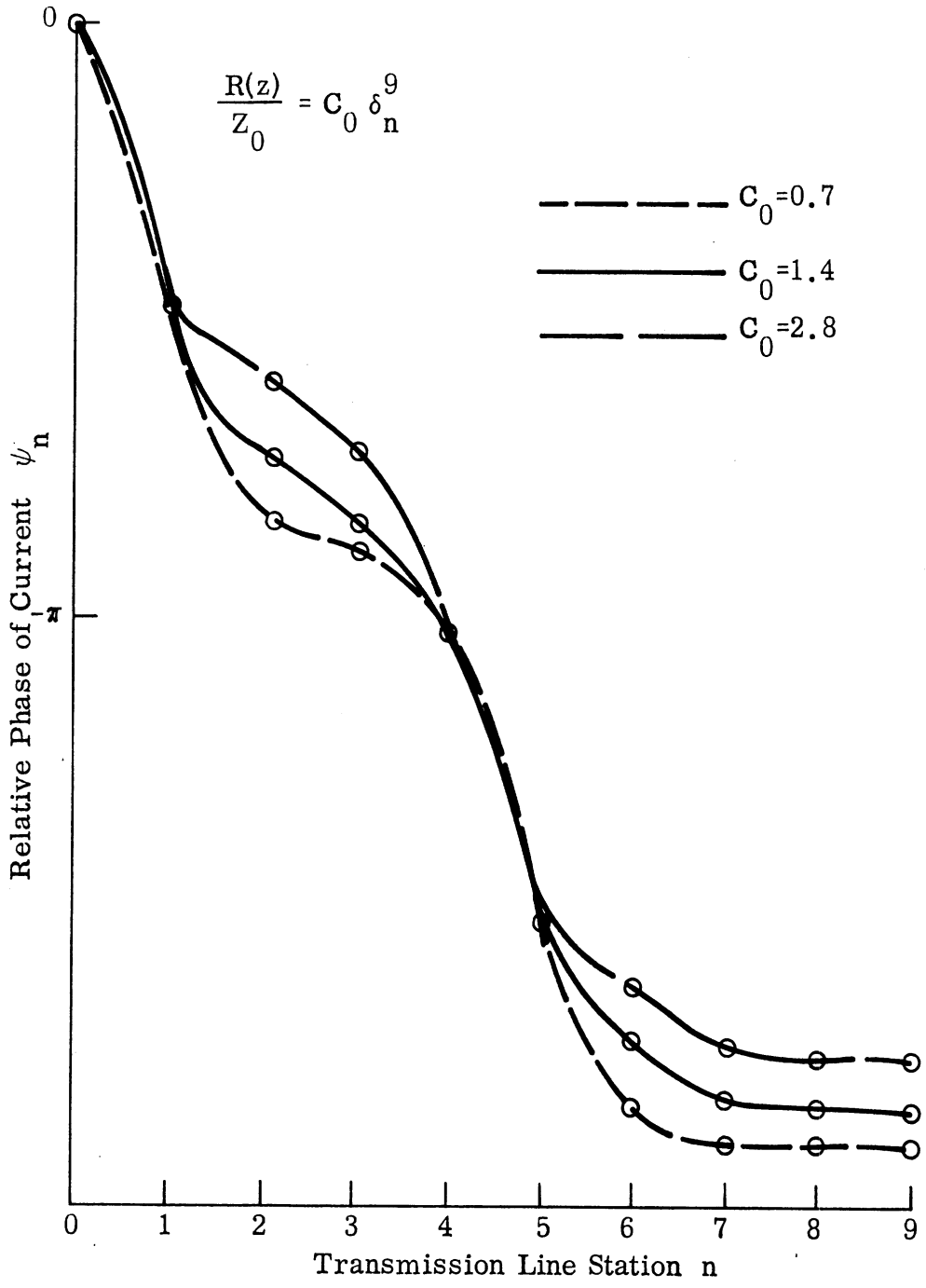

FIG. 2-35: PHASE OF CURRENT ALONG TRANSMISSION LINE PRODUCED BY DISCRETE IMPULSE RESISTANCE LOADING.

INVERSE	$\frac{R_n}{Z_0} = 18\left(\frac{1}{72}\right)\left(\frac{9}{10-n} - 1\right)$
EXPONENTIAL	$\frac{R_n}{Z_0} = 18\left(\frac{1}{9}\right)\left(\frac{1.5^{n-1} - 1}{1.5^{8} - 1}\right)$
LINEAR	$\frac{R_n}{Z_0} = 7.2\ \frac{n-1}{72}$
LOGARITHMIC	$\frac{R_n}{Z_0} = 8.3\ \frac{\log n}{9 \log 9}$
UNIFORM	$\frac{R_n}{Z_0} = 3.6\ \left(\frac{1}{9}\right)$
IMPULSE	$\frac{R_n}{Z_0} = 1.4\ \delta_n^9$

TABLE 2-4: PREFERENTIAL ORDER OF VARIOUS DISCRETE RESISTANCE DISTRIBUTIONS.

The impedance of a discrete resistance loaded transmission line as a function of position along the line can be calculated by repeated use of equations (2.50) through (2.56). Smith chart plots of such impedances for each of the individually optimized loading functions are shown in Figs. 2-36 through 2-41. It is observed from these plots that the relative effectiveness of the various loading functions in producing matched impedances along the transmission line is given by the same ranking as in Table 2-4. The transmission line input reflection coefficients $|\Gamma_{in}|$ plotted in Fig. 2-42, also show the same ranking. This figure displays in addition the dependence of $|\Gamma_{in}|$ on the parameter C_0 for each of the

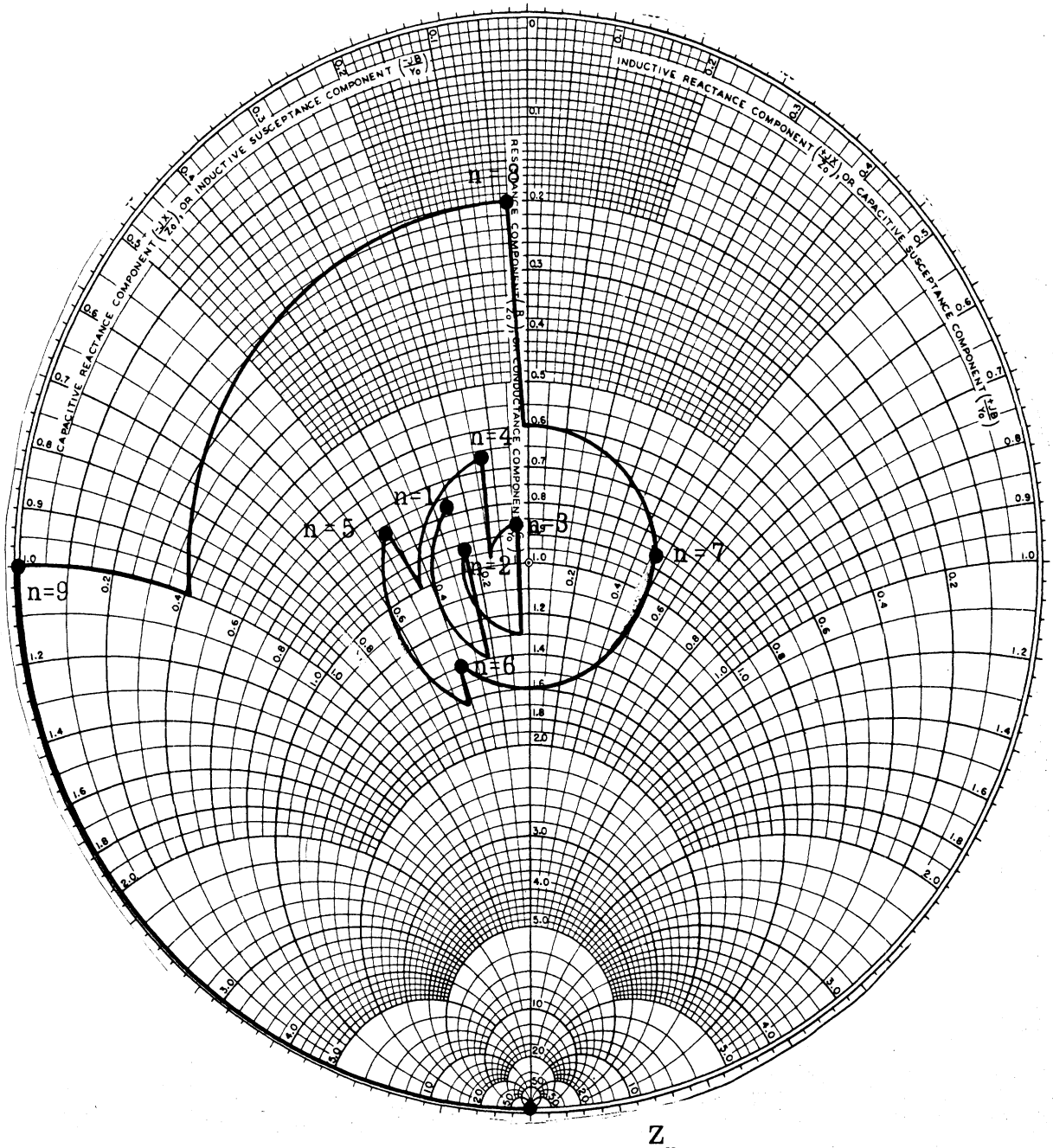

FIG. 2-36: IMPEDANCES ALONG TRANSMISSION LINE WITH UNIFORM DISCRETE RESISTANCE LOADING $\frac{R_n}{Z_0} = 0.4$.

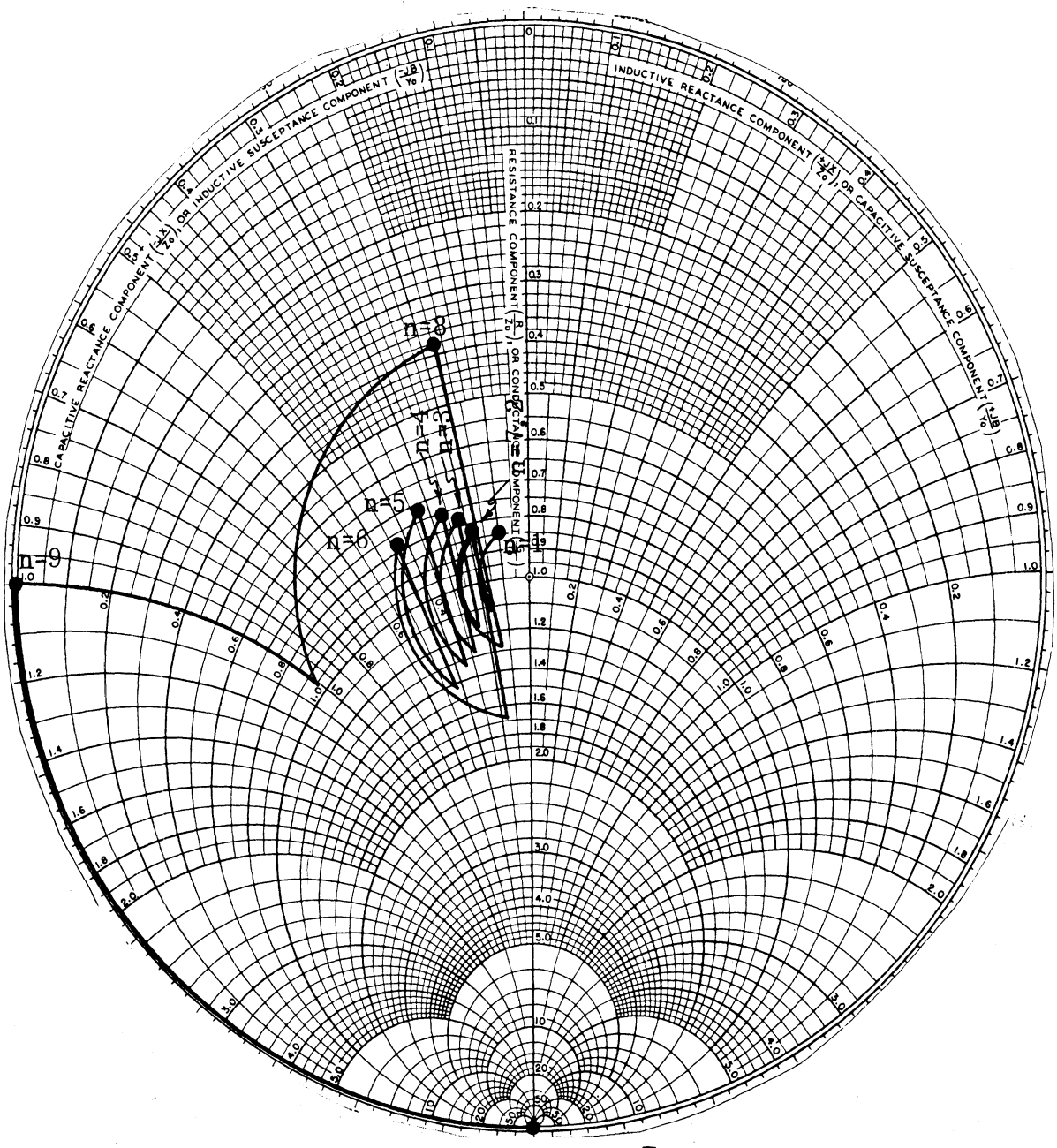

Normalized Impedance $\frac{Z_n}{Z_0}$

FIG. 2-37: IMPEDANCES ALONG TRANSMISSION LINE WITH LOGARITHMIC DISCRETE RESISTANCE LOADING $\frac{R_n}{Z_0} = 8.3 \frac{\log n}{9 \log 9}$.

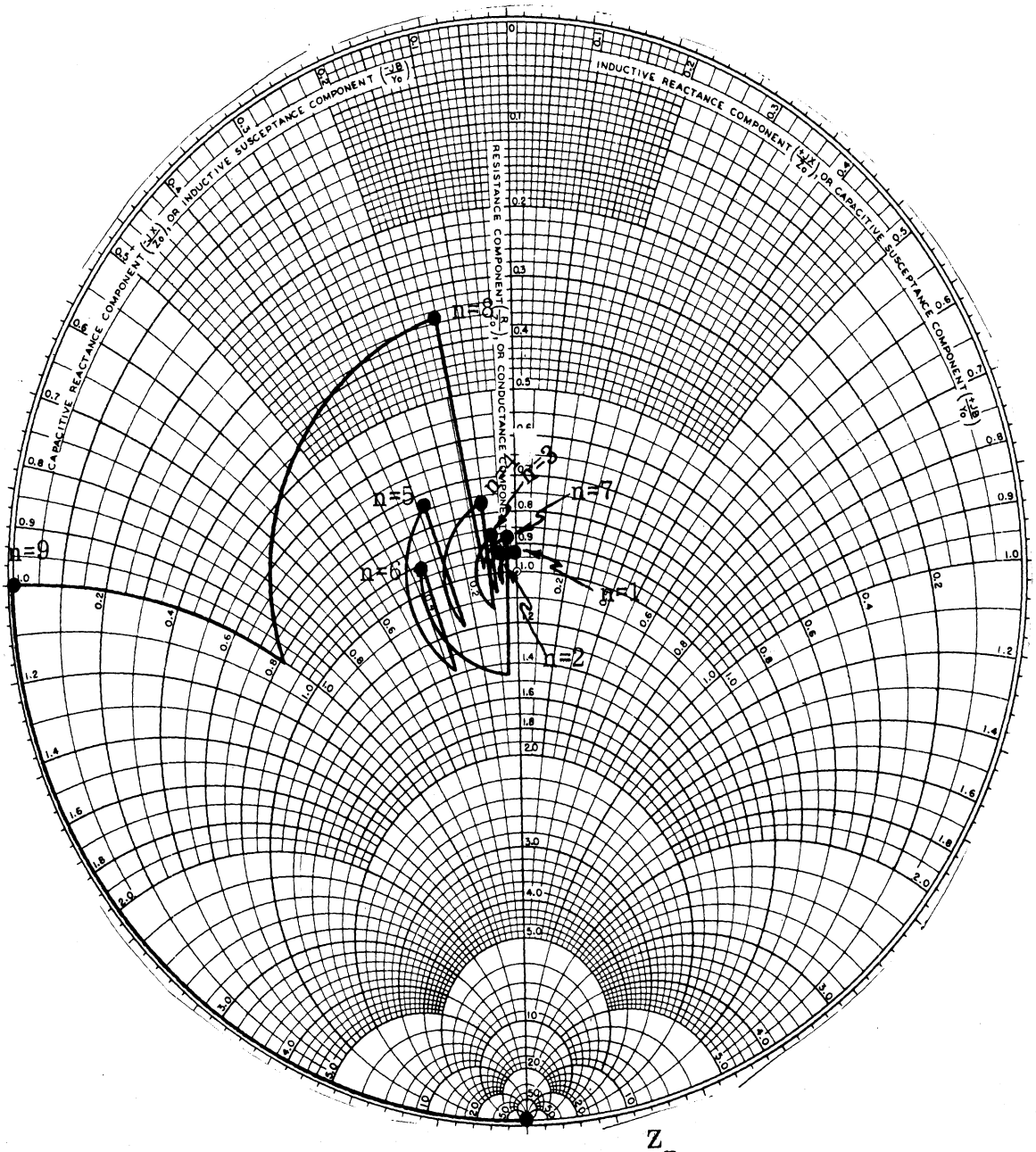

Normalized Impedance $\frac{Z_n}{Z_0}$

FIG. 2-38: IMPEDANCES ALONG TRANSMISSION LINE WITH LINEAR DISCRETE RESISTANCE LOADING

$$\frac{R_n}{Z_0} = 7.2\,\frac{n-1}{72}\ .$$

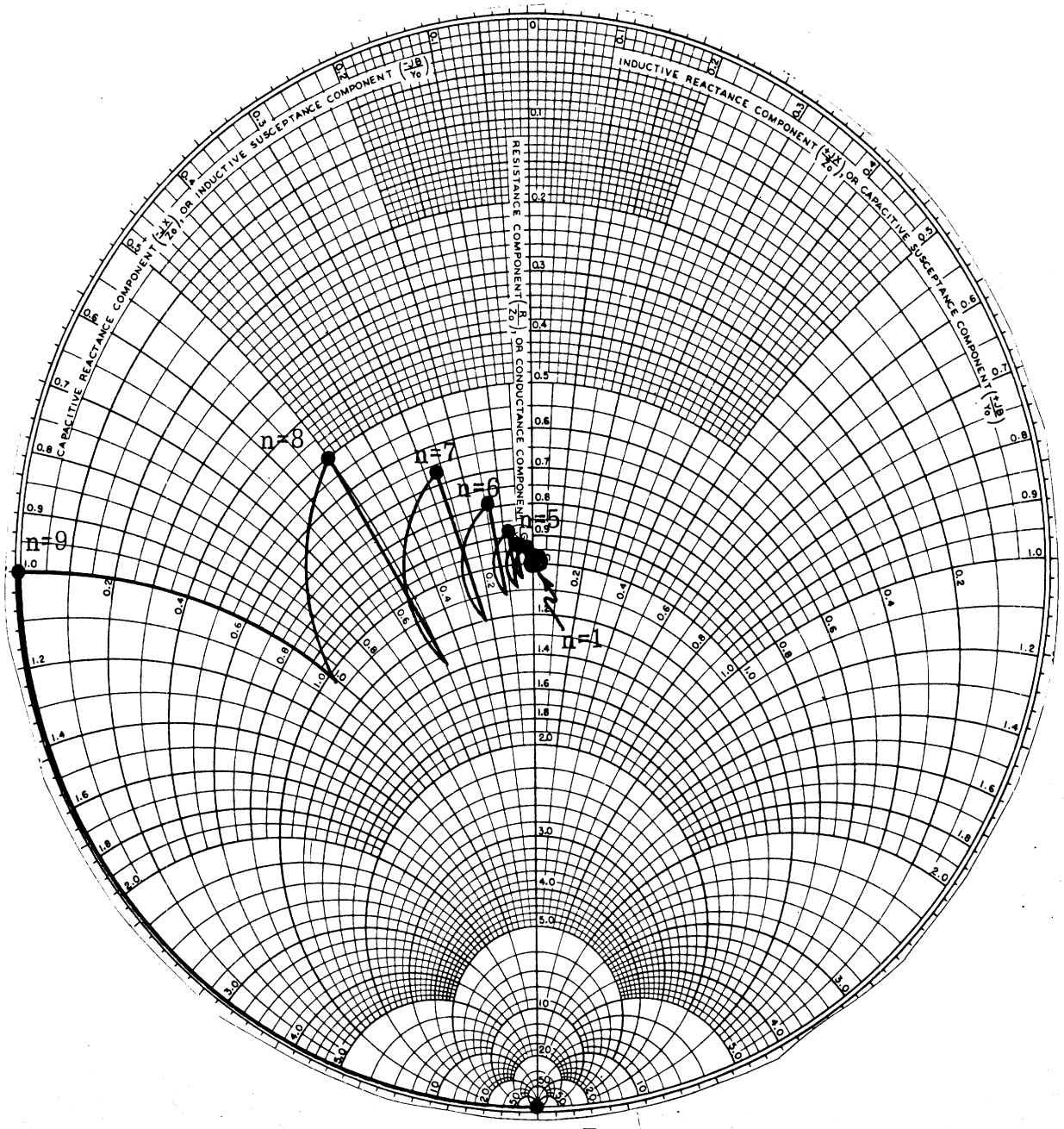

Normalized Impedance $\frac{Z_n}{Z_0}$

FIG. 2-39: IMPEDANCES ALONG TRANSMISSION LINE WITH INVERSE DISCRETE RESISTANCE LOADING

$$\frac{R_n}{Z_0} = 18\left(\frac{1}{72}\right)\left(\frac{9}{10-n} - 1\right).$$

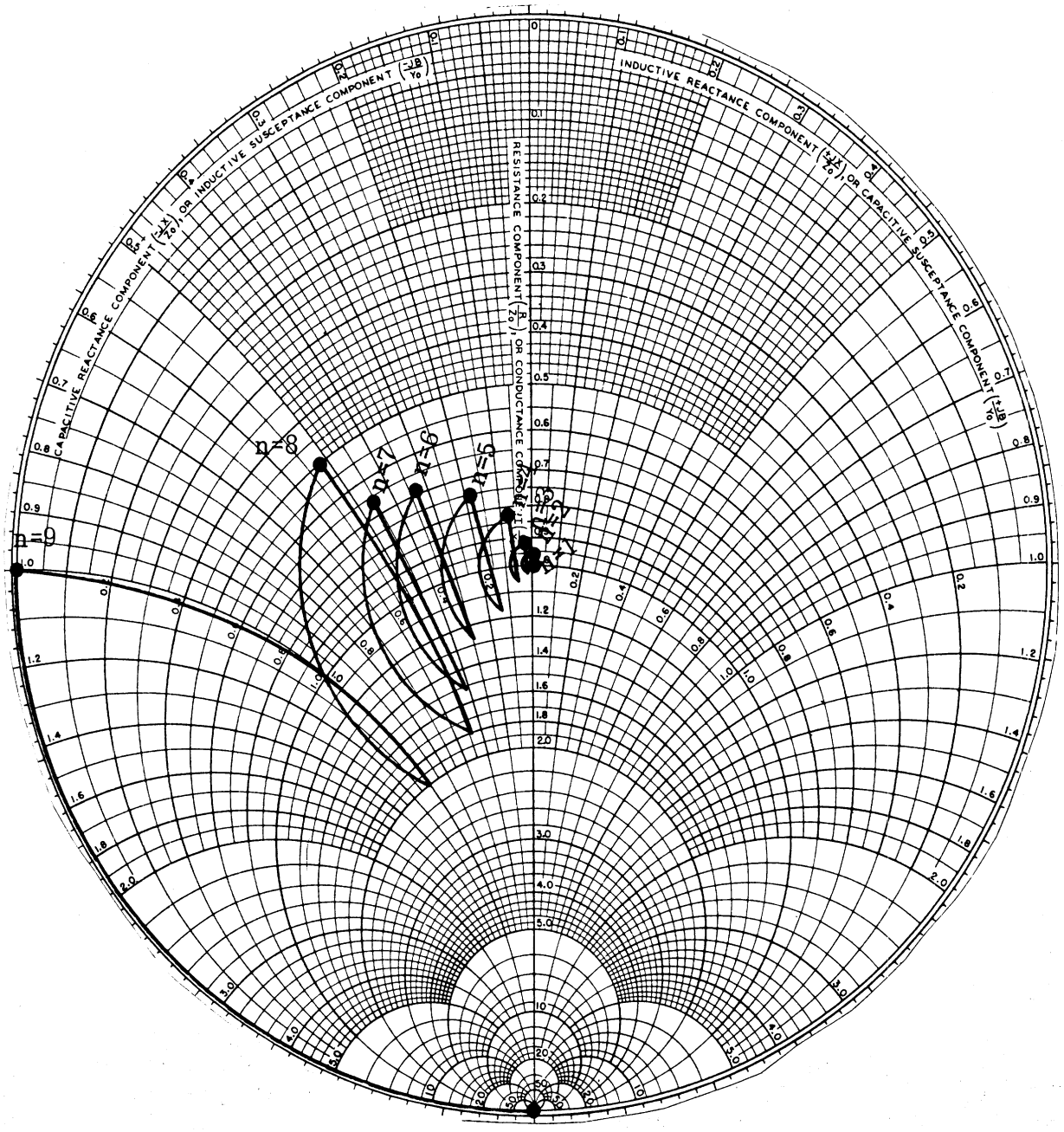

FIG. 2-40: IMPEDANCES ALONG TRANSMISSION LINE WITH EXPONENTIAL DISCRETE RESISTANCE LOADING $\frac{R_n}{Z_0} = 18\left(\frac{1}{9}\right)\left(\frac{1.5^{n-1}-1}{1.5^{8}-1}\right)$.

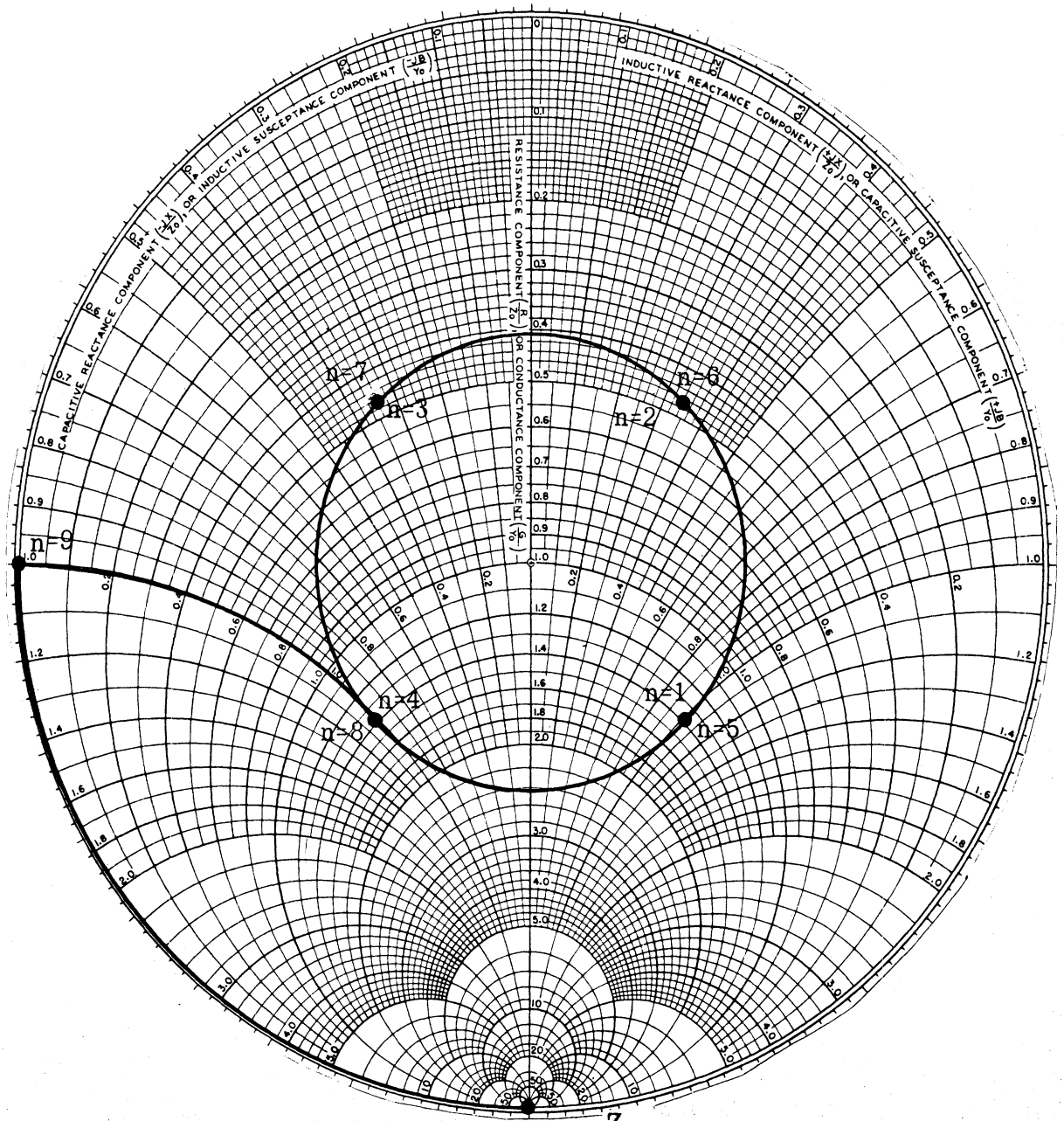

FIG. 2-41: IMPEDANCES ALONG TRANSMISSION LINE WITH IMPULSE DISCRETE RESISTANCE LOADING $\frac{R_n}{Z_0} = 1.4\ \delta_n^9$.

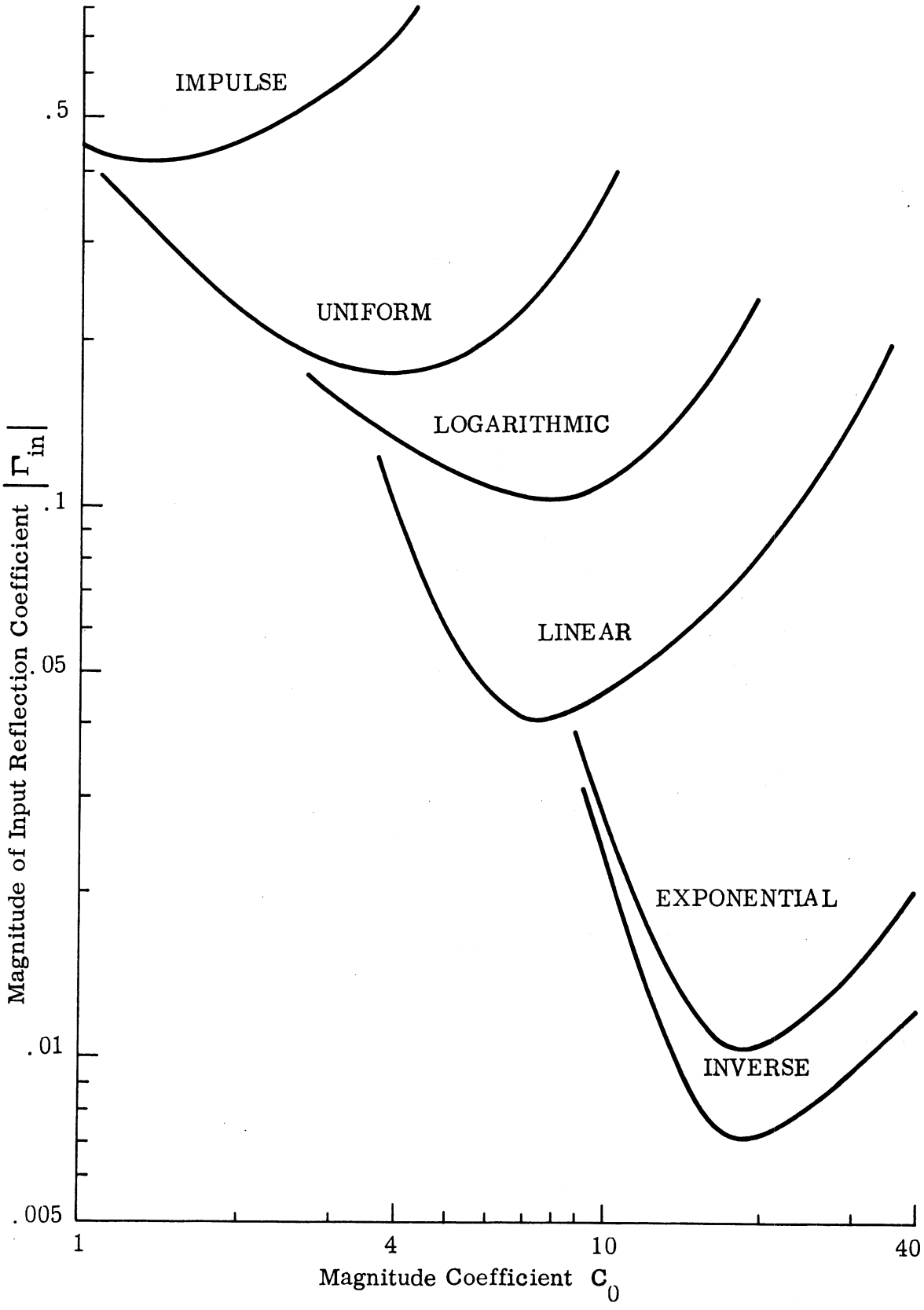

FIG. 2-42: INPUT REFLECTION COEFFICIENTS PRODUCED BY VARIOUS DISCRETE RESISTANCE DISTRIBUTIONS

functional forms of discrete resistance loading. The values of C_0 which minimize $|\Gamma_{in}|$ are seen to be the same as the optimum values of Table 2-3 which maximize radiation from the transmission line.

Throughout this analysis of the discrete resistance loading of transmission lines, the results have been virtually identical to those obtained previously for continuous resistance loading. The 1/8 wavelength spacing of resistances produces very nearly the same complex current distribution and transmission line impedances as a continuum of resistance loading. Detailed conclusions about the results parallel those of the continuous loading case and need not be repeated.

2.9 Excitation Voltage Source

The source of excitation of the resistance-loaded transmission lines which are investigated here is a transient voltage generator. It is convenient to synthesize the source waveform from its frequency spectral components and then apply the inverse Fourier transform to the transient analysis. In the interests of computational efficiency, the Fast Fourier Transform technique of truncating an infinite series is employed. Within any one period of the resulting periodic source voltage waveform, an arbitrarily close approximation to the idealized transient waveform of interest can be obtained.

A source waveform of particular interest in this study is the step function $u(t-t_0)$. The step function waveform is well suited to a time domain analysis of the transient features of transmission lines as has been shown for lossless lines [54, 55, 56]. The sharp, localized discontinuity in an ideal or approximate step function wave traveling on a transmission line serves to identify sharply the multiple reflections. Another advantage is that the step waveform possesses a derivative which is positive only and is of short duration. As the time variation in a waveform is the cause of radiation, this simplicity is desirable in analyzing the transient radiation

field of a transmission line. In these respects, a step function is superior to an impulse function which has both positive and negative derivatives and a correspondingly longer duration of its time variation. Ambiguities can arise through the overlap or merging of transient effects in the case of a non-zero rise time of an approximate step function. It is therefore desirable that the rise time of a practical approximate step function be as short as possible within the constraints of economical computations with the function's truncated series representation.

In the present investigation, it is computationally economical to approximate a step function waveform by a square wave which is an odd function of time with the time origin occurring at a step rise as in Fig. 2-43a. In this way, the waveform can be a simple sine series which involves only odd harmonics. Thus the voltage source waveform is

$$v_s(t) = \sum_{k=1}^{K} \frac{4(2K-1)}{\pi^2(2k-1)^2} \sin\frac{\pi(2k-1)}{2(2K-1)} \sin(2k-1)\omega_1 t \qquad (2.60)$$

where ω_1 is the fundamental radian frequency and t is time. Figures 2-43b and 2-43c show the approximate waveforms, including the Gibbs' phenomenon, that have been computed from (2.60) for K = 25 and K = 50.

Due to attenuation caused by the resistance loading of the transmission line, a step function wave traveling on the line will have appreciable amplitude at most for the first few of its multiple reflections from the ends of the line. For this reason, the duration τ of each step in the periodic square wave can be limited to the order of ten transmission line transit times:

$$\tau = 10\frac{h}{c}, \qquad (2.61)$$

where h is the transmission line length and c is the propagation velocity along the line.

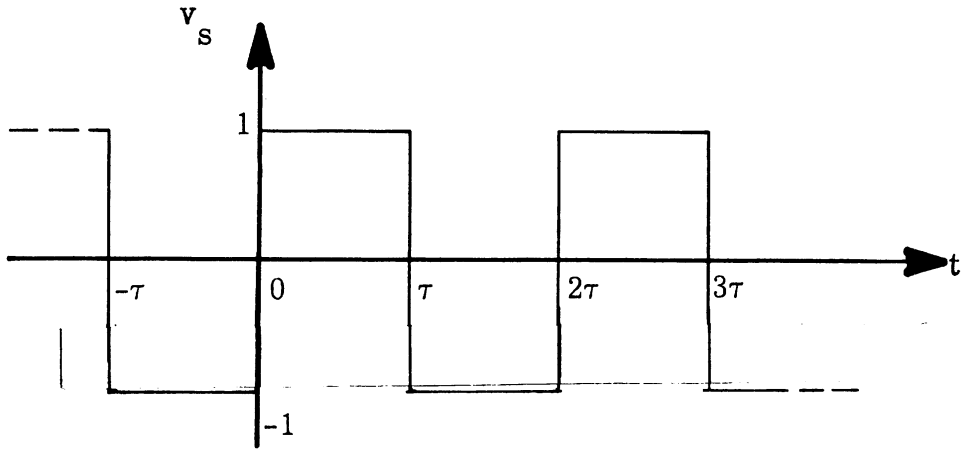

(A) Ideal Square Wave with Period 2τ.

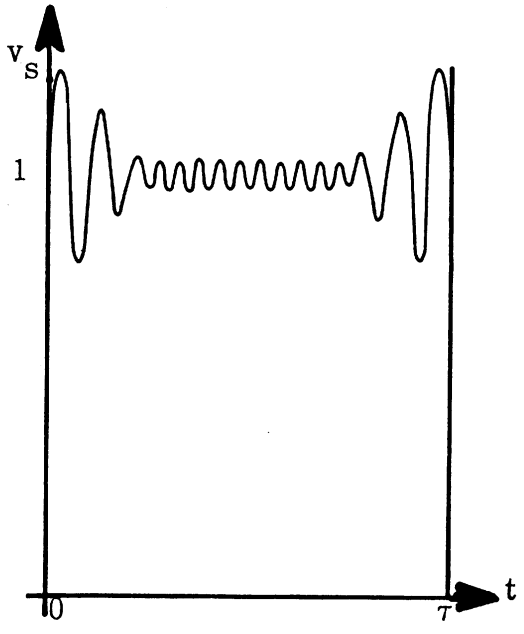

(B) 25-Term Approximation to Square Wave.

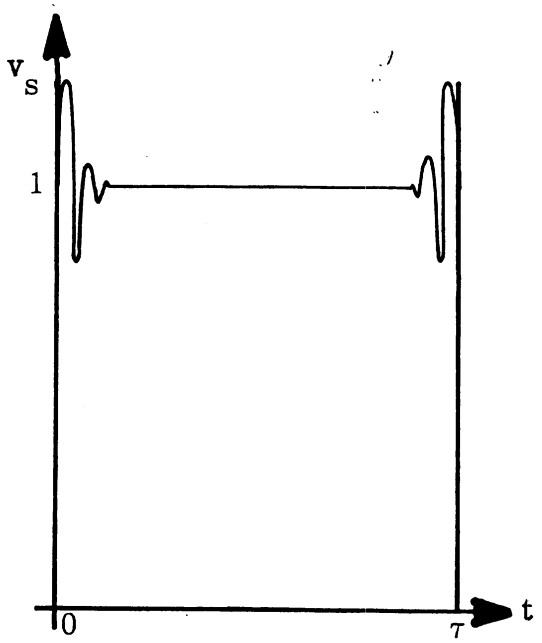

(C) 50-Term Approximation to Square Wave

FIG. 2-43: SQUARE WAVE VOLTAGE SOURCE WAVEFORM.

Once the transmission line responses to an approximate step function are determined, they can be differentiated with respect to time to yield approximate impulse responses. The impulse responses can then be convolved with any general source waveform to produce the transmission line responses to that general waveform. Numerical time domain convolution of a source waveform with an approximate impulse response whose features of interest lie within the short time τ can be performed efficiently.

The frequency spectral representation of the transient source voltage in convenient phasor notation is

$$v_s(t) = \sum V_s(\omega)\, e^{j\omega t} \tag{2.62}$$

where $V_s(\omega)$ is the complex amplitude

$$V_s(\omega) = -j\, \frac{4(2K-1)\,\omega_1^2}{\pi^2\,\omega^2}\, \sin\frac{\pi\,\omega}{2(2K-1)\omega_1} \,. \tag{2.63}$$

In the frequency domain, the Thevenin equivalent circuit of the excitation source consists of an ideal voltage source $V_s(\omega)$ in series with an internal impedance $Z_s(\omega)$ as indicated in Fig. 2-44. The input impedance of the resistance-loaded transmission line to which the excitation source is attached is designated $Z_{in}(\omega)$. In the frequency domain the input current is designated

$$I(0,\omega) = \frac{V_s(\omega)}{Z_s(\omega) + Z_{in}(\omega)} \,. \tag{2.64}$$

A representative illustration of these frequency domain quantities is provided by the case of an approximate step function voltage source driving the transmission line which was determined to be optimally loaded (2.31).

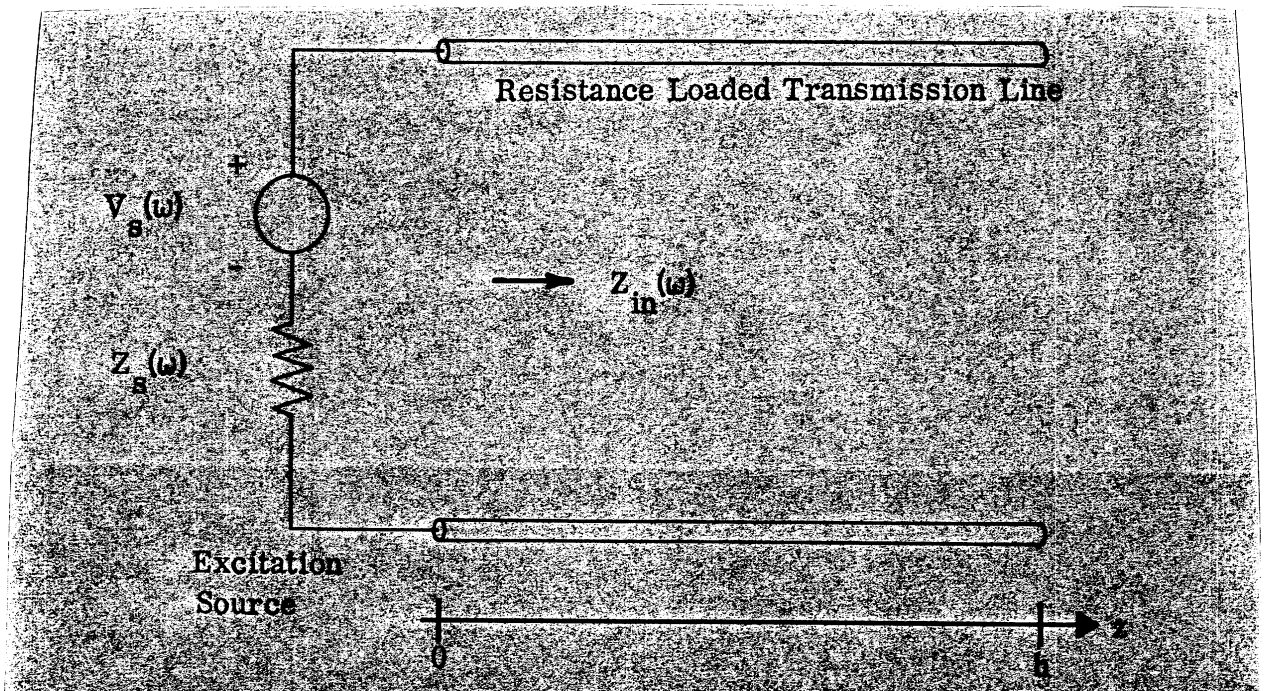

FIG. 2-44: TRANSMISSION LINE WITH SOURCE OF EXCITATION IN THE FREQUENCY DOMAIN

This loaded transmission line's input impedance, computed from (2.32) is shown in Fig. 2-45. A constant source impedance $Z_s(\omega)=Z_0=300$ ohms was used for these calculations inasmuch as it matches the high-frequency limit of $Z_{in}(\omega)$ and thereby represents an appropriate design goal for a generator. Figure 2-46 shows the frequency spectrum envelopes of the voltage source (2.63) and the resulting input current (2.64). In this illustration, K = 99 so that 50 odd harmonic components synthesize an approximate step function for the voltage source.

In the time domain, the shapes of the voltage source waveform (2.62) and the input current waveform

$$i(0, t) = \sum I(0,\omega)\, e^{j\omega t} \qquad (2.65)$$

are not the same. For the present illustration, Fig. 2-47 shows the approximate step function source voltage waveform and the resulting input current waveform.

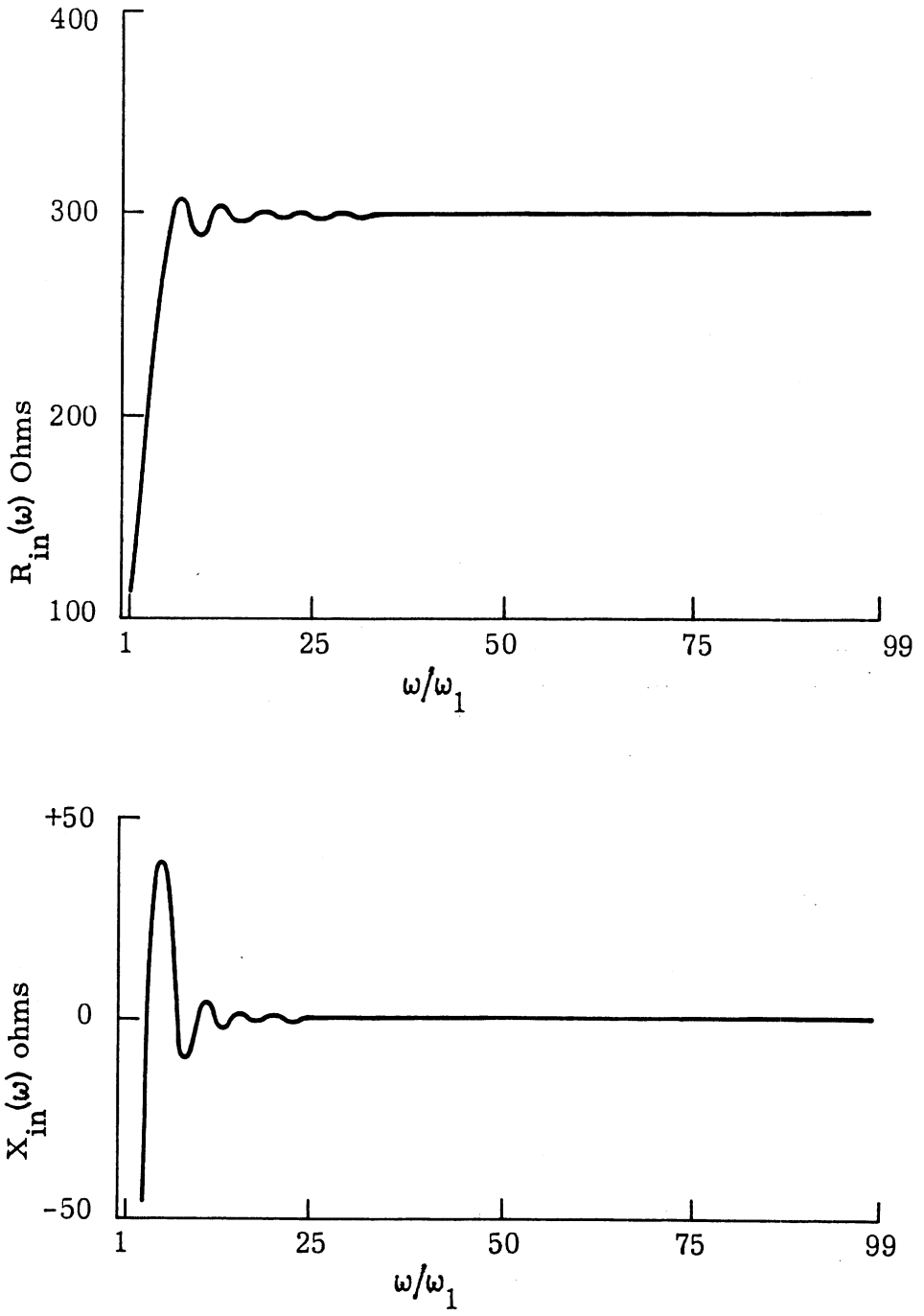

FIG. 2-45: INPUT IMPEDANCE VERSUS FREQUENCY FOR OPTIMUM RESISTANCE-LOADED TRANSMISSION LINE.

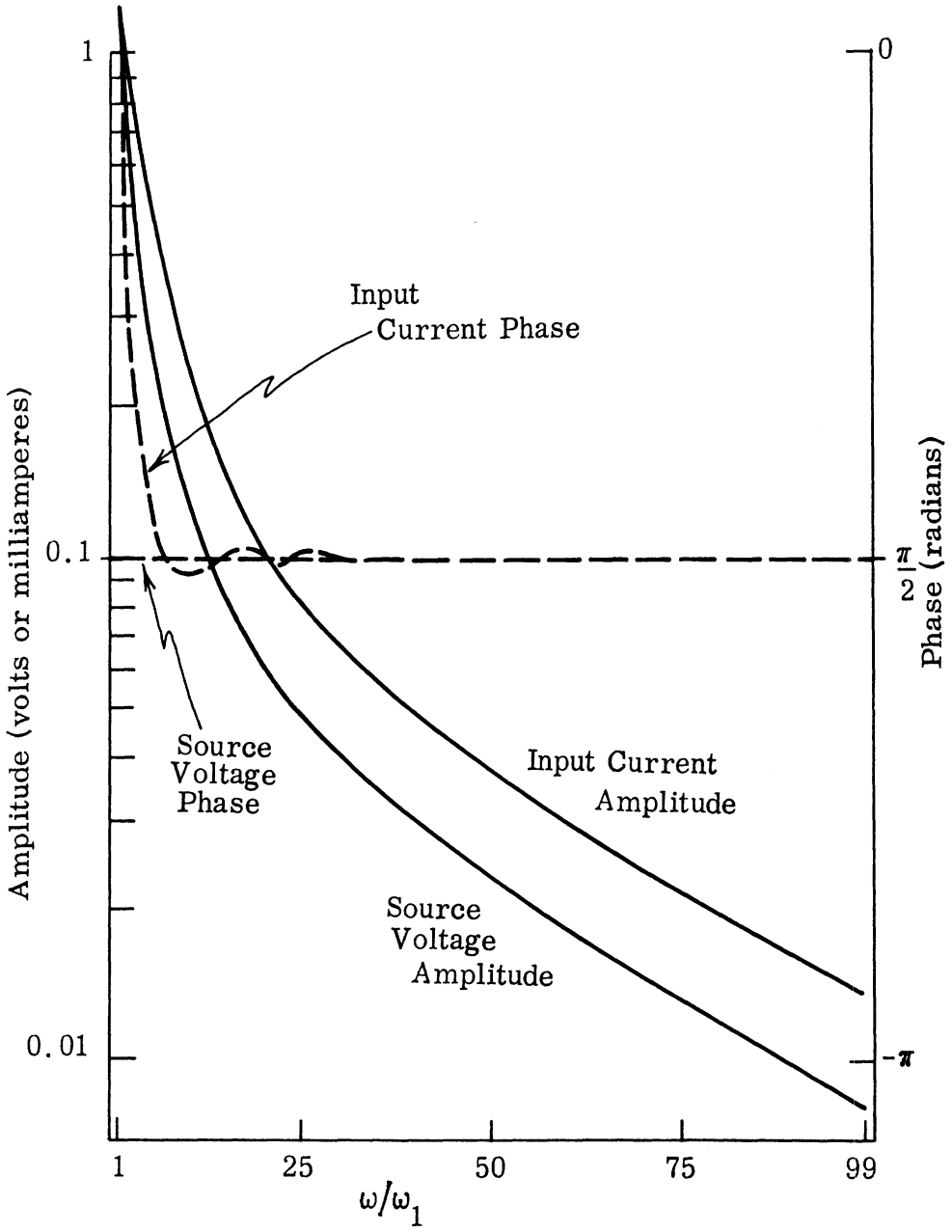

FIG. 2-46: FREQUENCY DOMAIN AMPLITUDE AND PHASE OF SOURCE VOLTAGE $V_s(\omega)$ AND INPUT CURRENT $I(0,\omega)$. $K = 50$.

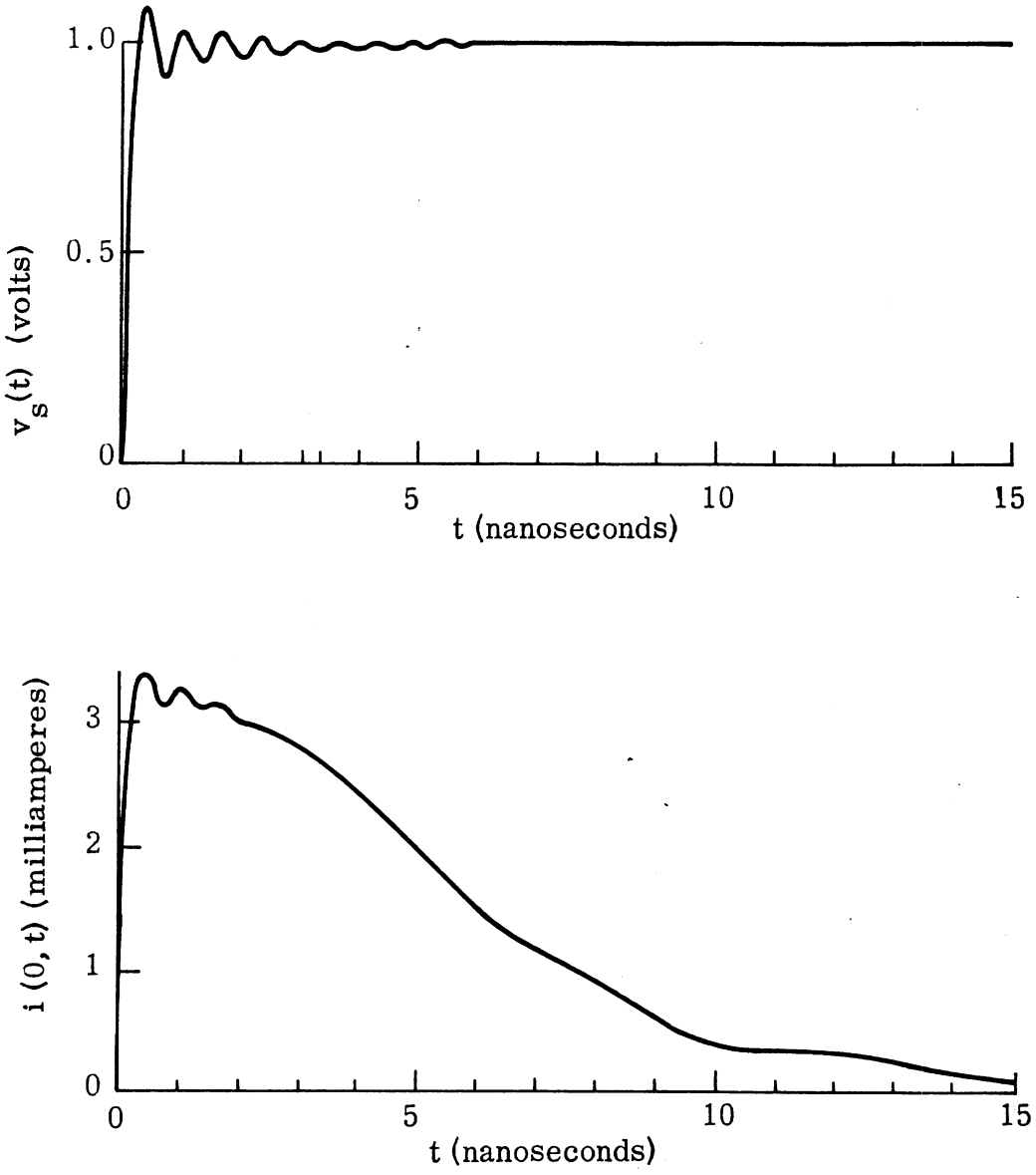

FIG. 2-47: TIME WAVEFORMS OF SOURCE VOLTAGE $v_s(t)$ AND INPUT CURRENT i (0, t). K = 50.

2.10 Transmission Line Waveforms

The time domain transient waveforms of current $i(z, t)$ and voltage $v(z, t)$ can be determined at any position along the transmission line in addition to $z = 0$. The computer program in Appendix A supplies $I(z,\omega)$. The same program also supplies $\frac{\partial I(z,\omega)}{\partial z}$ which can be converted directly to $V(z,\omega)$ by the transmission line relation

$$V(z,\omega) = \frac{j}{\omega C} \frac{\partial I(z,\omega)}{\partial z} .$$

Both $I(z,\omega)$ and $\frac{\partial I(z,\omega)}{\partial z}$ have been computed subject to the normalized boundary condition $I(0,\omega) = 1$ and must be adjusted to the input spectral weighting functions (2.64) and

$$V(z,\omega) = \frac{V_s(\omega)\ Z_{in}(\omega)}{Z_s(\omega) + Z_{in}(\omega)}$$

respectively. Inverse Fourier transformations can then yield $i(z,t)$ and $v(z,t)$. To illustrate the results of this procedure, $i(\frac{h}{2}, t)$ on the optimally-loaded (2.31) transmission line has been calculated for the case of the approximate step function voltage source excitation of Fig. 2-47. Figure 2-48 shows this transient current waveform at the midpoint of the transmission line. Relative to the input current of Fig. 2-47, this waveform is observed to be shifted to a later time by $\frac{h}{2c}$, to be attenuated and to be slightly changed in shape by dispersion.

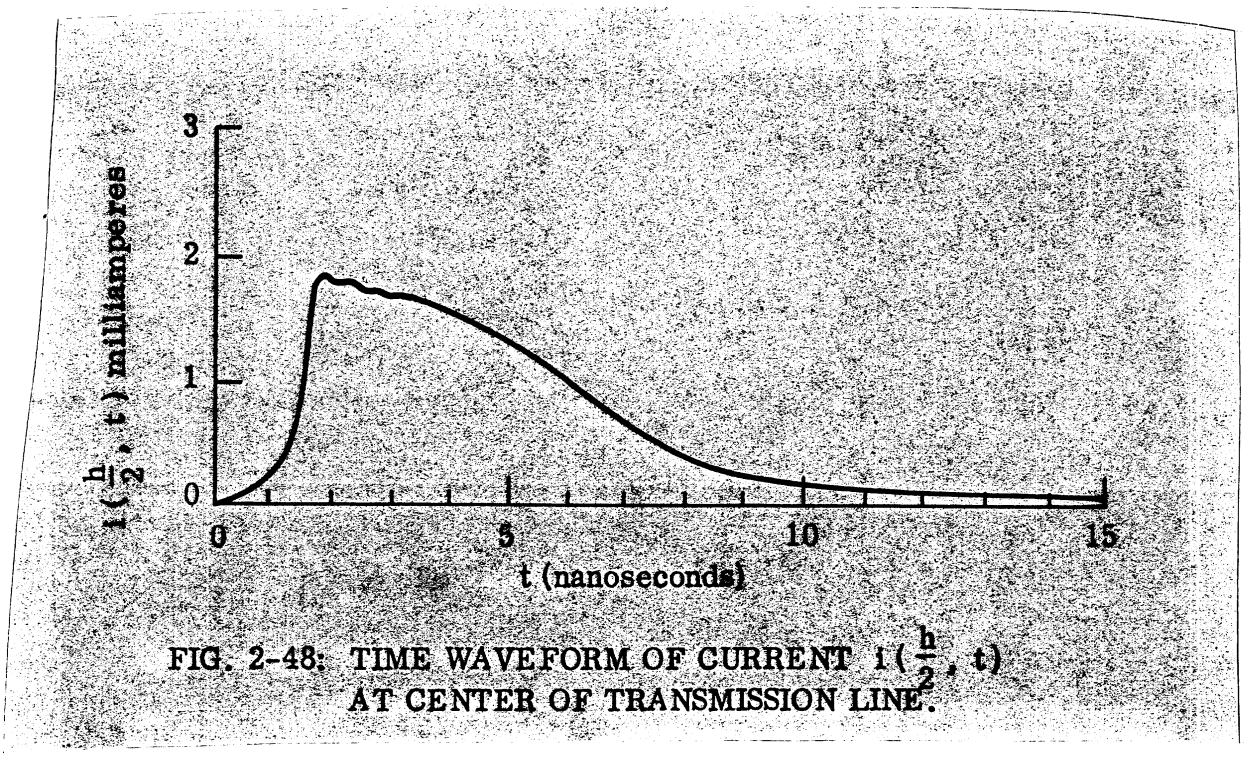

FIG. 2-48: TIME WAVEFORM OF CURRENT $i(\frac{h}{2}, t)$ AT CENTER OF TRANSMISSION LINE.

2.11 Radiation from Transmission Lines

A transient radiated field is produced by the current distributed along a resistance-loaded transmission line which is excited by a transient source. The time waveform of the radiated field is a function of the direction of radiation. The shape of the radiation pattern changes with time. To determine the transient radiated field, the analysis will first be carried out in the frequency domain and then be Fourier transformed into the time domain. The most difficult part of the analysis, that of finding the current distribution on the resistance loaded transmission line, is performed by the computer program in Appendix A. The current is renormalized in accordance with (2.64).

Figure 2-49 defines the centered coordinate system.

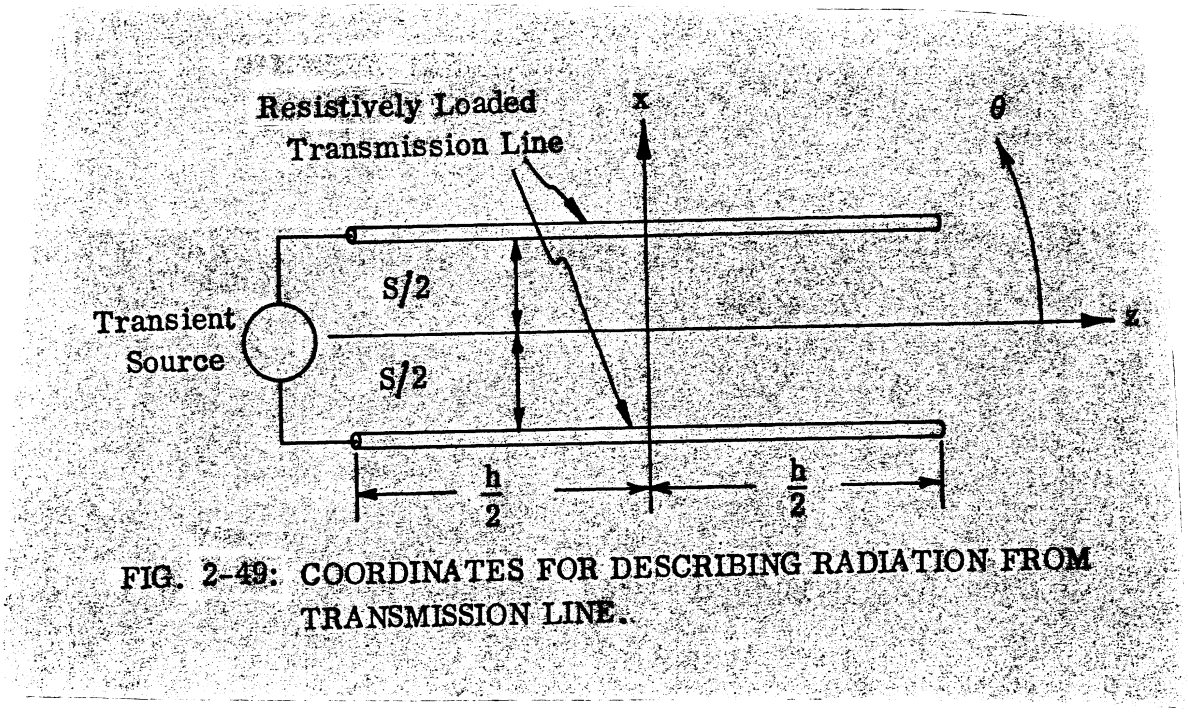

FIG. 2-49: COORDINATES FOR DESCRIBING RADIATION FROM TRANSMISSION LINE.

The vector current density on the balanced two-conductor transmission line is

$$\bar{J}(\bar{R},\omega) = \hat{z}\, I(z,\omega) \left[\delta(x-\frac{s}{2}) - \delta(x+\frac{s}{2})\right] \delta(y)\, U(\frac{h}{2} - |z|) \qquad (2.66)$$

where

$\bar{R}$ = the three-dimensional position vector whose origin is the center of the section of two-conductor transmission line,

s = the separation distance between the two parallel conductors of the transmission line which lies in the xz plane,

$\delta(\cdot)$ = the Dirac delta function,

$U(\cdot)$ = the unit step function,

a caret ($\wedge$) denotes a unit vector.

In terms of the dyadic free space Green's function $\bar{\bar{G}}_0(\bar{R}|\bar{R}')$[50], the far zone electric field radiated by the transmission line is

$$\bar{E}_{TL}(\bar{R}, \omega) = -j\omega\mu \iiint_{V'} \bar{\bar{G}}_0(\bar{R}|\bar{R}') \cdot \bar{J}(\bar{R}')\, dV' \tag{2.67}$$

where μ is the permeability of the medium which is assumed to be constant, primes (') identify source coordinates, unprimed coordinates are observation coordinates, V' is the three-dimensional source volume. The dyadic free space Green's function can be expressed as

$$\bar{\bar{G}}_0(\bar{R}|\bar{R}') = \left(\hat{\hat{U}} + \frac{1}{k^2}\nabla'\nabla'\right)\frac{e^{-jk|\bar{R}-\bar{R}'|}}{4\pi|\bar{R}-\bar{R}'|} \tag{2.68}$$

where $\hat{\hat{U}}$ = the unit dyad,

$k = \frac{\omega}{c}$,

c = velocity of electromagnetic wave propagation in the medium.

For $R >> R'$,

$$|\bar{R} - \bar{R}'| = \sqrt{R^2 + R'^2 - 2\bar{R}\cdot\bar{R}'}$$

$$\approx R\sqrt{1 - 2\frac{\hat{R}\cdot\bar{R}'}{R}}$$

$$\approx R - \hat{R}\cdot\bar{R}' \,. \tag{2.69}$$

The radiation field of the transmission line becomes

$$\bar{E}_{TL}(\bar{R}, \omega) \approx -j\omega\mu \frac{e^{-jkR}}{4\pi R} \int_{-\frac{h}{2}}^{\frac{h}{2}} \left(\hat{\hat{U}} + \frac{1}{k^2} \nabla' \nabla' \right) e^{-jk \hat{R} \cdot \bar{R}'} \cdot \hat{Z}$$

$$I(z', \omega)\, dz' \tag{2.70}$$

which can be simplified by a vector identity to

$$\bar{E}_{TL}(\bar{R}, \omega) \approx j\omega\mu \frac{e^{-jkR}}{4\pi R} \hat{R} \times \left[\hat{R} \times \hat{z} \int_{-\frac{h}{2}}^{\frac{h}{2}} e^{jk\hat{R}\cdot\bar{R}'} I(z', \omega)\, dz' \right]. \tag{2.71}$$

From the particular geometry of the transmission line in the spherical coordinate system (R, θ, ϕ),

$$\hat{R} \cdot \bar{R}' = z' \cos\theta \pm \frac{s}{2} \sin\theta \cos\phi \tag{2.72}$$

and

$$\bar{E}_{TL}(\bar{R}, \omega) \approx -\hat{\theta}\, j\omega\mu \frac{e^{-jkR}}{2\pi R} \sin\theta \sin\left(\frac{ks}{2} \sin\theta \cos\phi\right) \cdot$$

$$\cdot \int_{-\frac{h}{2}}^{\frac{h}{2}} I(z', \omega)\, e^{jk' \cos\theta}\, dz', \tag{2.73}$$

Equation (2.73) describes the far field radiated from a transmission line which consists of two parallel conductors. The conductors may be thin wires or parallel plates provided that the cross-sectional dimensions of the plates are small compared to all wavelengths of interest. $\bar{E}_{TL}(\bar{R}, \omega)$ may be small in magnitude due to the two opposing currents separated by the

dimension s which may be small in terms of wavelengths. Radiation from a generator structure could in general be comparable in magnitude to that from the two-conductor line. The generator structure could be modeled approximately in simple cases as an electrically small Hertzian diople carrying the current $I(0,\omega)$. Its radiation field

$$\bar{E}_G(\bar{R},\omega) \approx \hat{\alpha}\, j\omega\mu\, I(0,\omega)\, s\, \frac{e^{-jk\left(R+\frac{h}{2}\cos\alpha\right)}}{2\pi R}\sin\alpha \qquad (2.74)$$

could be superimposed on the field radiated by the transmission line. Here, α is the polar angle relative to the x axis. The total radiated field is thus

$$\bar{E}(\bar{R},\omega) = \bar{E}_{TL}(\bar{R},\omega) + \bar{E}_G(\bar{R},\omega) \quad . \qquad (2.75)$$

The radiated field's time domain waveform is given by the inverse Fourier transforms of (2.73) and (2.74).

$$\bar{e}_{TL}(\bar{R},t) \approx -\hat{\theta}\frac{\mu \sin\theta}{4\pi^2 R}\int_{-\infty}^{\infty} \omega \sin\left(\frac{\omega s}{2c}\sin\theta\cos\phi\right)\cdot \int_{-\frac{h}{2}}^{\frac{h}{2}} I(z',\omega)\, e^{j\omega\left(t-\frac{R}{c}+\frac{z'}{c}\cos\theta\right)}\, dz'\, d\omega \,, \qquad (2.76)$$

and then

$$\bar{e}_G(R,t) \approx \hat{\alpha}\frac{\mu s \sin\alpha}{4\pi^2 R}\int_{-\infty}^{\infty} j\omega\, I(0,\omega)\, e^{j\omega\left(t-\frac{R}{c}-\frac{h}{2}\cos\alpha\right)}\, d\omega \,, \qquad (2.77)$$

$$\bar{e}(\bar{R},t) = \bar{e}_{TL}(\bar{R},t) + \bar{e}_G(\bar{R},t) \quad . \qquad (2.78)$$

Here again for reasons of economy, the Fast Fourier Transform technique of using a finite number K of discrete frequencies can be employed to evaluate the radiated transient waveform numerically. Appendix B is a listing of the computer program which calculates the time domain transient waveform radiated from a resistance-loaded transmission line. The program is capable of computing the transient waveform at any far zone distance and in any direction from the transmission line. The program also allows any length h and conductor spearation s for the transmission line.

To illustrate the radiation of transient signals, a transmission line loaded by the optimum resistance distribution (2.31) is considered to be excited by an approximate step voltage source (2.60) of long duration (2.61). The transient source voltage waveform was shown in Fig. 2-47. The transient waveforms radiated in various θ directions in the xz plane are shown in Fig. 2-50. The xz plane is the plane of maximum radiation. The time scale in this figure has been translated to $t - \frac{R}{c}$ for convenient comparison with the source waveform.

Each waveform in Fig. 2-50 consists of a positive pulse followed at a later time by a smaller negative pulse. The larger positive pulse is radiation from the positive transient current waveform, Fig. 2-47, as that wave travels along the transmission line from the generator to the open-circuit termination. During its transit along the loaded transmission line, the current waveform undergoes attenuation and a change in shape due to phase dispersion. For this reason, the shape of the positive radiated pulse would be difficult to estimate without a detailed computation. The smaller negative pulse in the radiated waveform is radiation from the attenuated, dispersed, negative current waveform which is reflected from the open circuit termination and travels back along the transmission line to the generator. In this example, negligible current is re-reflected from the generator because of transmission line attenuation and the good impedance match (2.47) from the

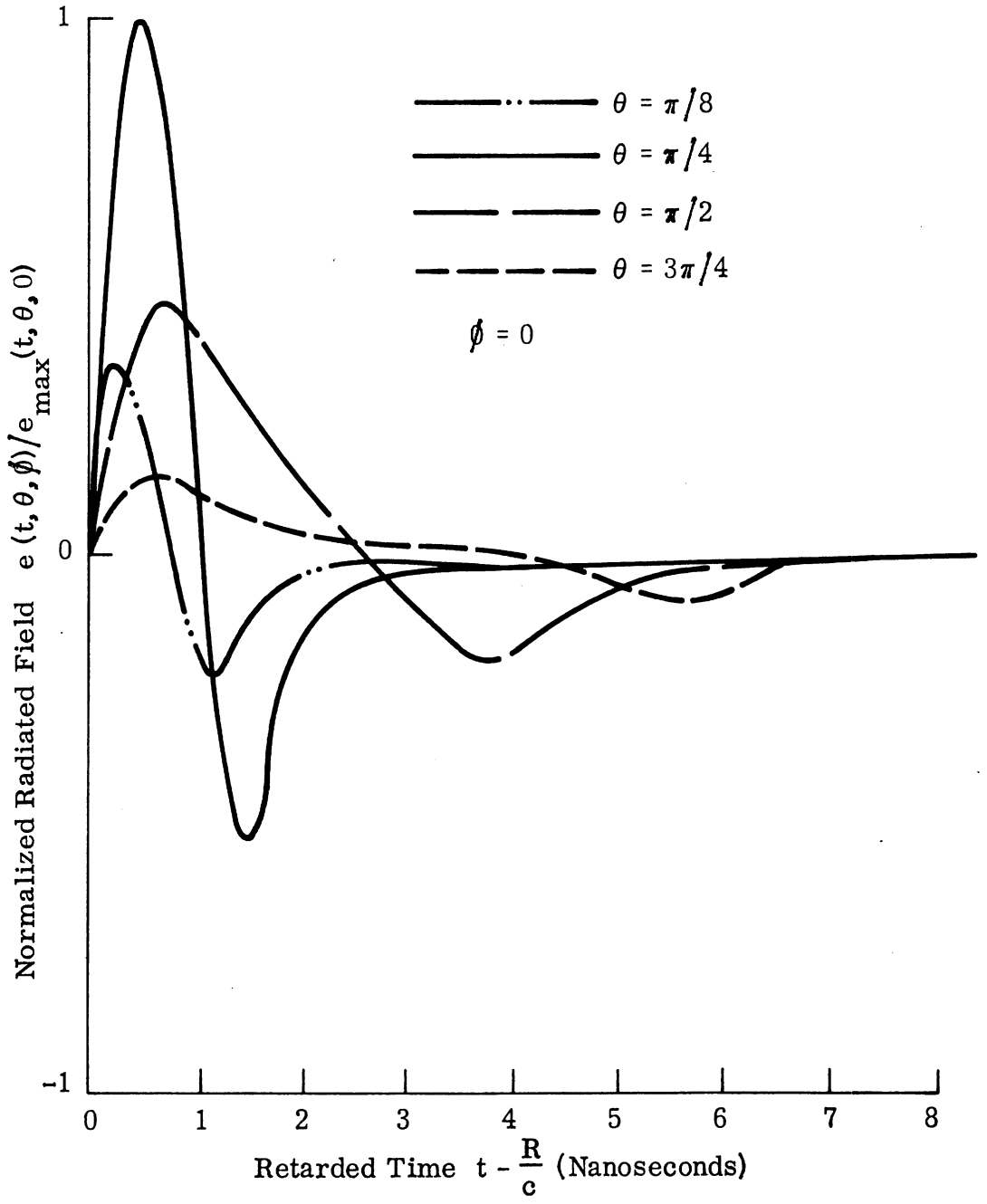

FIG. 2-50: TRANSIENT TIME WAVEFORMS RADIATED IN VARIOUS θ DIRECTIONS FROM STEP-EXCITED TRANSMISSION LINE WITH OPTIMUM RESISTANCE LOADING.

transmission line to the generator.

Figure 2-50 shows that the time elapsed between positive and negative pulse grows progressively longer as the radiation direction angle θ becomes progressively larger. These time delays from the computed transient waveforms are in excellent agreement with the known values

$$\Delta t = \frac{h}{c}(1 - \cos\theta) \quad . \tag{2.79}$$

Figure 2-50 also shows that the peak of the transient waveform has a maximum intensity for radiation in a direction near ($\theta = \frac{\pi}{4}$, $\phi = 0$). This demonstrates that the current on the transmission line contains a large traveling wave component. The traveling wave property was indicated previously in the monochromatic analysis by the nearly linear phase variation (Fig. 2-11) of current along the transmission line. In the frequency domain, the effect of the current's linear phase progression with distance along the transmission line is to produce constructive interference for radiation in the direction

$$\theta = \cos^{-1}\left(\frac{1}{k_0}\frac{d\psi}{dz}\right) \quad . \tag{2.80}$$

This angle is different for the different frequency components of the current waveform so that the direction of maximum radiation in the time domain is modified. Further, the $\sin\theta$ terms in (2.76) weight broadside radiation more heavily than endfire radiation. The peak intensity of the radiated transient waveform as a function of direction is shown in Fig. 2-51. This plot is perhaps more useful than a radiation pattern. It differs from a radiation pattern in that the plotted field intensities do not occur simultaneously. Here, a radiation pattern is defined as a plot of relative radiated field intensity versus angle at one instant of time. Such patterns can be derived from a set of waveforms of the type illustrated in Fig. 2-50 but including a larger number of curves for finer increments of the angle parameter. Each value of the

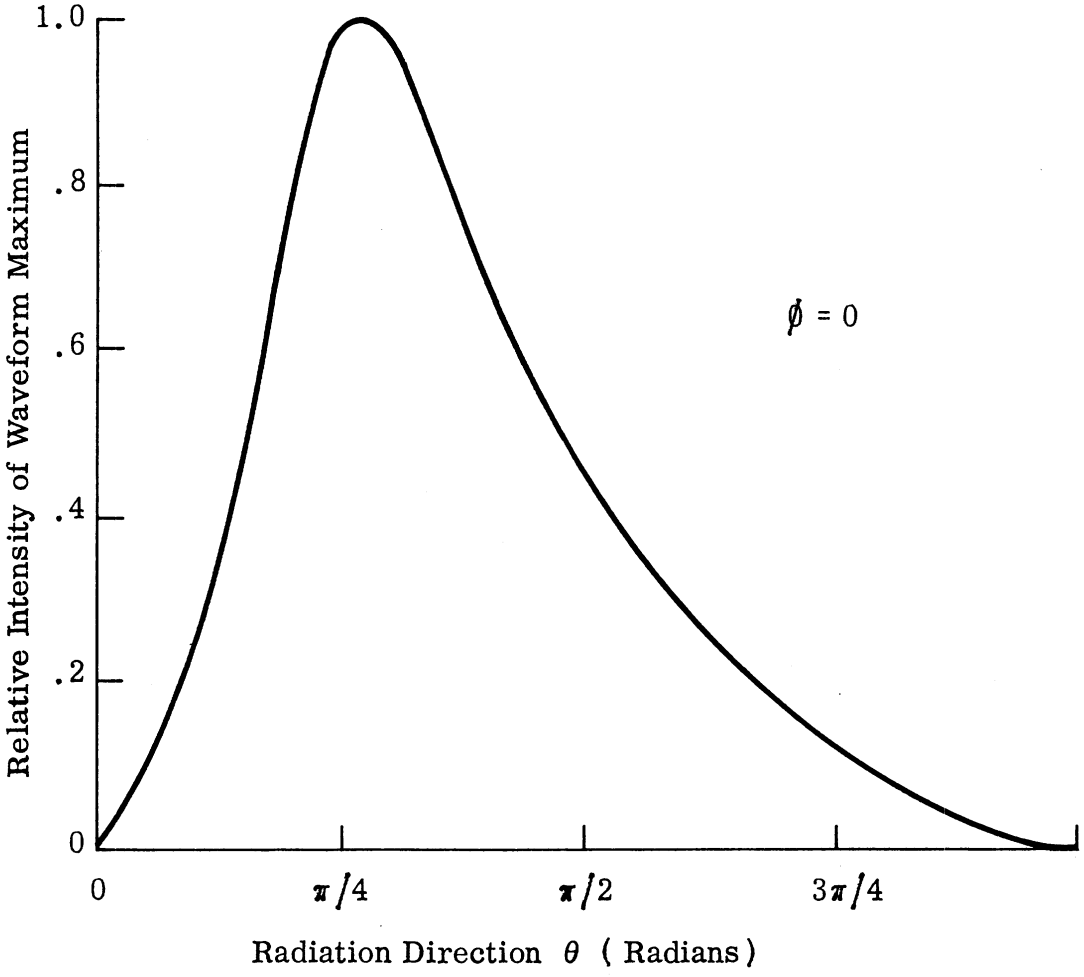

FIG. 2-51: MAXIMUM AMPLITUDE OF RADIATED TRANSIENT WAVEFORM AS A FUNCTION OF RADIATION DIRECTION.

abscissa in the figure generates a different radiation pattern which is valid at that time. Thus a time sequence of different radiation patterns characterizes transient radiation from the transmission line. Some sequential radiation patterns of the optimally loaded transmission line excited by an approximate step voltage are shown in Fig. 2-52.

In discussing the temporal and spatial distribution of transient radiation from a transmission line, attention has been focused on the xz or $\phi = 0$ plane where the interesting properties are pronounced. In the yz or $\phi = \frac{\pi}{2}$ plane, radiation vanishes due to cancellation of the effects of the antisymmetrical currents in the two conductors of the transmission line. The xy or $\theta = \frac{\pi}{2}$ plane need not receive much attention because the radiated waveforms and radiation patterns do not provide much new information. The conductor separation s as a practical example has been made small relative to all wavelengths of interest as well as to the transmission line length h. Figure 2-53 shows that the transient waveforms radiated in the xy plane have nearly the same shape. The amplitudes of these waveforms are nearly proportional to $\cos\phi$ as seen in (2.76) for $s << k$. It is evident that the xy plane radiation patterns derived from a set of waveforms like Figure 2-53 will have nearly the same shape for all values of time.

2.12 Reception by Transmission Lines

Transient electromagnetic radiation incident on a resistively loaded transmission line will produce a transient voltage v_L across a load impedance Z_L. The transmission line considered here is terminated with Z_L at one end and an open circuit at the other end. Figure 2-49 represents the geometry if the source is replaced by Z_L. The present analysis of reception uses the concept of the vector effective height function [57, 58, 59] of the loaded transmission line. This approach takes advantage of the previous determinations of current distributions and input impedances.

The received signal can be formulated as

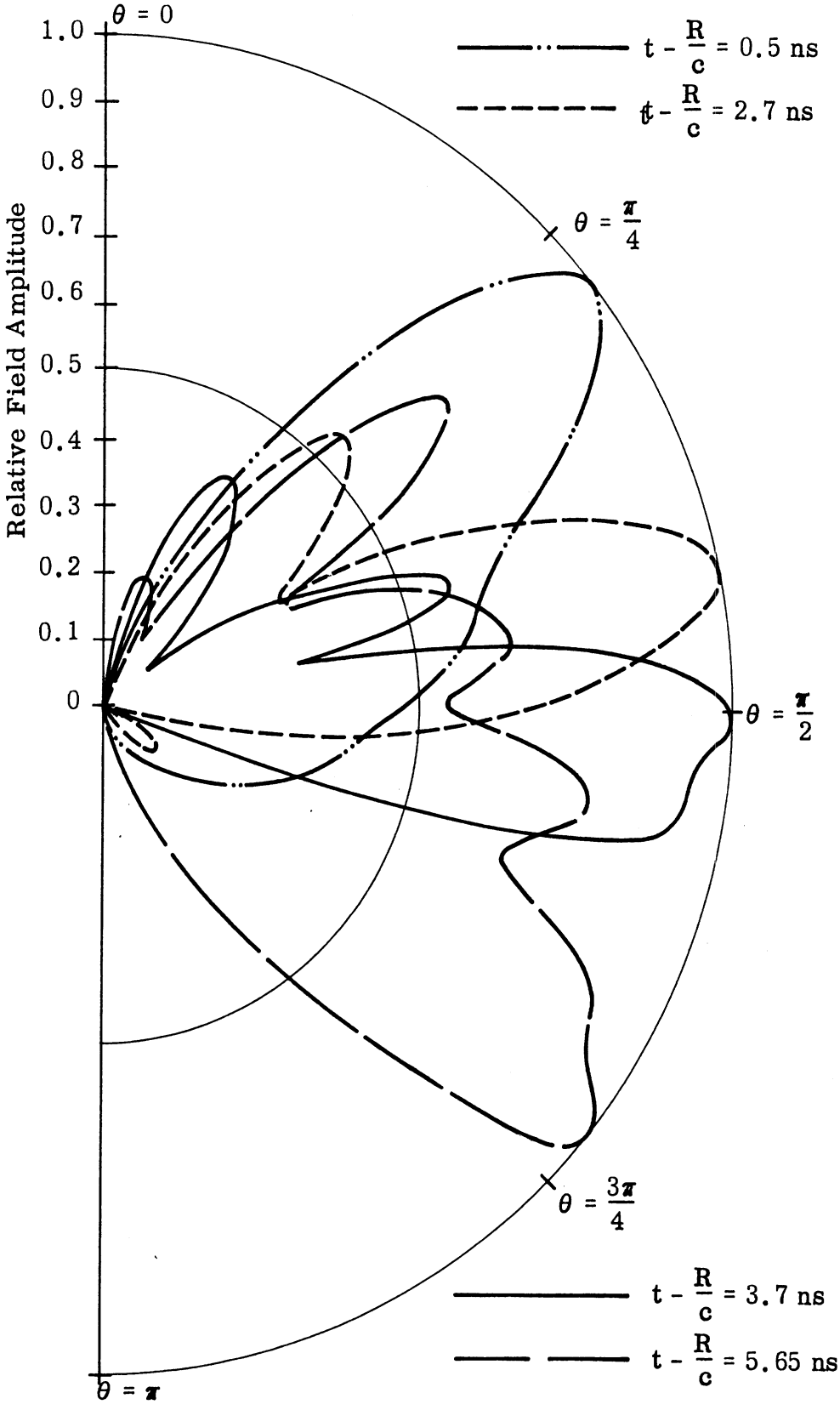

FIG. 2-52: TIME SEQUENCE OF RADIATION PATTERNS FOR OPTIMALLY LOADED TRANSMISSION LINE EXCITED BY APPROXIMATE STEP VOLTAGE.

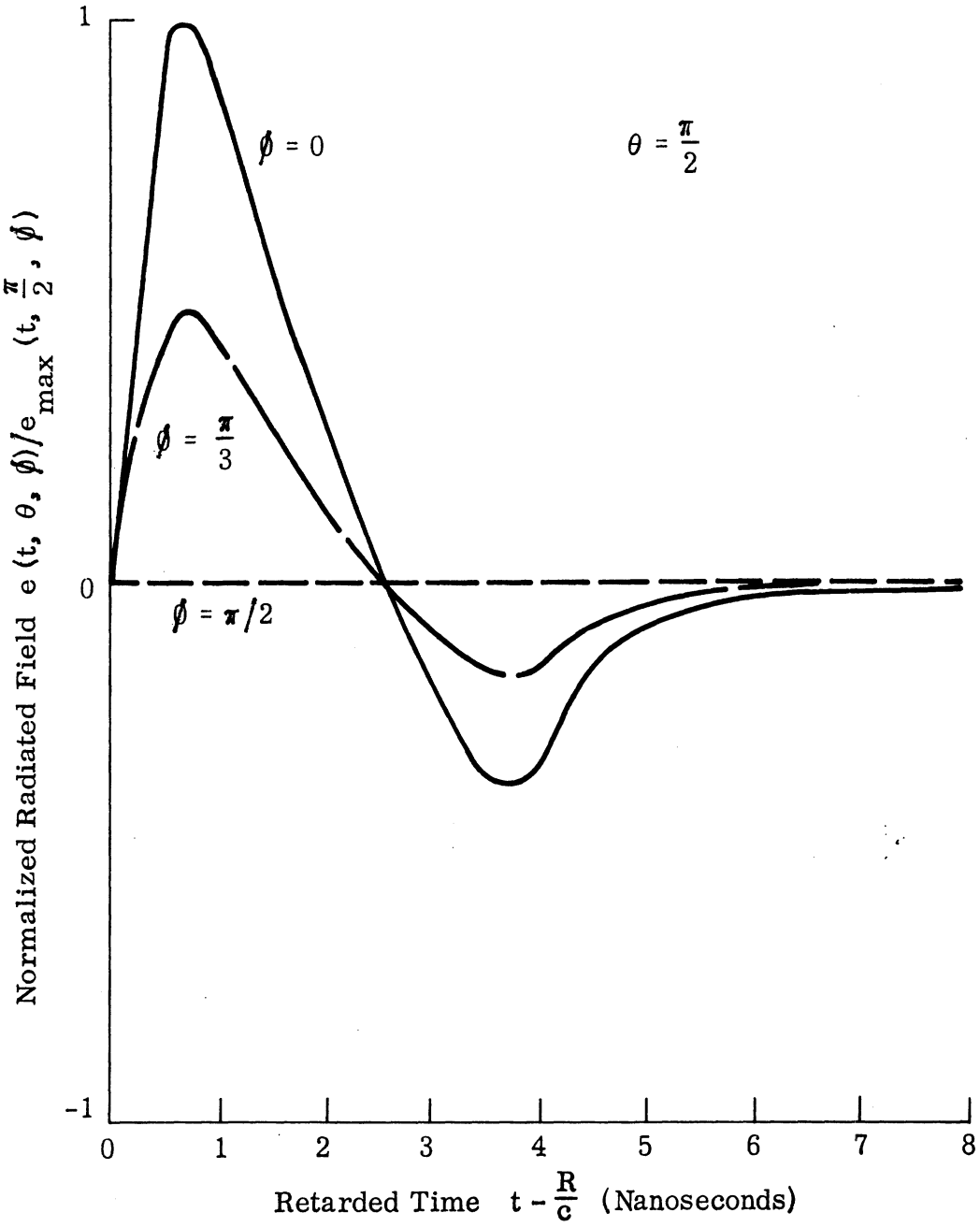

FIG. 2-53: TRANSIENT TIME WAVEFORMS RADIATED IN VARIOUS BROADSIDE DIRECTIONS FROM STEP-EXCITED TRANSMISSION LINE WITH OPTIMUM RESISTANCE LOADING.

$$v_L(\Omega,t) = \frac{1}{2\pi}\int_{-\infty}^{\infty} \frac{Z_L(\omega)\,\bar{E}_i(\Omega,\omega)\cdot\bar{h}(\Omega,\omega)\,e^{j\omega t}}{Z_L(\omega)+Z_{in}(\omega)}\,d\omega \qquad (2.81)$$

where Ω represents the two angular dimensions (θ, ϕ) of the incident wave direction,

$\bar{E}_i(\Omega,\omega)$ = the Fourier transform of the transient incident electric field,

$\bar{h}(\Omega,\omega)$ = the vector effective height function of the loaded transmission line.

Expressed in terms of the current density (2.66),

$$\bar{h}(\Omega,\omega) = \frac{1}{I_{in}(\omega)}\iiint_{V'} \hat{R}\times\bar{J}(\bar{R}',\omega)\times\hat{R}\,e^{jk(\hat{R}\cdot\bar{R}')}dV' \qquad (2.82)$$

where $I_{in}(\omega)$ is the input current. Here, as previously, primes identify the coordinates of a current density which would exist if the transmission line were excited by $I_{in}(\omega)$. The current density $\bar{J}(\bar{R}',\omega)$ is given by (2.66) so that

$$\hat{R}\times\bar{J}(\bar{R}'.\omega)\times\hat{R} = \left[(-\hat{x}\cos\phi - \hat{y}\sin\phi)\cos\theta + \hat{z}\sin\theta\right]\sin\theta$$
$$\left[\delta\left(x-\frac{s}{2}\right) - \delta\left(x+\frac{s}{2}\right)\right]\delta(y)\,u\left(\frac{h}{2}-|z|\right)I(z,\omega) \qquad (2.83)$$

The quantity $\hat{R}\cdot\bar{R}'$ can again be expanded in the form (2.72). Thus the transient received signal can be directly evaluated from (2.81) with the previously determined $I(z,\omega)$ and $Z_{in}(\omega)$. The shape of the received transient waveform will be different for different directions Ω of the incident wave in analogy with the radiated waveforms.

Due to the geometry of the transmission line, the most pronounced effects occur in the xz plane. In this plane, an incident plane wave

$$\bar{E}_i(\Omega,\omega) = (-\hat{x}\cos\theta + \hat{z}\sin\theta)\,E_i(\omega) \qquad (2.84)$$

will produce a received signal which can be expressed in the reduced form

$$v_L(\Omega, t) = \frac{\sin\theta}{\pi} \int_{-\infty}^{\infty} \frac{E_i(\omega)}{I_{in}(\omega)} \frac{Z_L(\omega)}{Z_L(\omega)+Z_{in}(\omega)} \sin\left(\frac{\omega s}{2c} \sin\theta \cos\phi\right) \cdot$$

$$\cdot \int_{-\frac{h}{2}}^{\frac{h}{2}} I(z', \omega)\, e^{j\omega\left(t + \frac{z'}{c}\cos\theta + \frac{\pi}{2\omega}\right)}\, dz'\, d\omega \,. \qquad (2.85)$$

2.13 Transient Coupling of Transmission Lines

A transmission line which is excited by a transient signal source will cause a different transient signal to be received in the load of a second, distant, transmission line. The far field coupling of transient signals from one loaded transmission line to another can be formulated compatibly by using the vector effective height function. The vector effective height functions of the two transmission lines can differ due to different resistance loading distributions. In the following expression for the received transient signal, the subscripts t and r identify quantities associated with the transmitting and receiving structures respectively.

$$v_r(\Omega, t) = \frac{\eta}{8\pi^2 cR} \int_{-\infty}^{\infty} \frac{\omega Z_L(\omega) V_s(\omega) \bar{h}_t(\Omega, \omega) \cdot \bar{h}_r(\Omega, \omega)}{\left[Z_s(\omega) + Z_{in\,t}\right]\left[Z_L(\omega) + Z_{in\,r}(\omega)\right]}$$

$$e^{j\omega\left(t - \frac{R}{c} - \frac{\pi}{2\omega}\right)}\, d\omega \qquad (2.86)$$

where η = the characteristic impedance of the medium,

R = the distance between the two transmission lines.

Chapter III

BICONICAL ANTENNA

3.1 Antenna Considerations

A transmission line of conical geometry is the basic structure of a biconical antenna. Analysis of a biconical antenna through its representation as a conical transmission line is the most accurate analysis available for this antenna[34, 35, ..., 48]. The transmission line approach serves to determine the current distribution along the antenna and thereby the input impedance as well as the radiation and reception properties. Figure 3-1 shows the symmetrical perfectly conducting biconical antenna with radial length h and cone half-angle θ_0. The ends of the cones are terminated in perfectly conducting spherical caps.

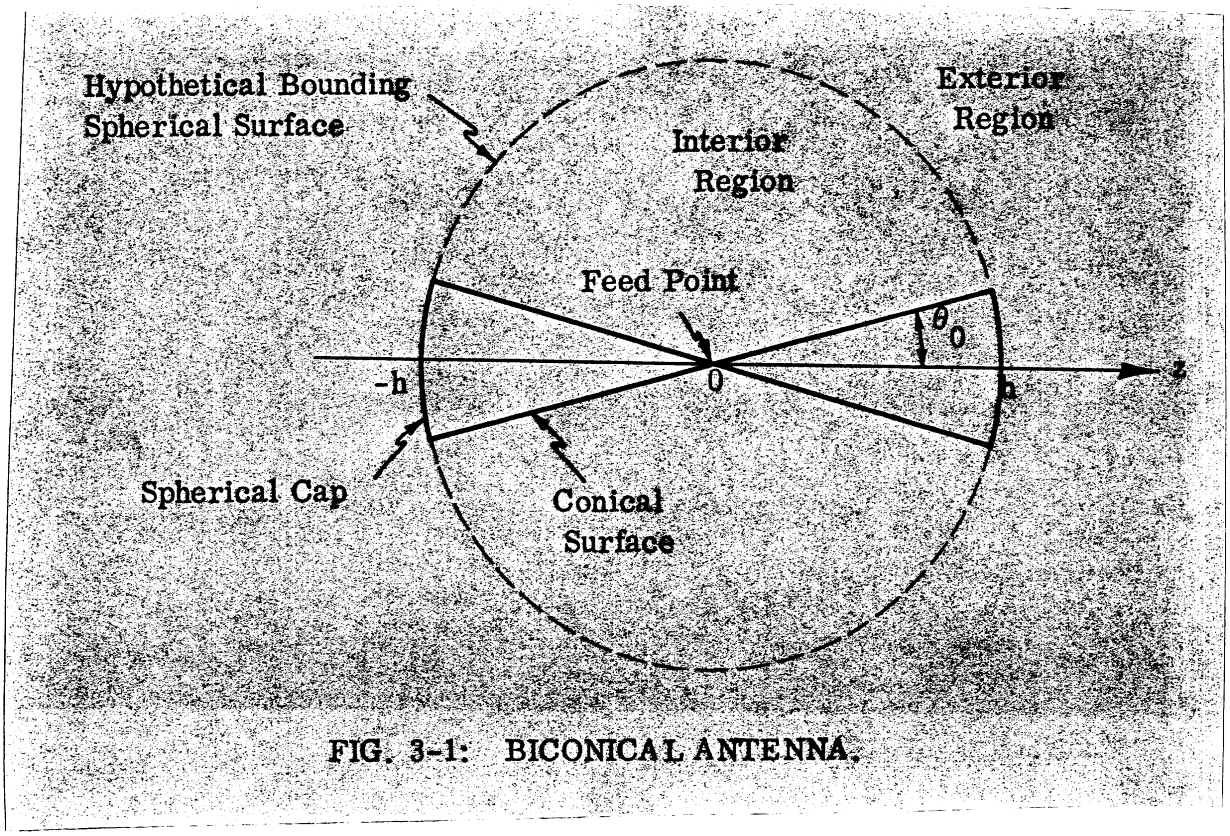

FIG. 3-1: BICONICAL ANTENNA.

The biconical antenna is well suited to transient analysis because it possesses a unique determinable input impedance in contrast to cylindrical antennas which have feed gap problems. Another advantage is that one of its

two dimensions is specified by an angle alone, implying relatively uniform performance over the wide frequency range required in transient analysis.

The thin, or small angle $\theta_0 \to 0$, biconical antenna will be treated here. For the small angle case, there exists an exact closed analytic form that can be used to express the continuity of fields between the antennas's interior and exterior regions. In contrast, the lack of a closed form representation in the wide angle case of $0 < \theta_0 < \frac{\pi}{2}$ requires a slowly convergent infinite series whose truncation would leave uncertainties in the antenna current distribution[49].

3.2 Antenna Fields

Only TM modes are supported by the antenna. Solution of the electromagnetic wave equation subject to the antenna boundary conditions shows that interior to the antenna's hypothetical bounding sphere there exists a dominant field

$$\bar{E}_D(\bar{R},\omega) = \hat{\theta}\,\frac{\eta\, I_0(\omega)}{2\pi R\sin\theta}\left[Z_c Y_t(\omega)\sin k(h-R) - j\cos k(h-R)\right], \tag{3.1}$$

$$\bar{H}_D(\bar{R},\omega) = \hat{\phi}\,\frac{I_0(\omega)}{2\pi R\sin\theta}\left[\sin k(h-R) - j\,Z_c\,Y_t(\omega)\cos k(h-R)\right], \tag{3.2}$$

and a complementary field

$$\bar{E}_c(\bar{R},\omega) = -\hat{R}\,\frac{j}{2\pi\omega\epsilon R^2}\sum_{n=0}^{\infty} a_n \frac{\sqrt{R}\,J_{n+1/2}(kR)}{\sqrt{h}\,J_{n+1/2}(kh)}\left[P_n(\cos\theta) - P_n(-\cos\theta)\right]$$

$$-\hat{\theta}\,\frac{j\eta}{2\pi R}\sum_{n=0}^{\infty}\frac{a_n}{n(n+1)}\,\frac{\sqrt{R}\,J'_{n+1/2}(kR) + \frac{1}{2k\sqrt{R}}\,J_{n+1/2}(kR)}{\sqrt{h}\,J_{n+1/2}(kh)}\cdot$$

$$\cdot\,\frac{\partial}{\partial\theta}\left[P_n(\cos\theta) - P_n(-\cos\theta)\right], \tag{3.3}$$

$$\bar{H}_c(\bar{R},\omega) = -\hat{\phi}\,\frac{1}{2\pi R}\sum_{n=0}^{\infty}\frac{a_n}{n(n+1)}\,\frac{\sqrt{R}\,J_{n+1/2}(kR)}{\sqrt{h}\,J_{n+1/2}(kh)}\,\frac{\partial}{\partial\theta}\left[P_n(\cos\theta) - P_n(-\cos\theta)\right]. \tag{3.4}$$

External to the boundary sphere, the field solution is

$$\bar{E}(\bar{R},\omega) = -\hat{R}\frac{1}{2\pi\omega\epsilon R^2}\sum_{\text{odd } m} b_m \frac{\sqrt{R}\, H^{(2)}_{m+1/2}(kR)}{\sqrt{h}\, H^{(2)}_{m1+/2}(kh)} P_m(\theta)$$

$$-\hat{\theta}\frac{j\eta}{2\pi R}\sum_{\text{odd } m}\frac{b_m}{m(m+1)}\frac{\sqrt{R}\, H^{(2)}_{m+1/2}(kR)+\frac{1}{2k\sqrt{R}} H^{(2)}_{m+1/2}(kR)}{\sqrt{h}\, H^{(2)}_{m+1/2}(kh)}\frac{dP_m(\theta)}{d\theta}, \tag{3.5}$$

$$\bar{H}(\bar{R},\omega) = -\hat{\phi}\frac{1}{2\pi R}\sum_{\text{odd } m}\frac{b_m}{m(m+1)}\frac{\sqrt{R}\, H^{(2)}_{m+1/2}(kR)}{\sqrt{h}\, H^{(2)}_{m+1/2}(kh)}\frac{dP_m(\theta)}{d\theta}. \tag{3.6}$$

Here, $\bar{R}$ = the three dimensional coordinates (R, θ, ϕ),

$\eta = \sqrt{\frac{\mu}{\epsilon}}$ the characteristic impedance of the medium,

$k = \frac{\omega}{c} = \omega\sqrt{\epsilon\mu}$ the propagation constant of the medium,

ϵ = the permittivity and μ = the permeability of the medium,

a, a_n, b_m = constant coefficients to be determined by boundary conditions.

The above field expressions were established by early investigators of the biconical antenna[37, 39, 40]. The transmission line character of the dominant field is emphasized by the form of (3.1) and (3.2) where

$$I_0(\omega) = \frac{j\,2\,\pi\,a}{\cos k\,h + j\,Z_c\,Y_t(\omega)\sin kh} \tag{3.7}$$

represents a current, Z_c represents the characteristic impedance of the conical transmission line and $Y_t(\omega)$ represents a terminating admittance produced by the spherical caps which terminate the transmission line. The total electric and magnetic fields in the interior region of the antenna are $\bar{E}(\bar{R},\omega) = \bar{E}_D(\bar{R},\omega) + \bar{E}_c(\bar{R},\omega)$ and $\bar{H}(\bar{R},\omega) = \bar{H}_D(\bar{R},\omega) + \bar{H}_c(\bar{R},\omega)$ respectively.

These fields can be integrated to give voltage and current quantities which are associated with the transmission line interpretation.

$$V(\bar{R},\omega) = \int_{\theta_0}^{\pi-\theta_0} \hat{\theta} \cdot \bar{E}(\bar{R},\omega)\ R\, d\theta \ . \tag{3.8}$$

$$I(\bar{R},\omega) = \oint \hat{\phi} \cdot \bar{H}(\bar{R},\omega)\ R \sin\theta_0\, d\phi \ . \tag{3.9}$$

In (3.8), integration of the $\bar{E}_c(\bar{R},\omega)$ component produces zero identically so that the complementary fields do not contribute to the voltage. In (3.9), the complementary wave contribution to the current vanishes at the bicone apex $R = 0$.

3.3 Antenna Impedances

As the voltage and current at the apex terminal of the biconical transmission line contain only dominant wave terms, the input impedance of the structure is uniquely determined from (3.1) and (3.2) to be

$$Z_{in}(\omega) = \frac{V(0,\omega)}{I(0,\omega)} = \frac{1 + j\, Z_c\, Y_t(\omega) \tan kh}{Z_c\, Y_t(\omega) + j \tan kh}\, Z_c \ . \tag{3.10}$$

The characteristic impedance experienced by the dominant mode on the biconical transmission line is determined by making the cones infinitely long and taking the quotient of the resulting outwardly traveling voltage and current waves.

$$Z_c = \frac{V^+(R,\omega)}{I^+(R,\omega)} = \frac{\eta}{\pi} \ell n \cot \frac{\theta_0}{2} \ . \tag{3.11}$$

The terminating admittance

$$Y_t(\omega) = \frac{I_D(h,\omega)}{V_D(h,\omega)} \tag{3.12}$$

is used to account for reflection of the dominant mode from the spherical caps that terminate the biconical transmission line. Evaluation of $Y_t(\omega)$ requires values for the a_n and b_m coefficients of the internal complementary and external fields which in general calls for the solution of an infinite set of linear equations. However, for the case of the small angle $\theta_0 \rightarrow 0$ biconical antenna, a closed form expression for $Y_t(\omega)$ exists[37, 60].

$$Y_t(\omega) = \frac{\pi}{4\eta \left(\ln \cot \frac{\theta_0}{2}\right)^2} \left\{ 2\, L(2kh) + e^{j2kh} \left[- L(4kh) + L(2kh) + \ell n\, 2 \right] \right.$$

$$\left. + e^{-j2kh} \left[L^*(2kh) - \ell n\, 2 \right] \right. . \qquad (3.13)$$

where $L(x) = Cin(x) + j\, Si(x)$,

$Cin(x) = C + \ln(x) - Ci(x)$,

$C = 0.577215665$ is Euler's constant.

The dominant mode impedance at any position R along the thin biconical antenna is

$$Z(R,\omega) = \frac{1 + j\, Z_c\, Y_t(\omega) \tan k(h - R)}{Z_c\, Y_t(\omega) + j \tan k(h - R)}\, Z_c \; . \qquad (3.14)$$

3.4 Transient Currents and Voltages

The thin biconical antenna is considered to be energized by the transient voltage source depicted in Fig. 2-44. The transient source voltage is given by (2.60) and (2.63) in the time and frequency domains respectively. For a thin biconical antenna where $\theta_o = 1$ degree and the resulting $Z_c = 567$ ohms, the antenna's frequency domain input current (2.64) is plotted in Fig. 3-2. The input current time domain transient waveform (2.65) is shown in Fig. 3-3.

The frequency spectral representation of the surface current density distributed over the biconical antenna due to the dominant interior field is

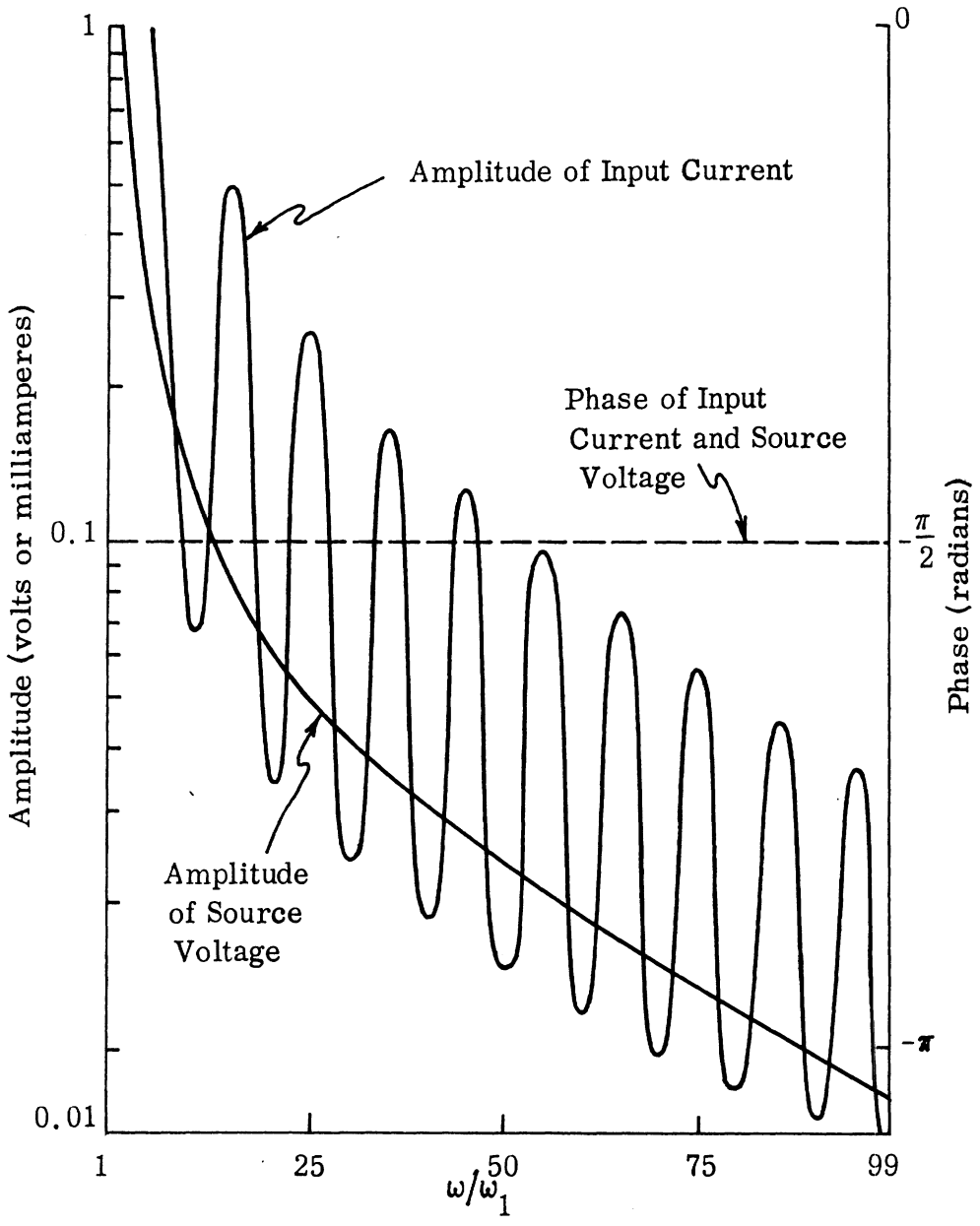

FIG. 3-2: FREQUENCY DOMAIN INPUT CURRENT OF BICONICAL ANTENNA, K = 50.

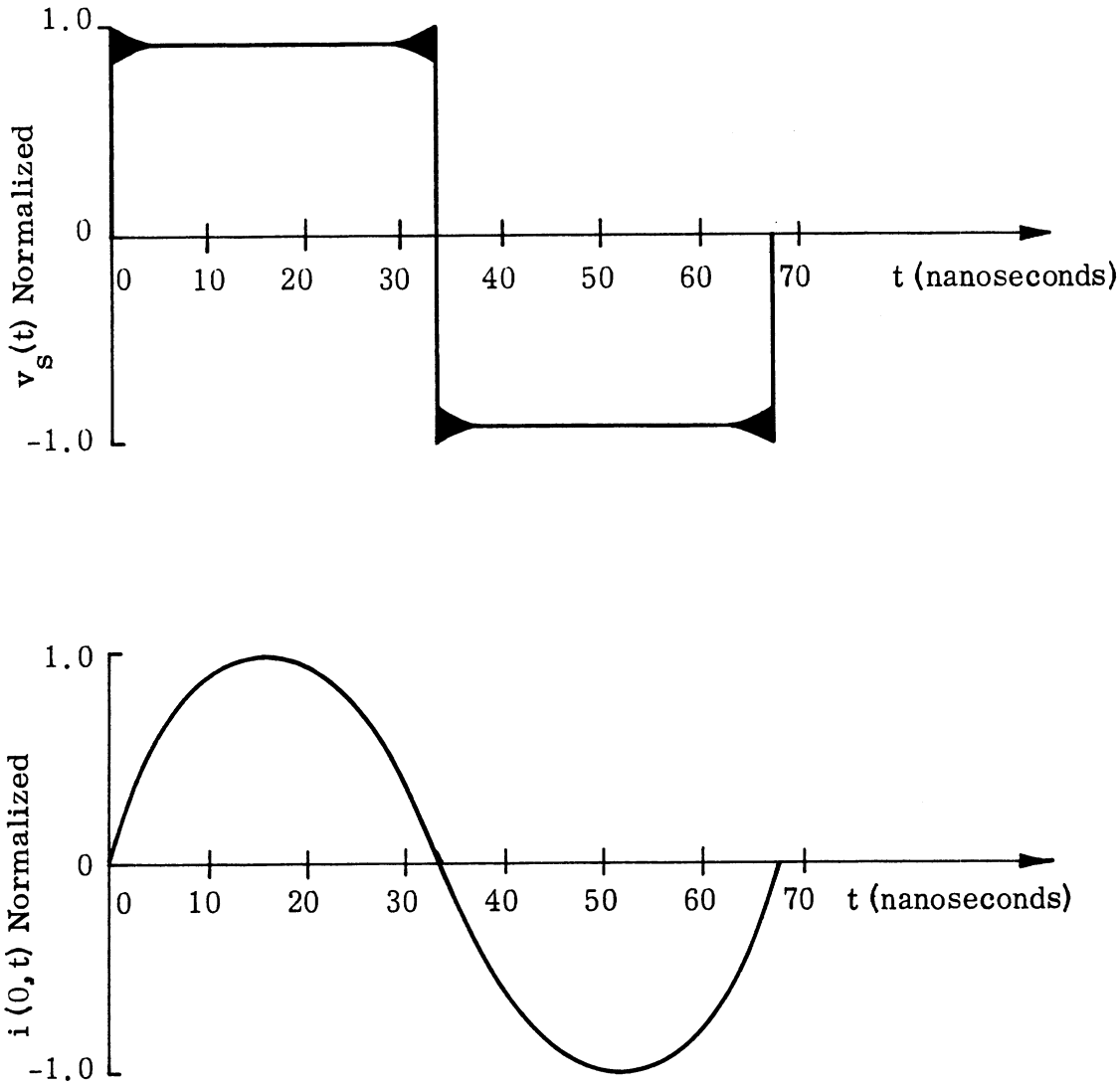

FIG. 3-3: TIME WAVEFORMS OF SOURCE VOLTAGE $v_s(t)$ AND INPUT CURRENT $i(0,t)$ OF BICONICAL ANTENNA.

$$\bar{J}(\bar{R},\omega) = \hat{R}\,\frac{I(R,\omega)\left[\delta(\theta-\theta_0)-\delta(\theta-\pi+\theta_0)\right]}{2\pi R^2 \sin\theta}\,, \tag{3.15}$$

where

$$I(R,\omega) = I_0(\omega)\left[\sin k(h-R) - j Z_c Y_t(\omega)\cos k(h-R)\right]. \tag{3.16}$$

As $\theta_0 \longrightarrow 0$, an approximation to the surface current density which may be used to compute the approximate radiated far field is

$$\bar{J}(\bar{R},\omega) \approx \hat{Z}\, I(Z,\omega)\, U(h-|Z|)\, \delta(x)\,\delta(y) \tag{3.17}$$

where

$$I(z,\omega) \approx I_0(\omega)\left[\sin k(h-|z|) - j Z_c Y_t(\omega)\cos k(h-|z|)\right]. \tag{3.18}$$

3.5 Radiation from Biconical Antenna

Far field radiation from the thin biconical antenna can be formulated in the frequency domain as

$$\bar{E}(\bar{R},\omega) = -j\omega\mu \int_{V'} \bar{\bar{G}}(\bar{R}|\bar{R}') \cdot \bar{J}(\bar{r}',\omega)\, dV'$$

$$= \frac{-j\omega\mu}{4\pi}\int_{V'}\left[\left(\hat{\hat{U}} + \frac{1}{k^2}\nabla'\nabla'\right)\frac{e^{-jk|\bar{R}-\bar{R}'|}}{|\bar{R}-\bar{R}'|}\right]\cdot J(r',\omega)\, dV', \tag{3.19}$$

where $\bar{J}(\bar{R},\omega)$ is the exact form (3.15). Relation (2.69) in addition to the relation

$$\nabla\,\nabla\, e^{jk\hat{R}\cdot\bar{R}'} = -k^2 \hat{R}\,\hat{R}\, e^{jk\hat{R}\cdot\bar{R}'} \tag{3.20}$$

produces

$$\bar{E}(\bar{R},\omega) = \frac{-j\omega\mu e^{-jkR}}{4\pi R}\int_{V'}\left(\hat{\hat{U}} - \hat{R}\,\hat{R}\right)\cdot\bar{J}(\bar{R}',\omega)\, e^{jk\hat{R}\cdot\bar{R}'}\, dV' \tag{3.21}$$

The identity

$$(\hat{\hat{U}} - \hat{R}\,\hat{R}) \cdot \bar{J}(\bar{R}', \omega) = \bar{J}(\bar{R}', \omega) - \hat{R}\left[\hat{R} \cdot \bar{J}(\bar{R}', \omega)\right] \tag{3.22}$$

leads to

$$\bar{E}(\bar{R}, \omega) = \frac{-j\omega\mu e^{-jkR}}{8\pi^2 R} \int_0^h \int_0^{\pi} \int_0^{2\pi} I(R', \omega)\left[\hat{R}' - (\hat{R} \cdot \hat{R}')\,\hat{R}\right] e^{jk(\hat{R} \cdot \hat{R}')R'} \cdot$$

$$\cdot \left[\delta(\theta' - \theta_0) - \delta(\theta' - \pi + \theta_0)\right] d\phi'\, d\theta'\, dR', \tag{3.23}$$

in which the quantity

$$\hat{R} \cdot \hat{R}' = \cos\theta' \cos\theta + \sin\theta' \sin\theta \cos(\phi - \phi') \quad . \tag{3.24}$$

Performing the θ' and ϕ' integrations and substituting Bessel function relations yield

$$\bar{E}(\bar{R}, \omega) = \frac{-j\omega\mu\, e^{-jkR}}{4\pi R} \int_{-h}^{h} I(R', \omega)\, e^{-jkR' \cos\theta_0 \cos\theta} \cdot$$

$$\cdot \left[(\hat{R}' - \hat{R} \cos\theta_0 \cos\theta)\, J_0(kR' \sin\theta_0 \sin\theta)\right.$$

$$\left. -j\,\hat{R} \sin\theta_0 \sin\theta\, J_1(kR' \sin\theta_0 \sin\theta)\right] dR', \tag{3.25}$$

where

$$I(-R', \omega) = -I(R', \omega) \quad . \tag{3.26}$$

An approximate form for the radiation field may be obtained in the case $\theta_0 \longrightarrow 0$ from (3.17) and (3.18). The identity

$$(\hat{\hat{U}} - \hat{R}\,\hat{R}) \cdot \bar{J}(\bar{R}', \omega) = -\hat{R} \times \left[\hat{R} \times \bar{J}(\bar{R}', \omega)\right] \tag{3.27}$$

converts (3.21) to

$$\bar{E}(\bar{R},\omega) \approx \frac{j\omega\mu\, e^{-jkR}}{4\pi R}\, \hat{R} \times (\hat{R} \times \hat{z}) \int_{-h}^{h} I(z',\omega)\, e^{jk\hat{R}\cdot\bar{R}'}\, dz' \qquad (3.28)$$

In this case,

$$\hat{R} \cdot \bar{R}' \approx z' \cos\theta \qquad (3.29)$$

so that

$$\bar{E}(\bar{R},\omega) \approx -\hat{\theta}\, \frac{j\omega\mu e^{-jkR}}{4\pi R} \sin\theta \int_{-h}^{h} I(z',\omega)\, e^{jkz'\cos\theta}\, dz' . \qquad (3.30)$$

The inverse Fourier transform of (3.30) gives the time domain transient waveform radiated by the biconical antenna.

$$\bar{e}(\bar{R},t) = -\hat{\theta}\, \frac{\mu \sin\theta}{8\pi^2 R} \int_{-\infty}^{\infty} \omega \int_{-h}^{h} I(z',\omega)\, e^{j\omega\left(t - \frac{R}{c} + \frac{z'}{c}\cos\theta + \frac{\pi}{2\omega}\right)}\, dz'\, d\omega . \qquad (3.31)$$

The Fast Fourier Transform techniques which have been described in Chapter II can be employed here as well for efficient computation. A computer program to compute the transient radiation field of the step-excited biconical antenna is similar in features and complexity to that in Appendix B.

To illustrate the results of calculating the radiated transient field from the preceding formulation, an example will be selected with parameters similar to the transmission line calculations of Chapter II. The duration of the source voltage step is $t = 10\frac{h}{c}$ and the half length of the thin biconical antenna is h = 1 meter in this example. For the sake of clarity in presenting these radiated transient waveforms, the source impedance is assumed to be conjugately matched to the antenna input impedance

$$Z_s(\omega) = Z_{in}^{*}(\omega) . \qquad (3.32)$$

In this way, re-reflection of antenna current waves from the source are avoided so that the radiated waveform is clearly related to a single outward and a single

inward traveling current step on each arm of the antenna. No loss in generality is created by the assumption of (3.32) for the present example. An inbound current wave on the antenna can experience reflection and distortion by a general source impedance and then be analyzed after reflection in exactly the same way as the initial outbound current wave. The formulation and computation of the radiated field allow any $Z_s(\omega)$.

Examples of calculated waveforms which are radiated in different θ directions are shown in Fig. 3-4. For visibility of details, the maximum field intensities have been normalized to unity. The time scale has been translated to $t - \frac{R}{c}$ where R is the observation distance from the apex feed point of the antenna. Marked differences are evident among the waveforms radiated in different directions. The basis for these differences as well as an understanding of the causal relationship between the transient antenna current and the radiated field can be supplied by the following rudimentary idealized time domain considerations.

Figure 3-5a depicts an idealized step function wave of current traveling from the source point of the antenna outward along each of the two thin biconical arms. It is assumed that the wave's velocity is c, the velocity of electromagnetic wave propagation in the surrounding medium. Due to the small value of $\theta_0 = 1$ degree, waves of net antenna current travel very nearly in the $\pm z$ directions. Hence

$$\bar{i}_+(z,t) = \hat{z}\, A\, u(h - |z|)\, u(t - \tfrac{|z|}{c}), \tag{3.33}$$

where A = the amplitude of the current step function. For the purposes of the present development, it is not necessary to consider attenuation and dispersion of the current wave. Similarly, Fig. 3-5b represents the inwardly traveling idealized step function wave of current after reflection from the ends $z = \pm h$ of the antenna,

$$\bar{i}_-(z,t) = -\hat{z}\, A\, u(h - |z|)\, u(t - \tfrac{2h - |z|}{c}) . \tag{3.34}$$

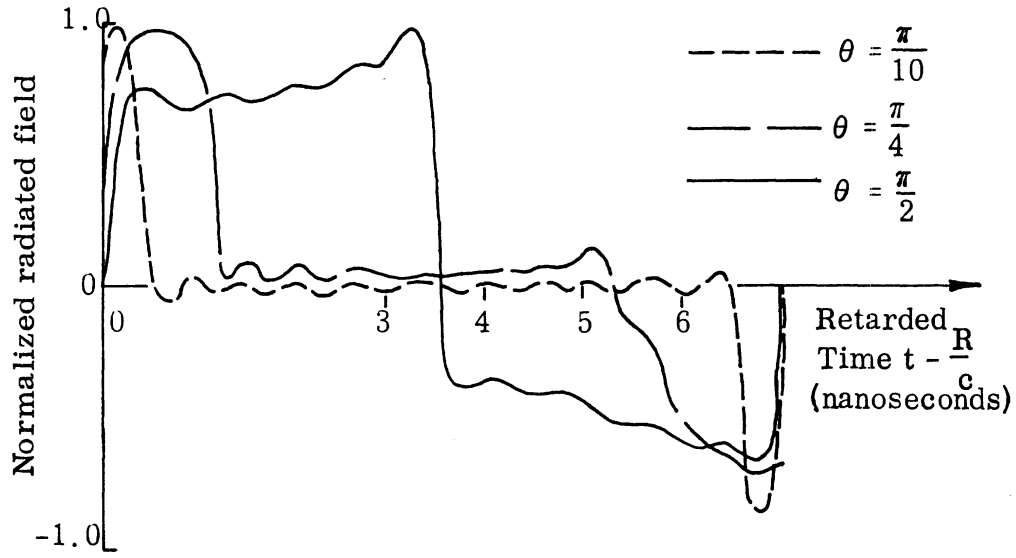

(A) Radiated Waveform for Step Function Input Current

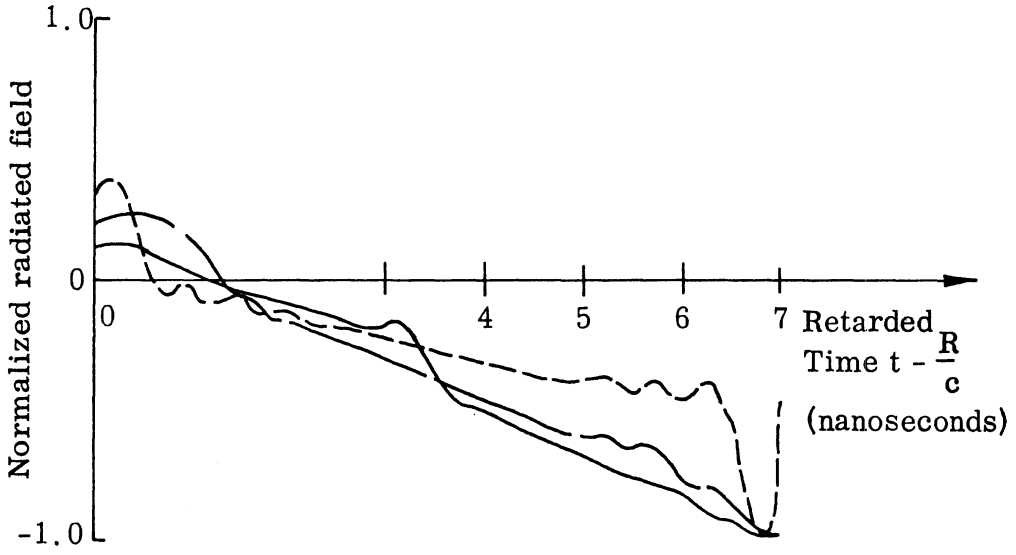

(B) Radiated Waveform for Input Current Which Results from Step Function Source Voltage.

FIG. 3-4: TRANSIENT WAVEFORMS RADIATED IN VARIOUS θ DIRECTIONS FROM STEP-EXCITED BICONICAL ANTENNA:

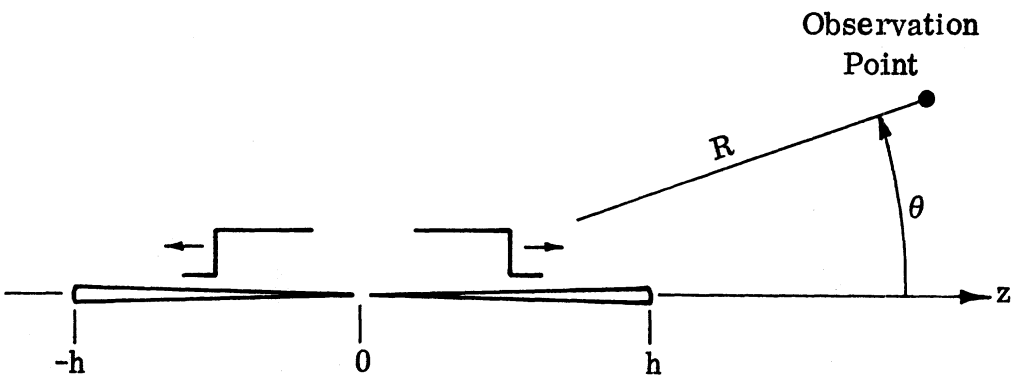

(A) Initial Outward Traveling Waves $\bar{i}_{+}(z, t)$.

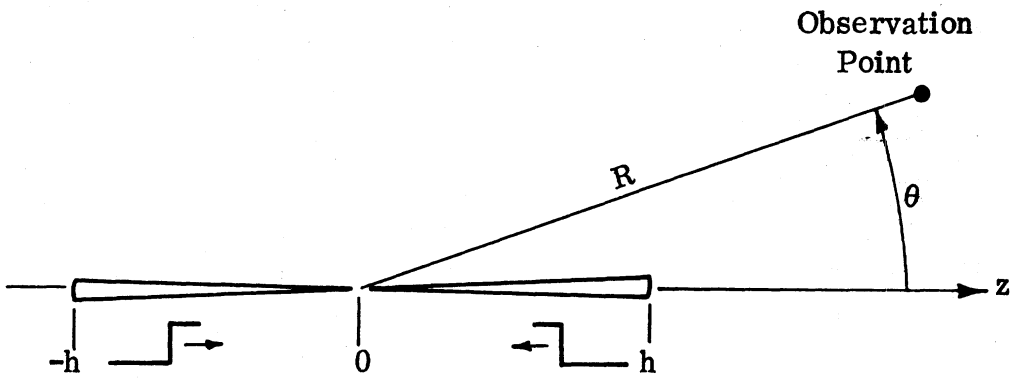

(B) Reflected Inward Traveling Waves $\bar{i}_{-}(z, t)$.

FIG. 3-5: IDEALIZED STEP FUNCTION CURRENT WAVES TRAVELING ON ARMS OF ANTENNA.

Here, the current reflection coefficient at the ends of the antenna has been approximated as $\Gamma = -1$.

The antenna's radiation field is proportional to the spatial integral over the antenna of the time derivative of the current distribution on the antenna. This current distribution, as a function of space and time, consists of the sequential superposition of the outward (3.33) and reflected (3.34) step functions traveling along the antenna. Thus the idealized radiated waveforms can be constructed in the manner sketched in Figs. 3-6, 3-7 and 3-8 for the observation directions $\theta = \frac{\pi}{4}$ and $\theta = \frac{\pi}{2}$ respectively. These idealized radiated waveforms approximate the computed waveforms of Fig. 3-4 quite well.

The idealized waveform construction aids in identifying the features of the computed waveforms. The first pulse in the radiated waveforms is caused by radiation from the abrupt change in current as that change propagates outward on each thin conical arm of the antenna. The far field radiation effects of both outward traveling current steps begin at $t = \frac{R}{c}$. The transit time of the current step waves from the bicone apex to the cone end caps is $\frac{h}{c}$. The duration of radiation from the two outwardly traveling current steps varies with the angular position of the far field observation point. It is

$$T = \frac{h}{c}(1 - \cos\theta) \tag{3.35}$$

for the current wave traveling outward on the +z arm and

$$T = \frac{h}{c}(1 + \cos\theta) \tag{3.36}$$

for the current wave traveling outward on the - z arm. As the radiated field intensity is proportional to $T^{-1/2}$, the first pulse in the radiated waveform for $\theta = \pi/10$ is mostly attributable to the outwardly traveling current step on the + z arm. For larger θ, the outwardly traveling current step on the - z arm makes a greater contribution. For $\theta = \pi/2$, both outwardly traveling current steps contribute equally to the first pulse in the radiated waveform.

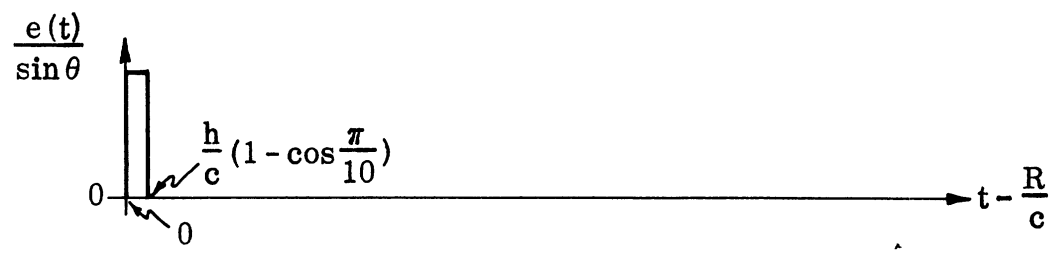

(A) Radiation from Current Step Traveling Outward on +z.

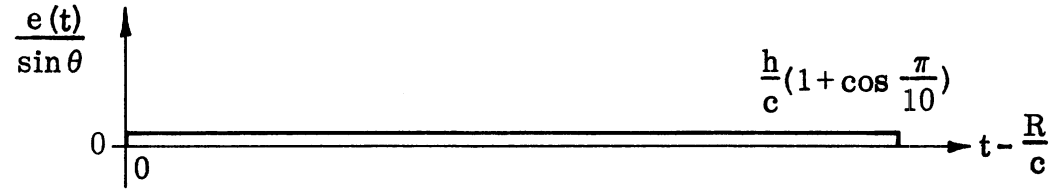

(B) Radiation from Current Step Traveling Outward on -z.

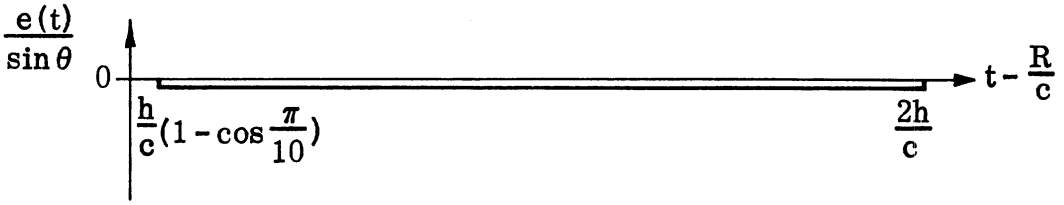

(C) Radiation from Current Step Traveling Inward on +z.

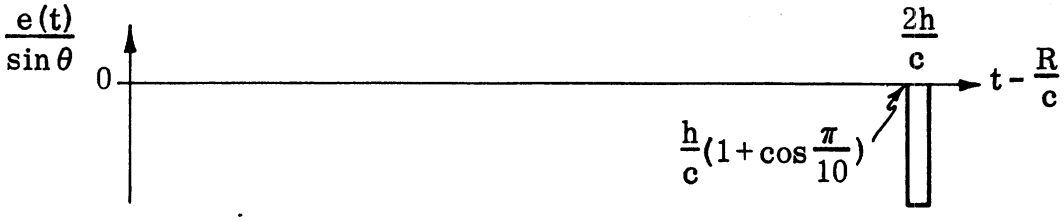

(D) Radiation from Current Step Traveling Inward on -z.

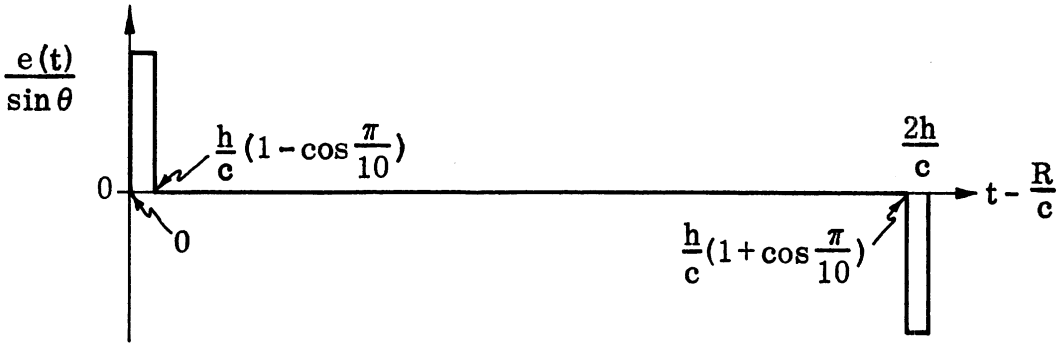

(E) Sum of (A), (B), (C), (D).

FIG. 3-6: COMPONENT IDEALIZATION OF TRANSIENT WAVEFORM RADIATED IN $\theta = \frac{\pi}{10}$ DIRECTION.

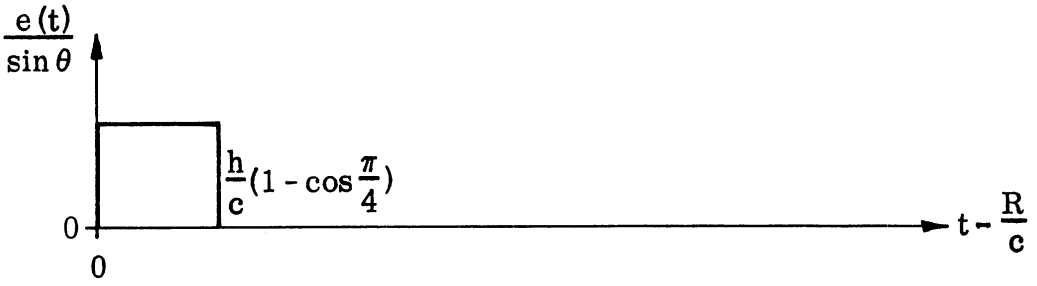

(A) Radiation from Current Step Traveling Outward on +z.

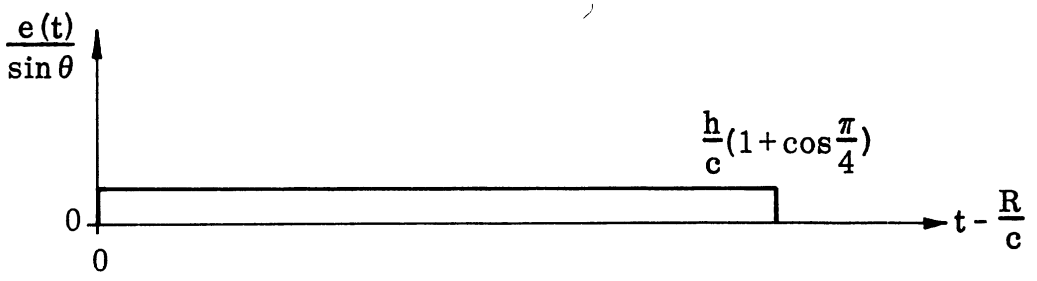

(B) Radiation from Current Step Traveling Outward on -z.

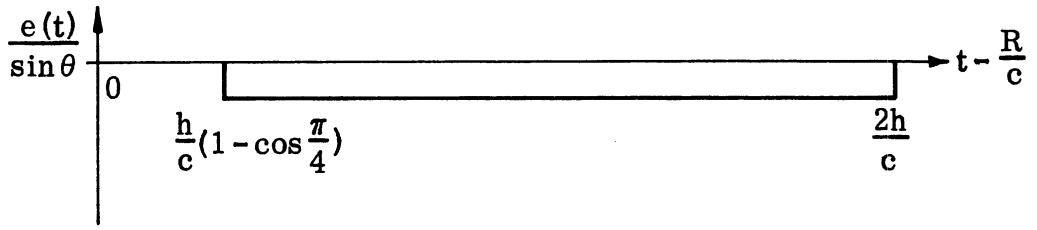

(C) Radiation from Current Step Traveling Inward on +z.

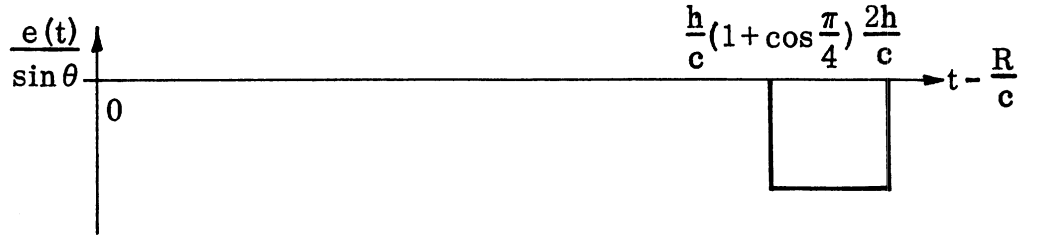

(D) Radiation from Current Step Traveling Inward on -z.

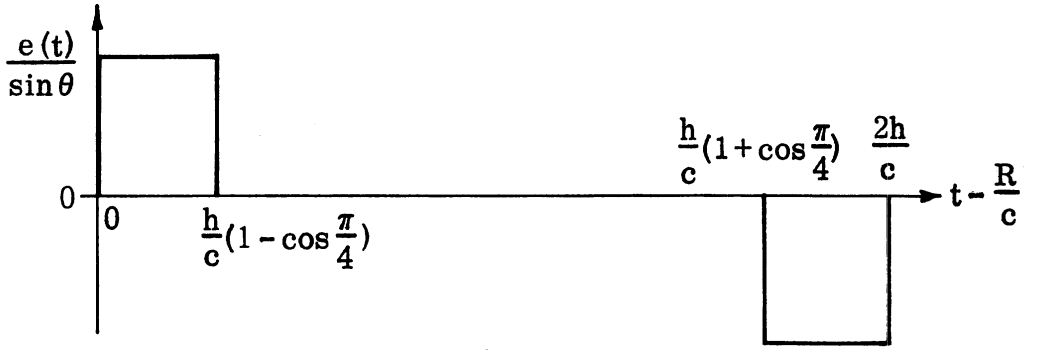

(E) Sum of (A), (B), (C), (D).

FIG. 3-7: COMPONENT IDEALIZATION OF TRANSIENT WAVEFORM RADIATED IN $\theta = \frac{\pi}{4}$ DIRECTION.

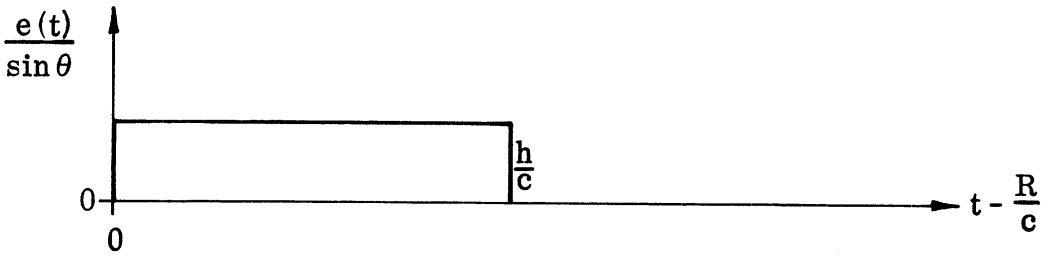

(A) Radiation from Current Step Traveling Outward on +z.

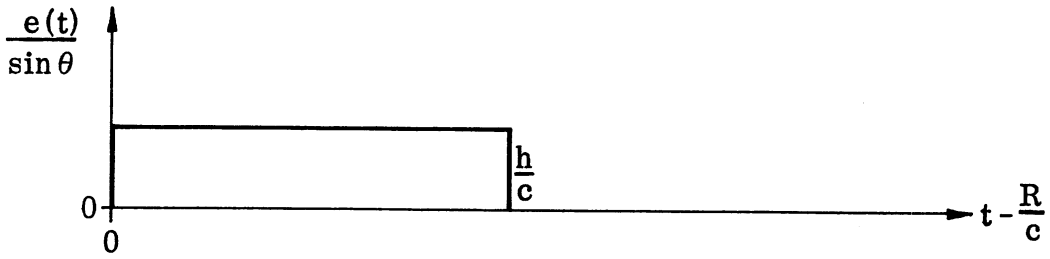

(B) Radiation from Current Step Traveling Outward on -z.

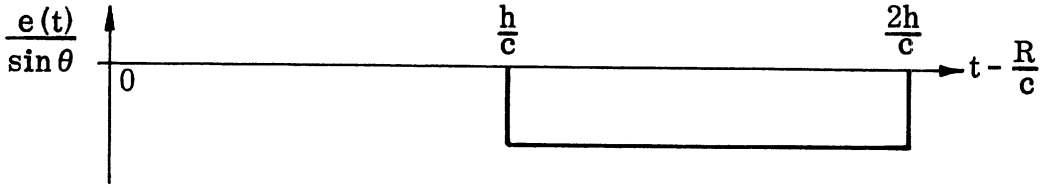

(C) Radiation from Current Step Traveling Inward on +z.

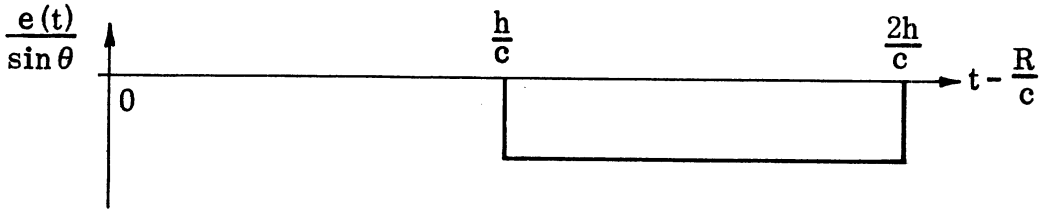

(D) Radiation from Current Step Traveling Inward on -z.

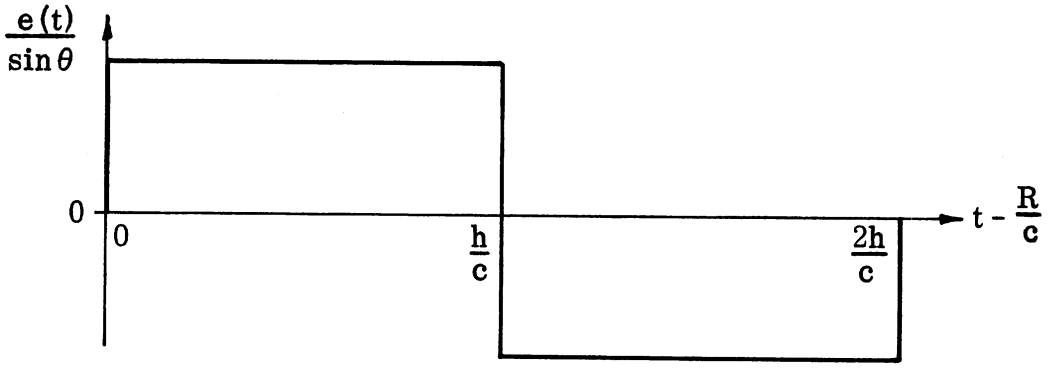

(E) Sum of (A), (B), (C), (D).

FIG. 3-8: COMPONENT IDEALIZATION OF TRANSIENT WAVEFORM RADIATED IN $\theta = \frac{\pi}{2}$ DIRECTION.

The second pulse in the radiated waveform is caused by radiation from the reflected current steps that propagate on the thin cones from the end caps to the bicone apex where they are assumed to be absorbed in the source impedance. The current of both reflected step waves is negative so that the second pulse in the waveform is negative.

Radiation due to the inwardly traveling current step on the + z arm first arrives at the far field observation point at $t = \frac{h}{c}(1 - \cos\theta) + \frac{R}{c}$ and persists until $t = \frac{2h}{c} + \frac{R}{c}$. Radiation due to the inwardly traveling current step on the -z arm arrives at $t = \frac{h}{c}(1 + \cos\theta) + \frac{R}{c}$ and persists until $t = \frac{2h}{c} + \frac{R}{c}$ also. During the period $\frac{h}{c}(1 + \cos\theta) + \frac{R}{c} \leq t \leq \frac{2h}{c} + \frac{R}{c}$, the two radiated fields add to produce the pulse. For $\theta = \pi/10$, most of the pulse is attributable to the reflected current on the - z arm because the contribution from the reflected current on the + z arm is smaller in amplitude and is distributed over a longer time. However, the latter contribution grows with increasing θ until at $\theta = \pi/2$ it is equal to the field radiated by the reflected current step on the - z arm. In the time period between the positive and negative pulses of the waveform, $\frac{h}{c}(1 - \cos\theta) + \frac{R}{c} < t < \frac{h}{c}(1 - \cos\theta) + \frac{R}{c}$, the positive field radiated from the outwardly traveling current step on the - z arm of the antenna is cancelled by the negative field radiated from the inwardly traveling reflected current step on the + z arm.

Radiated transient waveforms in the directions $\frac{\pi}{2} \leq \theta \leq \pi$ are related to the preceding according to

$$\bar{e}(\pi - \theta, t) = -\bar{e}(\theta, t) \quad . \tag{3.37}$$

3.6 Reception by Biconical Antenna

A transient plane electromagnetic wave incident on a biconical antenna will result in a transient voltage across a load impedance Z_L connected to the antenna terminals (Fig. 3-9). The previous determinations of antenna input impedance (3.10), current density on the antenna (3.15) and antenna input current

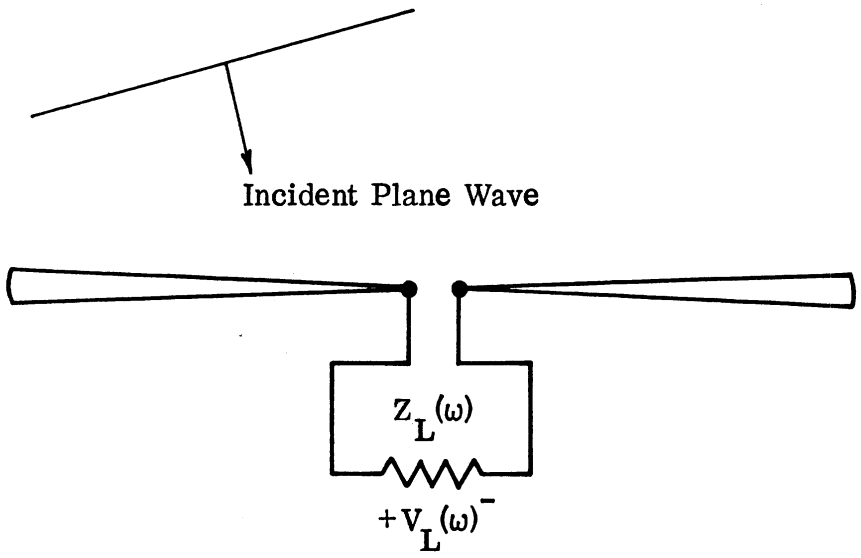

(A) Antenna with Load Impedance.

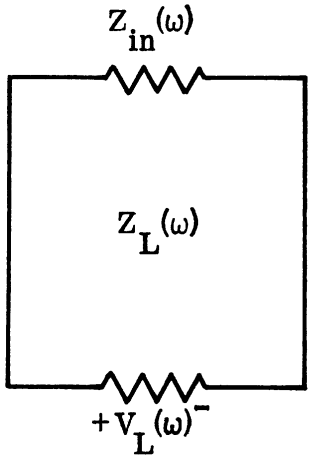

(B) Equivalent Circuit.

FIG. 3-9: BICONICAL ANTENNA IN RECEPTION.

$$I_{in}(\omega) = I(R = 0, \omega) = I_0(\omega) \left[\sin kh - j Z_c Y_t(\omega) \cos kh \right] \tag{3.38}$$

are directly applicable to the analysis of reception through use of the vector effective height function of the antenna

$$\bar{h}(\theta, \omega) = \frac{1}{I_{in}(\omega)} \iiint_{V'} \hat{R} \times \bar{J}(\bar{R}', \omega) \times \hat{R} \, e^{jk(\hat{R} \cdot \bar{R}')} \, dV' \,, \tag{3.39}$$

where primes denote the coordinates of the current density $\bar{J}$ which would exist if the antenna were driven by $I_{in}(\omega)$.. For the small angle $\theta_0 \longrightarrow 0$ biconical antenna, $\bar{J}(\bar{R}, \omega)$ can be expressed in the form (3.17),

$$\hat{R} \times \hat{Z} \times \hat{R} = -\hat{\theta} \sin\theta, \tag{3.40}$$

and

$$\hat{R} \cdot \bar{R}' = z' \cos\theta \,. \tag{3.41}$$

Thus

$$\bar{h}(\theta, \omega) = -\hat{\theta} \frac{2\pi \, 2 \sin\theta}{I_{in}(\omega) \left[\cos kh + j Z_c Y_t(\omega) \sin kh \right]} \int_{-h}^{h} \left[Z_c Y_t(\omega) \cos k(h - |z'|) + j \sin k(h - |z'|) \right] e^{jkz' \cos\theta} \, dz'. \tag{3.42}$$

The received voltage is then

$$v_L(\theta, t) = \frac{1}{2\pi} \int_{-\infty}^{\infty} \frac{Z_L(\omega) \, \bar{E}_i(\theta, \omega) \cdot \bar{h}(\theta, \omega) \, e^{j\omega t}}{Z_L(\omega) + Z_{in}(\omega)} \, d\omega \,, \tag{3.43}$$

where $\bar{E}_i(\theta, \omega)$ is the Fourier transform of the transient electric field intensity of the incident plane wave. The form of the integral (3.42) is similar to that of (3.30). The received transient waveforms will therefore vary with incidence angle in a manner analogous to the transmitting case which was shown in Fig. 3-4.

3.7 Transient Coupling of Biconical Antennas

The preceding separate analyses of transmission and reception of transient

signals by biconical antennas can be combined. The transient signal received by one biconical antenna in the radiation field of another biconical antenna that is driven by a transient source can be formulated in terms of vector effective height functions. The expression has already been presented as (2.86) when applied to transmission lines as the transmitting and receiving structures. The formulation applies to any transmitting and receiving combination of transmission lines and biconical antennas and to other antenna types for which $\bar{h}(\Omega, \omega)$ can be determined.

Chapter IV

CONCLUSIONS

The current on a resistively loaded transmission line can be expressed in an exact closed functional form when the resistance varies linearly with distance along the line. The expression consists of complex Airy functions. For nonlinear resistance distributions, a numerical solution for the current can be obtained.

Materially different current distributions are produced by different resistance functions. Of the resistance distribution functions investigated, the optimum was found to be

$$R(z) = \frac{9}{4} Z_0 \frac{z}{1 - z} .$$

This resistance loading function produces the best input impedance match as well as a current traveling wave of maximum amplitude on a transmission line with an open circuit termination. An exponential function is nearly as effective. Other functions create a greater input impedance mismatch and produce either a greater attenuation of current or allow the current to deviate by more than a prescribed amount from a traveling wave. Uniform resistance loading, which is the most commonly encountered type due to its analytic tractability, and a single discrete resistance, which is perhaps the simplest to fabricate, are particularly poor for impedance matching and minimizing reflections. Properties of resistance distributions which are responsible for producing the desired features in a current distribution are evident. High resistance near the end of the transmission line is needed to reduce the reflected wave. Low resistance loading over the rest of the line is necessary to retain a large amplitude of the outward traveling current wave. The proper smooth transition between low and high resistance regions is needed to reduce the net reflections from the transition.

The analysis of transmission lines loaded by continuous resistance distributions requires a large amount of computer time. Significantly less

computation is required for analysis of transmission lines loaded by lumped resistances at discrete positions along the lines. The construction cost of a discretely loaded line should also be lower. Results of the discrete analysis approach those of the continuous analysis when the separation of the discrete resistances is on the order of 1/8 of the shortest wavelength of interest.

For nonuniform resistance loadings, a transmission line may be considered to possess a characteristic impedance which is a function of position along the line and differs in the two directions. Expressions for this quantity can be derived by the technique of invariant imbedding.

An improvement in precision over previously published analyses of transient radiation from biconical antennas is possible by concentrating on thin biconical antennas. Small cone angles allow the use of a closed form expression for an effective terminating admittance. This improvement over the usual truncated infinite series improves the accuracy of the expressions for current distribution and input impedance. These in turn improve the accuracy of expressions for the radiated field and received signal.

When the resistively loaded transmission lines and thin biconical antennas investigated here are driven by a transient source, their transient radiated waveforms are direction-dependent and their radiation patterns are time-dependent. These results, as determined by the Fourier transform approach, agree with a rudimentary time domain view which ascribes radiation to temporal variations in currents that travel on the structures. In the case of a resistively loaded transmission line, attenuation and distortion of current waves as they traverse the line influence the shape of the radiated waveform and the radiation pattern. Thus the resistance distribution function is a possible means of controlling radiated pulse shapes for the electromagentic pulse simulation problem.

Chapter V

RECOMMENDATIONS

Topics for further research became apparent during the course of this investigation. Analysis of transient radiation and reception from additional types of antennas would be valuable. Examples are planar and conical logarithmic or Archimedean spiral antennas which characteristically have broad bandwidths. For the purpose of determining radiation fields, such antennas might be modeled adequately as spiraled transmission lines. As radiators, these antennas may have properties of interest to the electromagnetic pulse simulation problem. As receivers of transient signals, spiral antennas are interesting due to their common operational use where exposure to an electromagnetic pulse is a consideration.

An investigation, using the EMF method[41], of the input impedance of a resistively loaded linear antenna could be attempted. The resistance can be in the form of continuous and discrete series resistance loading similar to that of the transmission lines in the present dissertation. If successful, this investigation could lead to a study of transient radiation and reception by resistively loaded linear antennas that applies the results of the loaded transmission line work.

The transmission line, or perhaps a linear antenna, analysis could be extended to include resistances that are more complicated than the monotonically increasing functions of distance that have been covered.

There would be some practical value to a catalog of time domain waveforms radiated from linear antennas for a range of antenna lengths, resistance distributions and source waveforms. This type of data would be useful to those involved in electromagnetic pulse simulation.

REFERENCES

1. Manneback, Chas., "Radiation from Transmission Lines," A.I.E.E. J. Feb. 1923, 42, pp. 289-301.

2. Getsinger, W.T., "Analysis of Certain Transmission Line Networks in the Time Domain," IRE Trans. MTT, May, 1960, pp.301-309.

3. Frey, W. and P.Althammer, "The Calculation of Electromagnetic Transients in Lines by Means of a Digital Computer", Brown Boveri Rev., Vol. 48, No. 5/6, 1961, pp. 344-355.

4. Wu, T.T., "Theory of the Dipole Antenna and the Two-Wire Transmission Line," J. Math Phys., Vol. 2, July/August 1961, pp. 550-574.

5. Arismander, A., W.S. Price, A.J.McElroy, " A Digital Computer Iterative Method for Simulating Switching Surge Responses of Power Transmission Networks," AIEE Trans. P.A.S., Feb. 1962, pp. 983-998.

6. Youla, D.C., "Analysis and Synthesis of Arbitrarily Terminated Lossless Nonuniform Lines," IEEE Trans. Circuit Theory, September, 1964, pp. 363-372.

7. Uram, R. and R.W.Miller, "Mathematical Analysis and Solution of Transmission-line Transients, I - Theory", IEEE Trans. PAS, November, 1964, pp. 1116-1123.

8. Uram, R and W.E.Ferro, "Mathematical Analysis and Solution of Transmission-line Transients, II - Applications", IEEE Trans. PAS, November, 1964, pp. 1123-1137.

9. Arlett, P.L. and R. Murray-Shelley, "An Improved Method for the Calculation of Transients on Transmission Lines Using a Digital Computer," Proc. Power Industry Computer Applications Conference (sponsored by IEEE Power Group), 1965, pp. 195-211.

10. Wohlers, M.R., "A Realizability Theory for Smooth Lossless Transmission Lines, " IEEE Trans. Circuit Theory, December, 1966 pp. 356-363.

11. Branin, F.H. Jr., "Transient Analysis of Lossless Transmission Lines," IEEE Proc. November, 1967, pp. 2012-2013.

12. Liu, Y.K., "Transient Analysis of TEM Transmission Lines," Proc. IEEE, June, 1968, pp. 1090-1092.

References, continued

13. Boonyubol, C., and C. Calabrese, "Equivalent Distributed-Parameter Simulation for Transient Study of a Transmission Line," Paper 68-CP-655-PWR, 1968 IEEE Summer Power Meeting, Chicago.

14. Matick, R.E., "Transmission Lines for Digital and Communications Networks," McGraw-Hill, 1969.

15. Metzger, G. and J-P Vabre, "Transmission Lines with Pulse Excitation," Academic Press, 1969, 208 p.

16. Dvorak, V., "Transient Analysis of Nonuniform Transmission Lines," Proc. IEEE, May 1970, pp. 844-845.

17. Haack, G.R., "Comment on Transient Analysis of Lossy Transmission Lines," Proc. IEEE, June 1971, pp. 1022-1023.

18. Shah, K.R. and Y. Yavin, "Equivalent Representation of Lossy Transmission Lines," IEEE Proc., August 1971, pp. 1258-1261.

19. Wu, T.T. and R.W.P.King, "The Cylindrical Antenna with Nonreflecting Resistive Loading," IEEE Trans. AP, May 1965, pp. 369-373 and Nov. 1965, p. 998.

20. King, R.W.P. and T.T.Wu, "The Imperfectly Conducting Cylindrical Transmitting Antenna," IEEE Trans. AP, September, 1966, pp. 524-534.

21. King, R.W.P., C.W.Harrison, E.A.Aronson, "The Imperfectly Conducting Cylindrical Transmitting Antenna: Numerical Results," IEEE Trans. AP, September, 1966, pp. 535-542.

22. Shen, L.C. and T.T.Wu, "Cylindrical Antenna with Tapered Resistive Loading," Radio Science, February, 1967, pp. 191-201.

23. Taylor, C.D., C.W.Harrison, E.A.Aronson, "Resistive Receiving and Scattering Antennas," IEEE Trans. AP, May, 1967, pp. 371-376.

24. Harrington, R.F. and J.R.Mautz, "Straight Wires with Arbitrary Excitation and Loading", IEEE Trans. AP, July, 1967, pp. 502-515.

25. Shen, L.C., "An Experimental Study of the Antenna with Nonreflective Resistive Loading," IEEE Trans.AP, September, 1967. pp. 606-611.

26. Shen, L.C., "An Experimental Study of Imperfectly Conducting Dipoles," IEEE Trans. AP, November, 1967, pp.782-784.

References, continued

27. Taylor, C. D., "Cylindrical Transmitting Antenna: Tapered Resistivity and Multiple Impedance Loadings," IEEE Trans AP, March, 1968, pp. 176-179.

28. Taylor, C.D. and T.H.Shumpert, "Electromagnetic Pulse Generation by an Impedance Loaded Dipole Antenna," IEEE Trans. AP, January, 1970, pp. 110-112.

29. Popovic, B.D., "Theory of Imperfectly Conducting Thin Cylindrical Dipoles," Proc. IEE (London), 1970, pp. 2205-2208.

30. Lally, J.F. and D.T.Rouch, "Experimental Investigation of the Broadband Properties of a Continuously Loaded Resistive Monopole," IEEE Trans. AP, November, 1970, pp. 764-768.

31. Popovic, B.D., and Z.D.Popovic, "Imperfectly Conducting Cylindrical Antenna: Variations Approach," IEEE Trans AP, May 1971, pp. 435-436.

32. Popovic, B.D., "Theory of Cylindrical Antennas with Arbitrary Impedance Loading," Proc. IEE (London), October, 1971, pp. 1327-1332.

33. Auckenthaler, Alethia M. and C. Leonard Bennett, "Computer Solution of Transient and Time Domaine Thin-Wire Antenna Problems," IEEE Trans. MTT, November, 1971, pp. 892-893.

34. Howe, G.W.O., "The Nature of the Electromagnetic Waves Employed in Radio Telegraphy and the Mode of their Propagation," Elec. Rev., September 26, 1963, pp. 486-489.

35. Schelkunoff, S.A., "Transmission Theory of Spherical Waves," Trans. A.I.E.E., 1938, pp. 744-750.

36. Barrow, W.L., L.O.Chu and J.J.Jarson, "Biconical Electromagnetic Horns," Proc. IRE, 27, December, 1939, pp. 769-779.

37. Schelkunoff, S.A., "Theory of Antennas of Arbitrary Size and Shape," Proc. IRE, 29, September, 1941, pp. 493-521.

38. Schelkunoff, S.A., "Principal and Complementary Waves in Antennas," Proc. IRE, January, 1946, pp. 23p-32p.

39. Smith, P.D.P., "The Conical Dipole of Wide Angle," J.A.P. 19, January, 1948, pp. 11-23.

40. Tai, C-T, "On the Theory of Biconical Antennas," J.A.P., 19, December, 1948, pp. 1155-1160.

References, continued

41. Tai, C-T, "A Study of the e.m.f. Method", J.A.P., July 1947, pp. 717-723.

42. Tai, C-T, "Application of a Variational Principle to Biconical Antennas," J.A.P., 20, November, 1949, pp. 1076-1084.

43. Schelkunoff, S.A., "General Theory of Symmetric Biconical Antennas," J.A.P., 22, November, 1951, pp. 1330-1332.

44. Meier, J.A. and A. Leitner, "Biconical Antenna", Interim Technical Report No. 6, Dept. of Math. and Physics, Michigan State Univ., June, 1957.

45. Plonus, Martin A., "A Study of the Biconical Antenna," University of Michigan Radiation Laboratory, May, 1961.

46. Plonus, Martin A., "Application of Selective Mode Coupling in the Solution to Biconical Antennas," Chapter in Electromagnetic Theory and Antennas-2, MacMillan, 1963, edited by E.C.Jordan, pp. 1155-1166.

47. Papas, C.H. and R.W.P.King, "Input Impedance of Wide-Angle Conical Antennas," Cruft Laboratory Report, Harvard University, December, 1968.

48. Collin, Robert E. and F.J.Zucker, "Antenna Theory," McGraw-Hill Book Co., 1969, pp. 483-522.

49. Harrison, C.W. and C.S.Williams, Jr., "Transients in Wide-Angle Conical Antennas," IEEE Trans AP, March, 1965, pp. 236-246.

50. Tai, C-T., Dyadic Green's Functions in Electromagnetic Theory, Intext Educational Publishers, 1971.

51. Wait, J.R., "Electromagnetic Waves in Stratified Media," Pergamon Press, 1962, pp. 75, 97.

52. Woodward, P.M. and A.M., "Fourplace Tables of the Airy Function in the Complex Plane," London Philosophical Magazine, 37, (7), 1946, pp. 236-261.

53. Abramowitz, M. and I.A.Stegun, "Handbook of Mathematical Functions," N.B.S. Applied Math. Series - 55, U.S. Gov't. Printing Office, 1964, pp. 446-447.

54. Kimbark, E.W., "Electrical Transmission of Power and Signals", 1949, pp. 153-165.

References, continued

55. Weber, E., "Linear Transient Analysis - Volume II," John Wiley and Sons, 1956, pp. 285-315.

56. Magnusson, P.G., "Transmission Lines and Wave Propagation," Allyn and Bacon, 1965, pp. 100-118.

57. Sinclair, G., "The Transmission and Reception of Elliptically Polarized Waves," Proc. IRE, February, 1950, pp. 148-151.

58. Collin, R.E. and F.J.Zucker, "Antenna Theory - Part I", McGraw-Hill Book Co., New York, 1969, pp. 93-135.

59. Tai, Chen-To., "Theory of Receiving Antennas", Internal Memorandum University of Michigan, Radiation Laboratory, October, 1972.

60. Rice, S.O., "Sum of Series of the Form $\sum_{0}^{\infty} A_n J_{n+\alpha}(z) J_{n+\beta}(z)$", Phil. Mag., 35, 1944, pp. 686-693.

Appendix A

COMPUTATION OF CURRENT ON RESISTIVELY LOADED TRANSMISSION LINES

The amplitude and phase of the current in the frequency domain can be computed numerically as a function of position along the resistance-loaded transmission line as described in Chapter II. The FORTRAN program which was written specifically to compute the current by solving equation (2.24) with boundary conditions (2.25) is listed below. The program is compatible with the Michigan Terminal System at the University of Michigan as of January 1, 1973.

Input data, with the following nomenclature, is required by the program:

KMAX = the number of frequencies for which the current distribution is to be computed,

F1 = the fundamental frequency,

XMAX = the length of the transmission line,

ZC = the characteristic impedance of the associated unloaded transmission line,

RR = the resistance distribution function,

FFF = the frequency generating function.

Output data from the computations includes a printed record of the following quantities:

FF = the individual frequencies,

NNN = the frequency-dependent number of equispaced positions along the transmission line for which computed results are recorded,

RIN = the input resistance of the loaded transmission line at each frequency,

XIN = the input reactance of the loaded transmission line at each frequency.

The input resistance and reactance of the loaded transmission line for each frequency are also put into file storage for use in subsequent computations of transient waveforms and radiation patterns. In addition, the amplitude and phase of the current at all frequencies and all positions along the transmission line are stored in a separate file for use in subsequent computations.

With comments removed for brevity, the program listing is as follows.

```
      EXTERNAL AFCT,FCT,DFCT,OUTP
      NAMELIST/HAL/KMAX,F1,XMAX,ZC
      COMMON KMAX, F1, FF, ZC, Z(331), YMOD(331), YARG(331),
     &NN,DIDZRE(331),DIDZIM(331)
      DIMENSION B(4,4),C(4,4),R(4),Y(4),DERY(4),AUX(20,4),
     &A(4,4),PRMT(5),BDUM(4,4),CDUM(4,4),RDUM(4),DERYDM(4)
      COMPLEX CRNT, DIDZ, ZQUAD
      DATA B/1.,4*0.,1.,10*0./,C/0.,0.,1.,4*0.,1.,8*0./,R/1.,
     &3*0./,DERY/4*1./,BCD/'*'/
      READ (5,HAL)
      WRITE (6,HAL)
      WRITE(6,20)
   20 FORMAT('0')
      WRITE(6,28)
      DO 180 K=1,KMAX
      FF=FFF(K)
      XINC=XMAX/(1+AINT(10.66667E-8*FF*XMAX))
      PRMT(1)=0.
      PRMT(2)=XMAX
      PRMT(3)=XINC
      PRMT(4)=.01
      NDIM=4
      NN=0
      DO 10 I=1,4
      RDUM(I)=R(I)
      DERYDM(I)=DERY(I)
      DO 10 J=1,4
      BDUM(I,J)=B(I,J)
      CDUM(I,J)=C(I,J)
   10 CONTINUE
      CALL LBVP(PRMT, BDUM, CDUM, RDUM, Y, DERYDM, NDIM, IHLF,
     &AFCT,FCT,DFCT,OUTP,AUX,A)
      NNN=2+AINT(10.66667E-8*FF*XMAX)
      CRNTRE=YMOD(1)*COS(YARG(1))
      CRNTIM=YMOD(1)*SIN(YARG(1))
      CRNT=CMPLX(CRNTRE,CRNTIM)
      DIDZ=CMPLX(DIDZRE(1),DIDZIM(1))
      ZQUAD=.47746483E8*ZC*DIDZ/(FF*CRNT)
      RIN=-AIMAG(ZQUAD)
      XIN=REAL(ZQUAD)
      WRITE(6,29) K,FF,NNN,YMOD(NN),RIN,XIN
      WRITE(7) RIN,XIN
      DO 180 I=1,NN
      G=ABS(Z(I)-(AINT(Z(I)/(XINC-.000001)))*XINC)
      IF(G.LE.0.00001) WRITE(8) YMOD(I),YARG(I)
      IF(G.LE.0.00001) WRITE(9) DIDZRE(I),DIDZIM(I)
  180 CONTINUE
   28 FORMAT('K',T8,'FREQUENCY',T23,'NNN',T32,
     &'END CURRENT',T54,'RIN',T69,'XIN')
   29 FORMAT(I3,3X,E12.6, 4X,I4,6X,E10.4,9X,E11.4,4X,E11.4)
      END
```

```
      SUBROUTINE AFCT(X,A)
      COMMON KMAX, F1, FF, ZC, Z(331), YMOD(331), YARG(331),
     &NN,DIDZRE(331),DIDZIM(331)
      DIMENSION A(4,4)
      A(1,1)=0.
      A(1,2)=0.
      A(1,3)=1.
      A(1,4)=0.
      A(2,1)=0.
      A(2,2)=0.
      A(2,3)=0.
      A(2,4)=1.
      A(3,1)=-.43864908E-15*(FF**2)
      A(3,2)=-.20943951E-7*FF*RR(X)/ZC
      A(3,3)=0.
      A(3,4)=0.
      A(4,1)=.20943951E-7*FF*RR(X)/ZC
      A(4,2)=-.43864908E-15*(FF**2)
      A(4,3)=0.
      A(4,4)=0.
      RETURN
      END


      SUBROUTINE FCT(X,F)
      DIMENSION F(4)
      F(1)=0.
      F(2)=0.
      F(3)=0.
      F(4)=0.
      RETURN
      END


      SUBROUTINE DFCT(X,DF)
      DIMENSION DF(4)
      DF(1)=0.
      DF(2)=0.
      DF(3)=0.
      DF(4)=0.
      RETURN
      END
```

```
      SUBROUTINE OUTP(X,Y,DERY,IHLF,NDIM,PRMT)
      DIMENSION PRMT(1),Y(1),DERY(1)
      COMMON KMAX, F1, FF, ZC, Z(331), YMOD(331), YARG(331),
     &NN,DIDZRE(331),DIDZIM(331)
      IF (NN .GT. 400) PRMT(5)=1
      NN=NN+1
      Z(NN)=X
      YMOD(NN)=SQRT(Y(1)**2+Y(2)**2)
      YARG(NN)=ATAN2(Y(2),Y(1))
      DIDZRE(NN)=Y(3)
      DIDZIM(NN)=Y(4)
      RETURN
      END

      SUBROUTINE LBVP(PRMT,B,C,R,Y,DERY,NDIM,IHLF,AFCT,FCT,
     1DFCT,OUTP,AUX,A)
      DIMENSION PRMT(1),B(1),C(1),R(1),Y(1),DERY(1),
     1AUX(20,1),A(1)
      IF(PRMT(3)*(PRMT(2)-PRMT(1)))2,1,3
    1 IHLF=12
      RETURN
    2 IHLF=13
      RETURN
      IB=0
      IC=0
      DO 7 K=1,NDIM
      AUX(15,K)=DERY(K)
      AUX(1,K)=1.
      AUX(17,K)=1.
      KK=KK+NDIM
      DO 4 I=1,NDIM
      II=KK+I
      IF(B(II))5,4,5
    4 CONTINUE
      IB=IB+1
      AUX(1,K)=0.
    5 DO 6 I=1,NDIM
      II=KK+I
      IF(C(II))7,6,7
    6 CONTINUE
      IC=IC+1
      AUX(17,K)=0.
    7 CONTINUE
      IF(IC-IB)8,11,11
    8 H=PRMT(2)
      PRMT(2)=PRMT(1)
      PRMT(1)=H
      PRMT(3)=-PRMT(3)
      DO 9 I=1,NDIM
```

```
      AUX(17,I)=AUX(1,I)
      II=NDIM*NDIM
      DO 10 I=1,II
      H=B(I)
      B(I)=C(I)
   10 C(I)=H
   11 X=PRMT(2)
      CALL FCT(X,Y)
      CALL DFCT(X,DERY)
      DO 12 I=1,NDIM
      AUX(18,I)=Y(I)
   12 AUX(19,I)=DERY(I)
      K=0
      KK=0
  100 K=K+1
      IF(AUX(17,K)) 108,108,101
  101 X=PRMT(2)
      CALL AFCT(X,A)
      SUM=0.
      GL=AUX(18,K)
      DGL=AUX(19,K)
      II=K
      DO 104 I=1,NDIM
      H=-A(II)
      DERY(I)=H
      AUX(20,I)=R(I)
      Y(I)=0.
      IF(I-K) 103,102,103
  102 Y(I)=1.
  103 DGL=DGL+H*AUX(18,I)
  104 II=II+NDIM
      XEND=PRMT(1)
      H=.0625*(XEND-X)
      ISW=0
      GOTO 400
  105 IF(IHLF-10) 106,106,117
  106 DO 107 I=1,NDIM
      KK=KK+1
      H=C(KK)
      R(I)=AUX(20,I)+H*SUM
      II=I
      DO 107 J=1,NDIM
      B(II)=B(II)+H*Y(J)
  107 II=II+NDIM
      GOTO 109
  108 KK=KK+NDIM
  109 IF(K-NDIM) 100,110,110
  110 X=PRMT(4)
      CALL GELG(R,B,NDIM,1,X,I)
      IF(I) 111,112,112
```

```
111 IHLF=14
    RETURN
112 PRMT(5)=0.
    IHLF=-I
    X=PRMT(1)
    XEND=PRMT(2)
    H=PRMT(3)
    DO 113 I=1,NDIM
113 Y(I)=R(I)
    ISW=1
114 ISW2=12
    GOTO 200
115 ISW3=-1
    GOTO 300
116 IF(IHLF)400,400,117
117 RETURN
200 CALL AFCT(X,A)
    IF(ISW)201,201,205
201 LL=0
    DO 203 M=1,NDIM
    HS=0.
    DO 202 L=1,NDIM
    LL=LL+1
202 HS=HS-A(LL)*Y(L)
203 DERY(M)=HS
204 GOTO(502,504,506,407,415,418,608,617,632,634
   1ISW2
205 CALL FCT(X,DERY)
    DO 207 M=1,NDIM
    LL=M-NDIM
    HS=0.
    DO 206 L=1,NDIM
    LL=LL+NDIM
206 HS=HS+A(LL)*Y(L)
207 DERY(M)=HS+DERY(M)
    GOTO 204
300 IF(ISW)301,301,305
301 CALL FCT(X,R)
    GU=0.
    DGU=0.
    DO 302 L=1,NDIM
    GU=GU+Y(L)*R(L)
302 DGU=DGU+DERY(L)*R(L)
    CALL DFCT(X,R)
    DO 303 L=1,NDIM
303 DGU=DGU+Y(L)*R(L)
    SUM=SUM+.5*H*((GL+GU)+.1666667*H*(DGL-DGU))
    GL=GU
    DGL=DGU
```

```
304 IF(ISW3)116,422,618
305 CALL OUTP(X,Y,DERY,IHLF,NDIM,PRMT)
    IF(PRMT(5))117,304,117
400 N=1
    XST=X
    IHLF=0
    DO 401 I=1,NDIM
    AUX(16,I)=0.
    AUX(1,I)=Y(I)
401 AUX(8,I)=DERY(I)
    ISW1=1
    GOTO 500
402 X=X+H
    DO 403 I=1,NDIM
403 AUX(2,I)=Y(I)
404 IHLF=IHLF+1
    X=X-H
    DO 405 I=1,NDIM
405 AUX(4,I)=AUX(2,I)
    H=.5*H
    N=1
    ISW1=2
    GOTO 500
406 X=X+H
    ISW2=4
    GOTO 200
407 N=2
    DO 408 I=1,NDIM
    AUX(2,I)=Y(I)
408 AUX(9,I)=DERY(I)
    ISW1=3
    GOTO 500
409 DO 414 I=1,NDIM
    Z=ABS(Y(I))
    IF(Z-1.)410,411,411
410 Z=1.
411 DELT=.06666667*ABS(Y(I)-AUX(4,I))
    IF(ISW)413,413,412
412 DELT=AUX(15,I)*DELT
413 IF(DELT-Z*PRMT(4))414,414,429
414 CONTINUE
    X=X+H
    ISW2=5
    GOTO 200
415 DO 416 I=1,NDIM
    AUX(3,I)=Y(I)
416 AUX(10,I)=DERY(I)
    N=3
    ISW1=4
    GOTO 500
```

```
417 N=1
    X=X+H
    ISW2=6
    GOTO 200
418 X=XST
    DO 419 I=1,NDIM
    AUX(11,I)=DERY(I)
419 Y(I)=AUX(1,I)+H*(.375*AUX(8,I)+.7916667*AUX(9,I)
   1-.2083333*AUX(10,I)+.04166667*DERY(I))
420 X=X+H
    N=N+1
    ISW2=11
    GOTO 200
421 ISW3=0
    GOTO 300
422 IF(N-4)423,600,600
423 DO 424 I=1,NDIM
    AUX(N,I)=Y(I)
424 AUX(N+7,I)=DERY(I)
    IF(N-3)425,427,600
425 DO 426 I=1,NDIM
    DELT=AUX(9,I)+AUX(9,I)
    DELT=DELT+DELT
426 Y(I)=AUX(1,I)+.3333333*H*(AUX(8,I)+DELT+AUX(10,I))
    GOTO 420
427 DO 428 I=1,NDIM
    DELT=AUX(9,I)+AUX(10,I)
    DELT=DELT+DELT+DELT
428 Y(I)=AUX(1,I)+.375*H*(AUX(8,I)+DELT+AUX(11,I))
    GOTO 420
429 IF(IHLF-10)404,430,430
430 IHLF=11
    X=X+H
    IF(ISW)105,105,114
500 Z=X
    DO 501 I=1,NDIM
    X=H*AUX(N+7,I)
    AUX(5,I)=X
501 Y(I)=AUX(N,I)+.4*X
    X=Z+.4*H
    ISW2=1
    GOTO 200
502 DO 503 I=1,NDIM
    X=H*DERY(I)
    AUX(6,I)=X
503 Y(I)=AUX(N,I)+.2969776*AUX(5,I)+.1587596*X
    X=Z+.4557372*H
    ISW2=2
    GOTO 200
```

```
504 DO 505 I=1,NDIM
    X=H*DERY(I)
    AUX(7,I)=X
505 Y(I)=AUX(N,I)+.2181004*AUX(5,I)-3.050965*AUX(6,I)
   1+3.832865*X
    ISW2=3
    GOTO 200
506 DO 507 I=1,NDIM
5070Y(I)=AUX(N,I)+.1747603*AUX(5,I)-.5514807*AUX(6,I)
   1+1.205536*AUX(7,I)+.1711848*H*DERY(I)
    X=Z
    GOTO(402,406,409,417),ISW1
600 ISTEP=3
601 IF(N-8)604,602,604
602 DO 603 N=2,7
    DO 603 I=1,NDIM
    AUX(N-1,I)=AUX(N,I)
603 AUX(N+6,I)=AUX(N+7,I)
    N=7
604 N=N+1
    DO 605 I=1,NDIM
    AUX(N-1,I)=Y(I)
605 AUX(N+6,I)=DERY(I)
    X=X+H
606 ISTEP=ISTEP+1
    DO 607 I=1,NDIM
   0DELT=AUX(N-4,I)+1.333333*H*(AUX(N+6,I)+AUX(N+6,I)-AUX
   1(N+5,I)+AUX(N+4,I)-AUX(N+4,I)))
    Y(I)=DELT-.9256198*AUX(16,I)
607 AUX(16,I)=DELT
    ISW2=7
    GOTO 200
608 DO 609 I=1,NDIM
   0DELT=.125*(9.*AUX(N-1,I)-AUX(N-3,I)+3.*H*(DERY(I)+
   1AUX(N+6,I)+AUX(N+6,I)-AUX(N+5,I)))
    AUX(16,I)=AUX(16,I)-DELT
609 Y(I)=DELT+.0743817*AUX(16,I)
    DELT=0.
    DO 616 I=1,NDIM
    Z=ABS(Y(I))
    IF(Z-1.)610,611,611
610 Z=1.
611 Z=ABS(AUX(16,I))/Z
    IF(ISW)613,613,612
612 Z=AUX(15,I)*Z
613 IF(Z-PRMT(4))614,614,628
614 IF(DELT-Z)615,616,616
615 DELT=Z
616 CONTINUE
    ISW2=8
    GOTO 200
```

```
617 ISW3=1
    GOTO 300
618 IF(H*(X-XEND))619,621,621
619 IF(ABS(X-XEND)-.1*ABS(H))621,620,620
620 IF(DELT-.02*PRMT(4))622,622,601
621 IF(ISW)105,105,117
622 IF(IHLF)601,601,623
623 IF(N-7)601,624,624
624 IF(ISTEP-4)601,625,625
625 IMOD=ISTEP/2
    IF(ISTEP-IMOD-IMOD)601,626,601
626 H=H+H
    IHLF=IHLF-1
    ISTEP=0
    DO 627 I=1,NDIM
    AUX(N-1,I)=AUX(N-2,I)
    AUX(N-2,I)=AUX(N-4,I)
    AUX(N-3,I)=AUX(N-6,I)
    AUX(N+6,I)=AUX(N+5,I)
    AUX(N+5,I)=AUX(N+3,I)
    AUX(N+4,I)=AUX(N+1,I)
    DELT=AUX(N+6,I)+AUX(N+5,I)
    DELT=DELT+DELT+DELT
627 AUX(16,I)=8.962963*(Y(I)-AUX(N-3,I))-3.361111*H*
   1DERY(I)+DELT+AUX(N+4,I))
    GOTO 601
628 IHLF=IHLF+1
    IF(IHLF-10)630,630,629
629 IF(ISW)105,105,114
630 H=.5*H
    ISTEP=0
    DO 631 I=1,NDIM
   0Y(I)=.00390625*(80.*AUX(N-1,I)+135.*AUX(N-2,I)+40.*AUX
   1(N-3,I)+AUX(N-4,I))-.1171875*(AUX(N+6,I)-6.*AUX(N+5,I)
   0AUX(N-4,I)=.00390625*(12.*AUX(N-1,I)+135.*AUX(N-2,I)+
   1108.*AUX(N-3,I)+AUX(N-4,I))-.0234375*(AUX(N+6,I)+18.*
   2AUX(N+5,I)-9.*AUX(N+4,I))*H
   29.*AUX(N+4,I))*H
    AUX(N-3,I)=AUX(N-2,I)
631 AUX(N+4,I)=AUX(N+5,I)
    DELT=X-H
    X=DELT-(H+H)
    ISW2=9
    GOTO 200
632 DO 633 I=1,NDIM
    AUX(N-2,I)=Y(I)
    AUX(N+5,I)=DERY(I)
633 Y(I)=AUX(N-4,I)
    X=X-(H+H)
    ISW2=10
    GOTO 200
```

```
634 X=DELI
    DO 635 I=1,NDIM
    DELI=AUX(N+5,I)+AUX(N+4,I)
    DELT=DELT+DELT+DELT
   CAUX(16,I)=8.962963*(AUX(N-1,I)-Y(I))-3.361111*H*(AUX
   1(N+6,I)+DELT+DERY(I))
635 AUX(N+3,I)=DERY(I)
    GOTO 606
    END


    SUBROUTINE GELG(R,A,M,N,EPS,IER)
    DIMENSION A(1),R(1)
    IF(M)23,23,1
  1 IER=0
    PIV=0.
    MM=M*M
    NM=N*M
    DO 3 L=1,MM
    TB=ABS(A(L))
    IF(TB-PIV)3,3,2
  2 PIV=TB
    I=L
  3 CONTINUE
    TOL=EPS*PIV
    LST=1
    DO 17 K=1,M
    IF(PIV)23,23,4
  4 IF(IER)7,5,7
  5 IF(PIV-TOL)6,6,7
  6 IER=K-1
  7 PIVI=1./A(I)
    J=(I-1)/M
    I=I-J*M-K
    J=J+1-K
    DO 8 L=K,NM,M
    LL=L+I
    TB=PIVI*R(LL)
    R(LL)=R(L)
  8 R(L)=TB
    IF(K-M)9,18,18
  9 LEND=LST+M-K
    IF(J)12,12,10
 10 II=J*M
    DO 11 L=LST,LEND
    TB=A(L)
    LL=L+II
    A(L)=A(LL)
 11 A(LL)=TB
```

```
12 DO 13 L=LST,MM,M
   LL=L+I
   TB=PIVI*A(LL)
   A(LL)=A(L)
13 A(L)=TB
   A(LST)=J
   PIV=0.
   LST=LST+1
   J=0
   DO 16 II=LST,LEND
   PIVI=-A(II)
   IST=II+M
   J=J+1
   DO 15 L=IST,MM,M
   LL=L-J
   A(L)=A(L)+PIVI*A(LL)
   TB=ABS(A(L))
   IF(TB-PIV)15,15,14
14 PIV=TB
   I=L
15 CONTINUE
   DO 16 L=K,NM,M
   LL=L+J
16 R(LL)=R(LL)+PIVI*R(L)
17 LST=LST+M
18 IF(M-1)23,22,19
19 IST=MM+M
   LST=M+1
   DO 21 I=2,M
   II=LST-I
   IST=IST-LST
   L=IST-M
   L=A(L)+.5
   DO 21 J=II,NM,M
   TB=R(J)
   LL=J
   DO 20 K=IST,MM,M
   LL=LL+1
20 TB=TB-A(K)*R(LL)
   K=J+L
   R(J)=R(K)
21 R(K)=TB
22 RETURN
23 IER=-1
   RETURN
   END
```

Appendix B

COMPUTATION OF TRANSIENT RADIATION FIELD OF RESISTIVELY LOADED TRANSMISSION LINE

The time domain transient waveform of the electric field radiated by a resistively loaded transmission line can be computed from equation (2.76). a FORTRAN program which was written for this purpose is listed here. The program is compatible with the Michigan Terminal System at The University of Michigan as of January 1, 1973.

Input data required by the program include the input impedances and current distributions of the loaded transmission line. This data is available from a storage file into which it was placed by the program of Appendix A. The following additional input data, identified by program nomenclature, are also required:

ZS = source impedance,

S = separation between conductors of the transmission line, expressed in meters,

THETA = the polar observation angle θ,

PHI = the azimuth observation angle ϕ .

Computed output data include a printed record of the discrete Fourier spectral content of the approximate step function source voltage and the resulting source current. In addition, the far field radiated transient waveform is tabulated as well as plotted in a coarse graphical form.

The computer program is written in two separable parts to allow flexibility in its use. The parts may be applied to the computation of transient waveforms of voltage and current on the transmission line and far field radiation patterns. A listing of the program is as follows:

```
      DIMENSION RIN(99),XIN(99),A(99),B(99),D(99),F(99),
     &S(99),V(201),C(201)
      ZS=300.
      KMAX=99
      TINC=.16835E-9
      WRITE(6,100)
      WRITE(6,110)
      DO 10 K=1,KMAX,2
      READ(7) RIN(K),XIN(K)
      A(K)=(.80157*KMAX/K**2)*SIN(1.5708*K/KMAX)
      B(K)=ZS+RIN(K)
      D(K)=(B(K)**2+(XIN(K))**2)**.5
      F(K)=ATAN2(B(K),XIN(K))
      S(K)=A(K)/D(K)
      F(K)=F(K)-1.5707
      WRITE(10) S(K),F(K)
   10 WRITE(6,150) K,A(K),S(K),F(K)
      WRITE(6,100)
  100 FORMAT('0')
  110 FORMAT(T12,'HARMONIC',T23,'VOLTAGE AMPLITUDE',
     &T44,'CURRENT AMPLITUDE',T65,'CURRENT PHASE+PI')
  150 FORMAT(14X,I3,8X,E10.4,13X,E10.4,13X,E10.4)
      END

      NAMELIST/INPUT/KMAX,F1,JMAX,TINC,XMAX,S,THETA,PHI
      DIMENSION U(50),V(50),X(4075),Y(4075),E(201),TI(201),
     &IMAGE(1500)
      DATA E/50*0./,BCD/'*'/
      READ(5,INPUT)
      WRITE(6,INPUT)
      EMAX=.1E-10
      L=0
      DO 20 K=1,KMAX
      READ(10) U(K),V(K)
      FF=(2*K-1)*F1
      W=6.283185*FF
      NNN=2+AINT(10.66667E-8*FF*XMAX)
      XINC=XMAX/(NNN-1)
      C=W*XINC*COS(THETA)/.3E9
      D=W*TINC
      A=W*XINC*U(K)*SIN(W*S*SIN(THETA)
     &*COS(PHI)/.6E9)
      DO 10 N=1,NNN
      READ(8) X(L+N),Y(L+N)
      P=(N-1)*C+V(K)+Y(L+N)
      B=A*X(L+N)
      DO 10 J=1,JMAX
   10 E(J)=E(J)+B*COS((J-1)*D+P)
```

```
 20 L=L+NNN
    DO 30 J=1,JMAX
    TI(J)=J
    G=ABS(E(J))
 30 EMAX=AMAX1(EMAX,G)
    H=EMAX*SIN(THETA)
    WRITE(6,110) H
    WRITE(6,120)
    DO 40 J=1,JMAX
    E(J)=E(J)/EMAX
 40 WRITE(6,130) J,E(J)
    WRITE(6,100)
    WRITE(6,100)
    CALL PLOT1(0,3,16,2,48)
    CALL PLOT2(IMAGE,50.,0.,1.,-1.)
    CALL PLOT3(BCD,TI,E,50,4)
    CALL PLOT4(26,'NORMALIZED RADIATION FIELD')
    WRITE(6,140)
100 FORMAT('0')
110 FORMAT('MAXIMUM FIELD MAGNITUDE=',E12.6)
120 FORMAT('TIME INDEX',T14,'RADIATED FIELD')
130 FORMAT(3X,I3,10X,F10.4)
140 FORMAT(//T33,'TIME INDEX')
    END
```